D-33192
Version 6.0

Earth Observing System (EOS)
Tropospheric Emission Spectrometer (TES)

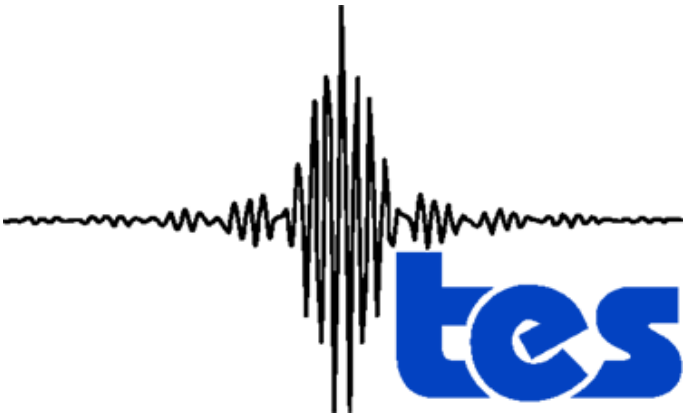

Data Validation Report
(Version F07_10 data)

Editors:

Robert Herman and Gregory Osterman

Contributors:

Matthew Alvarado, Christopher Boxe, Kevin Bowman, Karen Cady-Pereira, Tony Clough, Annmarie Eldering, Brendan Fisher, Dejian Fu, Robert Herman, Daniel Jacob, Line Jourdain, Susan Kulawik, Michael Lampel, Qinbin Li, Jennifer Logan, Ming Luo, Inna Megretskaia, Ray Nassar, Gregory Osterman, Susan Paradise, Vivienne Payne, Hank Revercomb, Nigel Richards, Mark Shephard, Dave Tobin, Solene Turquety, Felicia Vilnrotter, Kevin Wecht, Helen Worden, John Worden, Lin Zhang

June 20, 2014

JPL
Jet Propulsion Laboratory
California Institute of Technology
Pasadena, California

Earth Observing System (EOS)
Tropospheric Emission Spectrometer (TES)

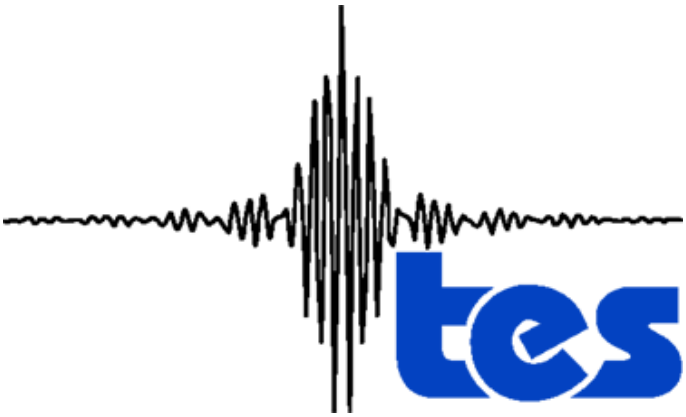

Data Validation Report
(Version F07_10 data)

Approved by:

_____
John Worden
TES Principal Investigator
Jet Propulsion Laboratory

_____
Douglas Shepard
TES Ground Data Systems Manager
Jet Propulsion Laboratory

For the Reader:

In order to successfully interpret TES data one must account for the variable vertical sensitivity of the TES product and the a priori constraints used to help convert measured radiances to vertical profiles of tropospheric composition.

Biases in the data can also vary with altitude. Comparisons between TES data and earth atmosphere models can also be challenging because of possible logarithmic differences between the data product, a priori, and model fields.

We therefore recommend that the scientist interested in TES data read Chapter 9 of the Level 2 TES Data User's Guide Version 6.0 (Herman and Kulawik (eds.) et al., 2013) on how to interpret and use TES data AND any published papers in which the data are used (all published papers using TES data are listed on the TES website). For example, these papers will discuss how biases are addressed or how logarithmic differences between TES data and model fields affect scientific interpretation.

Users should also read the quality statement associated with the version of the data. For most scientific applications a data user should select data using the master data quality flag ("speciesretrievalquality") and a check on the sensitivity with the DegreesOfFreedomForSignal data field. If these checks are removing too much data over the area of interest then the user should contact a member of the TES science team on how to use a subset of flags.

Revision History:

Version	Date	Description/Comments
1.0	8/15/2005	Initial Version of Validation Report for time frame "launch + 1 year"
2.0	1/4/2007	Validation Report for F03_03 data
3.0	11/5/2007	Validation Report for F04_04 data
4.0	11/23/2011	Validation Report for F05_05, F05_06, F05_07 data
5.0	4/8/2012	Validation Report for F06_08, F06_9 data
6.0	6/20/2014	Validation Report for F07_10 data

TABLE OF CONTENTS

LIST OF FIGURES

LIST OF TABLES

1. Overview of TES Product Validation

This document is intended to provide our best determination of the quality of the TES data products based on detailed comparisons between TES L2 data products and other independent data sets.

Validation is defined, for purposes of this report, as comparison between quantities measured by TES and other data products that represent the state of the atmosphere. This definition will evolve as the validation effort matures. Data used in these figures come from processing at the TES Science Computing Facility and are all publicly available.

The TES L2 nadir products have undergone extensive quality control and validation testing. Table 1-1 shows the definitions of data maturity developed by the Terra-MISR (Multi-angle Imaging SpectroRadiometer) team and adopted by the TES team (http://www-misr.jpl.nasa.gov/getData/maturityLevels/).

Using these definitions, the current validation status of the TES L2 data products are given in Table 1-2. Currently, all the TES L2 nadir products are ready for scientific use with the exception of the emissivity reported over land surfaces. TES methane products should be used in a manner similar to that outlined in Payne et al. 2009 (see Section 11). The TES limb products are provisionally validated but should not be used without working with the TES team. Limb data was taken only for the first 9 months of the TES mission and some special observations in 2006. The TES limb data is provisionally validated, but should be used only in collaboration with the TES science team at JPL. This validation report does not include analysis of the limb data validation.

Table 1-1 Definitions of Data Maturity based on those used by the EOS-Terra MISR Team

Term	Definition
Beta	Early release products for users to gain familiarity with data formats and parameters.
Provisional	Limited comparisons with independent sources have been made and obvious artifacts fixed.
Validated Stage 1	Biases are estimated from independent measurements at selected locations and times.
Validated Stage 2	Biases are estimated from more widely distributed independent measurements.
Validated Stage 3	Biases are estimated from independent measurements representing global conditions.
Note: TES L2 retrievals include fully characterized internal error estimates and do not obtain error estimates from external sources. Uncertainty in the TES validation work describes biases when compared to other data sources.	

Table 1-2 Current Validation Status of TES L2 Data Products

Species	Validation Status
Nadir Ozone	Validated Stage 3
Nadir Carbon Monoxide	Validated Stage 3
Nadir Temperature	Validated Stage 3
Nadir Water (Lower/Middle Troposphere)	Validated Stage 3
Nadir Water (Upper Troposphere)	Validated Stage 2
Sea Surface Temperature	Validated Stage 3
Nadir Methane	Validated Stage 2
Cloud Properties	Validated Stage 2
Water Isotopologue (HDO/H_2O)	Validated Stage 1
Nadir Carbon Dioxide	Validated Stage 2
Nadir Ammonia	Validated Stage 1
Nadir Formic Acid (HCOOH)	Provisional
Nadir Methanol (CH_3OH)	Provisional
Note: TES L2 limb products (Nitric Acid, Ozone, Temperature and Water) are provisionally validated but are not included in this report.	

In order to compare TES profile data with other measurements, vertical smoothing and sensitivity must be accounted for by applying the appropriate averaging kernels (such as those supplied with the TES data products). The error estimates included in the L2 data products are meaningful based on the current validation analysis.

1.1 Applicable Documents

Note: All TES documentation are available online at the TES website, http://tes.jpl.nasa.gov/documents/ and at the NASA (National Aeronautics and Space Administration) Langley Atmospheric Science Data Center (ASDC) https://eosweb.larc.nasa.gov/project/tes/tes_table (Documentation tab). All TES related publications are available at the TES web site http://tes.jpl.nasa.gov/documents/publications/

[1] Lewicki, S., D. Shepard, M. Madatyan and R. Morris (2013), TES Science Data Processing Standard and Special Observation Data Products Specifications, Version 13.0, JPL Internal Report D-22993, June 19, 2013, for public released data, software release 13.0.

[2] Robert Herman and Gregory Osterman (editors), Christopher Boxe, Kevin Bowman, Karen Cady-Pereira, Tony Clough, Annmarie Eldering, Brendan Fisher, Dejian Fu, Robert Herman, Daniel Jacob, Line Jourdain, Susan Kulawik, Michael Lampel, Qinbin Li, Jennifer Logan, Ming Luo, Inna Megretskaia, Ray Nassar, Gregory Osterman, Susan Paradise, Vivienne Payne, Hank Revercomb, Nigel Richards, Mark Shephard, Dave Tobin, Solene Turquety, Felicia Vilnrotter, Kevin Wecht, Helen Worden, John Worden, Lin Zhang (2012), Earth Observing System (EOS) Tropospheric Emission Spectrometer (TES) Data Validation Report (Version F06_08, F06_09 data), Version 5.0, JPL Internal Report D-33192, April 8, 2012.

[3] Robert Herman and Susan Kulawik (editors), Kevin Bowman, Karen Cady-Pereira, Annmarie Eldering, Brendan Fisher, Dejian Fu, Robert Herman, Daniel Jacob, Line Jourdain, Susan Kulawik, Ming Luo, Ruth Monarrez, Gregory Osterman, Susan Paradise, Vivienne Payne, Sassaneh Poosti, Nigel Richards, David Rider, Douglas Shepard, Mark Shephard, Felicia Vilnrotter, Helen Worden, John Worden, Hyejung Yun, Lin Zhang (2013), Earth Observing System (EOS) Tropospheric Emission Spectrometer (TES) Level 2 (L2) Data User's Guide (Up to & including Version 6 data), Version 6.0, JPL Internal Report D-38042, November 5, 2013.

2. An Overview of the TES Instrument and Data Products

This section provides information about the TES instrument and the L2 data products. More detailed information on the TES data products is available in the TES L2 Data User's Guide (Herman and Kulawik (eds.) et al., 2013) and the TES Data Product Specification Document (Lewicki et al., 2009).

2.1 Instrument Description

The Tropospheric Emission Spectrometer (TES) on EOS-Aura was designed to measure the global, vertical distribution of tropospheric ozone and ozone precursors such as carbon monoxide (Beer et al., 2001; Beer, 2006). TES is a nadir and limb viewing infrared Fourier transform spectrometer (FTS) (http://tes.jpl.nasa.gov/instrument/). The TES spectral range is from 650 to 3250 cm^{-1}. The apodized resolution for standard TES spectra is 0.10 cm^{-1}, however, finer resolution (0.025 cm^{-1}) is available for special observations. The footprint of each nadir observation is 5 km by 8 km, averaged over detectors. Limb observations (each detector) have a projection around 2.3 km x 23 km (vertical x horizontal).

TES is on the EOS-Aura platform (http://aura.gsfc.nasa.gov/) in a near-polar, sun-synchronous, 705 km altitude orbit. The ascending node equator crossings are near 1:45 pm local solar time.

2.2 TES Observation Modes

2.2.1 Global Surveys

TES makes routine observations in a mode referred to as the "global survey". A global survey is run every other day on a predefined schedule and collects 16 orbits (~26 hours) of continuous data. Each orbit consists of a series of repetitive units referred to as a sequence. A sequence is further broken down into scans. Global surveys are always started at the minimum latitude of an Aura orbit. Table 2-1 provides a summary of the initial and modified versions of the TES Global Surveys from Launch to the present day.

Table 2-1 Description of TES Global Survey Modifications

Start Date/ First Run ID	Scans	Sequences	Maximum Number of TES L2 Profiles	Along-Track Distance between Successive Nadir Scan Locations	Description
August 22, 2004 / First GS Run ID 2026 (First 4 GS runs were 4 orbits only) (First full GS is Run ID 2147/Sep 20, 2004)	3 Limb/ 2 Nadir	1152 sequences (72 per orbit)	Maximum of 4608 L2 profiles (1152 sequences x (3 Limb Scans+ 1 Nadir Scan))	~544 km	• At-launch Global Survey (Aura launched on July 15, 2004) • Each sequence composed of 2 calibration scans, 2 nadir viewing scans and 3 limb scans. • The two nadir scans were acquired at the same location on the spacecraft ground track. Their radiances were averaged, providing a single TES L2 profile.

Start Date/ First Run ID	Scans	Sequences	Maximum Number of TES L2 Profiles	Along-Track Distance between Successive Nadir Scan Locations	Description
May 21, 2005 / Run ID 2931	3 Nadir	1152 sequences (72 per orbit)	Maximum of 3456 L2 profiles (1152 sequences x 3 nadir scans)	~182 km	• Global survey was modified to conserve instrument life. • Three limb scans were eliminated and replaced by an additional nadir scan. • The 3 Nadir scans were acquired at locations equally spaced along the spacecraft ground track. The radiances of individual scans are not averaged.
January 10, 2006 / Run ID 3239.	3 Nadir	1136 sequences (71 per orbit)	Maximum of 3408 L2 profiles (1136 sequences x 3 nadir scans)	~182 km	• The last sequence in each orbit was replaced with an instrument maintenance operation.
June 6, 2008 / Run ID 7370.	3 Nadir	960 sequences (60 per orbit)	Maximum of 2880 L2 profiles (960 sequences x 3 nadir scans)	~182 km	• Global survey was modified to conserve instrument life. • No measurements poleward of 60°S latitude.
July 30, 2008 / Run ID 8187.	3 Nadir	768 sequences (48 per orbit)	Maximum of 2304 L2 profiles (768 sequences x 3 nadir scans)	~182 km	• Global survey was further modified to conserve instrument life. • No measurements poleward of 50°S, 70°N latitude.
April 7, 2010 / Run ID 11125	4 Nadir	512 sequences (32 per orbit)	Maximum of 2048 L2 profiles (512 sequences x 4 nadir scans)	Spacing regular, but no longer uniform (56, 195, 187, 122 km)	• Global survey was further modified to conserve instrument life. • No measurements poleward of 30°S, 50°N latitude. • Blackbody calibrations reduced: no calibrations within the GS, only one pre-GS and one post-GS.

2.2.2 Special Observations

Observations are sometimes scheduled on non-global survey days. In general these are measurements made for validation purposes or with highly focused science objectives. These non-global survey measurements are referred to as "special observations". Eight special observation scenarios have been used to date and are summarized in Table 2-2.

Table 2-2 Description of TES Special Observation Modes

Name	Dates	Pointing	Sequences	Scans per Sequence	Distance Between Scans	Comments
Step and Stare	March 1, 2013-present	Nadir	1	38	146 km	Continuous along-track nadir views, 50 degrees of latitude.
Step and Stare	April 20, 2012-present	Nadir	1	44	76 km	Continuous along-track nadir views, ~29 degrees of latitude.
Step and Stare	Sep 2004 through Aug 6, 2005	Nadir	6	25	40 km	Continuous along-track nadir views, ~45 degrees of latitude.
Step and Stare	July 1, 2007 through Dec 29, 2011	Nadir	1	165	45 km	Along track nadir observations spanning 65 degrees of latitude
Step and Stare	Jan 17, 2006 – Oct 8, 2006 and Spring 2008	Nadir	1	125	45 km	Continuous along-track nadir views, ~50 degrees of latitude.
Note: In 2008 both the 125 and 165 scan Step and Stare macros were used						
Transect	April 20, 2012 through present	Near Nadir	1	20	12 km	Hi density along-track or off nadir views.
Transect	Jan 16, 2006 through Dec 29, 2011	Near Nadir	1	40	12 km	Hi density along-track or off nadir views.
Transect	Aug 20, 2005 – Sept 2, 2005	Near Nadir	1	68	25 km	Hi density along-track or off nadir views.
Stare	April 20, 2012 through present	Near Nadir	1	14	0 km	All measurements at a single location.
Stare	Launch through Dec. 29, 2011	Near Nadir	1	32	0 km	All measurements at a single location.

Name	Dates	Pointing	Sequences	Scans per Sequence	Distance Between Scans	Comments
Limb Only	Jan 31, 2006 – May 20, 2006	Limb	1	62	45 km	Continuous along-track limb views, 25 degrees of latitude.
Limb HIRDLS	Feb 13, 2006 Only	Limb	142	3	182 km	2 orbits of continuous limb measurements for HIRDLS (High Resolution Dynamics Limb Sounder) comparison

2.3 TES Scan Identification Nomenclature

Each TES scan is uniquely identified by a set of three numbers called the run ID, the sequence ID and the scan ID. Each major unit of observation is assigned a unique run ID. Run IDs increase sequentially with time. The first on-orbit run ID is 2000. The sequence ID is assigned to repetitive units of measurements within a run. They start at 1 and are automatically incremented serially by the TES flight software. The scan ID is also incremented by the flight software each time a scan is performed. Each time the sequence is set to 1, the scan ID is reset to 0.

Each time TES makes a set of measurements, that data set is assigned an identification number (referred to as a "run ID"). A calendar of the TES run IDs for global surveys and a list of all TES run IDs (including observation data, time and date) can be found at http://tes.jpl.nasa.gov/data/datacalendar/)

2.4 Derived products and data visualization

The standard TES products are in HDF format, grouped based on runID at https://eosweb.larc.nasa.gov/project/tes/tes_table. The TES "Lite" products are in netcdf format, and grouped into a monthly based file (follow the link from http://tesweb.jpl.nasa.gov/data/ to "Lite Products"). The lite products are reported on the TES retrieval pressure grid which makes the products more compact, and combine datasets (e.g. H_2O and HDO fields) and apply know bias corrections to make the data easier to use. More information can be obtained from the Lite Products user's guide found at the same site. A daily-based product for ozone can be found http://tesweb.jpl.nasa.gov/data/ "Daily ozone". This is the same as the TES V004 O3 product grouped into daily-based files in netcdf format. A similar daily-based product for ozone for only global survey data including the instantaneous radiative forcing kernel can be found http://tesweb.jpl.nasa.gov/data/ "Daily ozone & IRK".

2.5 Where to Obtain TES Data

There are two locations for obtaining TES data. Links to both locations are available from the TES site at the Langley Atmospheric Science Data Center (ASDC) http://eosweb.larc.nasa.gov/. The supporting documentation necessary to use TES data is also available at the Langley ASDC site.

- The primary location for obtaining TES data is the Earth Observing System (EOS) Data Gateway http://reverb.echo.nasa.gov/reverb/ . This site makes available earlier versions of the TES data.
- A secondary location for obtaining TES data is the Langley ASDC data pool. The data pool has space limitations that make it somewhat dynamic, therefore older versions of TES data may not be available there.

The TES data files are listed in different ways for the different sites. The naming convention will be described in Section 2.6.

All TES data products are in HDF-EOS 5 format and are completely documented in the TES Data Product Specification documents referenced at http://tes.jpl.nasa.gov/documents/. The site also contains links to the TES documentation mentioned in this manuscript.

Routines for reading the TES Level 2 data products, written in Interactive Data Language (IDL), are available at ASDC TES site. We expect to have IDL routines for determining "C-Curve" ozone retrievals (see section 6.2.1.2 of the TES L2 Data User's Guide (Herman and Kulawik (eds.) et al., 2013)) available at the ASDC as well.

2.6 File Formats and Data Versions

Information about the TES data file content and format versioning can be found in the L2 product filenames. Table 2-3 provides information for differentiating between the TES versions. When ordering the data on the EOS Data Gateway, the TES level 2 products can be initially differentiated by the TES Product (ESDT or Earth Science Data Type) version label shown in the first column of Table 2-3. Once the data is downloaded, more information can be gathered from the TES version string in the filename.

The TES L2 Data Products are provided in files separated out by the atmospheric species being measured. The parts of the product filename are:

<inst.>-<platform>_<process level>-<species>-<TES view mode>_r<run id>_<version id>.he5

The TES Version String (version id), contains the Format and content version:

F<format version>_<science content version>

A change to the format version string corresponds to minor updates to the fields available within the file or minor bug fixes. Changes to the science content string reflect major changes in the science content of certain fields in the data products.

An example file name is:

TES-Aura_L2-O3-Nadir_r000002945_F04_04.he5

This particular file contains TES nadir measurements of ozone for run ID 2945 (000002945).

In addition to the atmospheric products, there are data files with additional (ancillary) data that are important for working with TES data. These ancillary files can be used with any species data file and contain the string "Anc" in the filename.

Table 2-3 provides a way to map the TES version string information to the TES data product version. For example, version F03_03 is the first version to contain limb data and version

F03_02 data was a significant upgrade to the science content in the data products and therefore is referred to as version 2 (V002) TES data. When ordering TES Level 2 data products through the EOS Data Gateway, the products will be grouped by the TES version number (ESDT) in a form that looks like:

TES/AURA L2 O3 NADIR V003.

If the TES data is ordered through the Langley ASDC Data Pool using the FTP (File Transfer Protocol) interface, the version 3 nadir ozone data will be listed in the form:

TL2O3N.003.

If the TES data is ordered through the Langley Data Pool using the Web interface, the version 3 nadir ozone data will be listed as:

TL2O3N.3.

While the data may be listed differently for the different sites for downloading the products, the filenames will be identical.

There are eight different versions of TES L2 data products. The current version is V006 (F07_10). Data from versions prior to V003 (F04_04) are no longer publicly available, but the evolution of the product versions and file formats is provided in this document back to V001 (F01_01 and F02_01).

Table 2-3 Description of the TES L2 Data Product Version Labels

TES Product (ESDT) Version	TES Version String	Format Version	Science Content Version	Description
V001	F01_01	1	1	The first publicly released L2 data
V001	F02_01	2	1	Bug fixes and additional fields
V002	F03_02	3	2	Some additional fields but major upgrade to scientific quality of data.
V002	F03_03	3	3	Limb data and some bug fixes
V003	F04_04	4	4	Improvements to nadir ozone, temperature, methane and to limb products. Fully processed from Sep 2004 through present.

TES Product (ESDT) Version	TES Version String	Format Version	Science Content Version	Description
V004	F05_05 or F05_06 F05_07 (Final V004)	5	5,6 or 7	Improvements to temperature and methane retrievals. F05_07 is the final V004 release using retrieval software R11.3 and when available should be used over F05_05 or F05_06. F05_07 differentiates between GMAO* versions used in retrieval by date and TES run ID (see below) F05_05 refers to data processed using GMAO GEOS-5.1.0 products using TES retrieval software release R11.2 F05_06 refers to data processed using GMAO GEOS-5.2.0 products using TES retrieval software release R11.2
V005	F06_08 or F06_09	6	8 or 9	F06_08 added Carbon Dioxide (CO_2) and Ammonia (NH_3) to the list of Standard Products. F06_09 added Nitrous Oxide (N_2O) to the list of Standard Products.
V006	F07_10	7	10	F07_10 added Formic Acid (HCOOH) and Methanol (CH_3OH) to the list of Standard Products.

** The TES processing software uses meteorological fields from the NASA Global Modeling and Assimilation Office (GMAO) GEOS (Goddard Earth Observing System) model as inputs to the Level 2 data retrievals.*

2.7 TES Standard L2 Products

Currently the TES data products available for any given run ID are listed in Table 2-4. The products are separated by species with an ancillary file providing additional data fields applicable to all species. A description of the contents of the product files, information on the Earth Science Data Type names and file organization can be found in the TES Data Processing Specification (DPS) document (Lewicki, et al., 2009).

Table 2-4 Description of the TES L2 Data Product Files Currently Available

TES L2 Standard Data Product	TES View Mode	Description
Ozone	Nadir and Limb	TES ozone profiles and some geolocation information
Temperature	Nadir and Limb	TES atmospheric temperature profiles and some geolocation information.
Water Vapor	Nadir and Limb	TES nadir water vapor profiles and some geolocation information
Carbon Monoxide	Nadir	TES nadir carbon monoxide profiles and some geolocation information
Carbon Dioxide	Nadir	TES nadir carbon dioxide profiles and some geolocation information
Ammonia	Nadir	TES nadir ammonia profiles and some geolocation information
HDO	Nadir and Limb	TES HDO (Hydrogen Deuterium Monoxide) profiles and some geolocation information
Methane	Nadir	TES nadir methane profiles and some geolocation information
Nitric Acid	Limb	TES limb nitric acid profiles and some geolocation information
Formic Acid	Nadir	TES nadir formic acid profiles and some geolocation information
Methanol	Nadir	TES nadir methanol profiles and some geolocation information
Ancillary	Nadir and Limb	Additional data fields necessary for using retrieved profiles.
Summary	Nadir and Limb	Provides information on retrieved volume mixing ratios/temperatures without averaging kernel, error matrices.
Supplemental	Nadir and Limb	Provides information on non-retrieved species that are used in the Level 2 retrievals (climatologies, covariance matrices, etc.)

TES retrieves surface temperature and it is reported in each nadir species file, however the value in the atmospheric temperature file is the one that should be used for scientific analysis.

2.8 References

2.8.1 TES References

[1] Beer, R., T. A. Glavich, and D. M. Rider (2001), Tropospheric emission spectrometer for the Earth Observing System's Aura satellite, *Applied. Optics, 40 (15),* 2356-2367, May 20, 2001.

[2] Beer, R. (2006), TES on the Aura Mission: Scientific Objectives, Measurements and Analysis Overview, *IEEE Transactions on Geoscience and Remote Sensing, 44 (No.5), Special Issue on Aura,* 1102-1105, May 2006.

[3] Lewicki, S., D. Shepard, M. Madatyan and S. Gluck (2009), TES Science Data Processing Standard and Special Observation Data Products Specifications, Version 11.9, JPL Internal Report D-22993, May 26, 2009, for public released data, software release 11.3.

[4] Robert Herman and Susan Kulawik (editors), Kevin Bowman, Karen Cady-Pereira, Annmarie Eldering, Brendan Fisher, Dejian Fu, Robert Herman, Daniel Jacob, Line Jourdain, Susan Kulawik, Ming Luo, Ruth Monarrez, Gregory Osterman, Susan Paradise, Vivienne Payne, Sassaneh Poosti, Nigel Richards, David Rider, Douglas Shepard, Mark Shephard, Felicia Vilnrotter, Helen Worden, John Worden, Hyejung Yun, Lin Zhang (2013), Earth Observing System (EOS) Tropospheric Emission Spectrometer (TES) Level 2 (L2) Data User's Guide (Up to & including Version 6 data), Version 6.0, JPL Internal Report D-38042, November 5, 2013.

3. Executive Summary

Below is a summary of each data validation section.

- **Section 4 – L1B Radiance:**

Though this report is focused primarily on the TES Level 2 data products, it is important to understand that the L1B radiance products have also undergone a rigorous validation as reported in Shephard et al. (2008) and in the TES Validation Report V003 (Osterman et al., 2007). The fundamental measurement of the Tropospheric Emission Spectrometer (TES) on board the Aura spacecraft is upwelling infrared spectral radiances. Accurate radiances are critical for trace gas profile retrievals for air quality as well as sensitivity to climate processes. For example, any radiometric systematic errors (*e.g.* calibration) not addressed in the L1B radiances will propagate as errors into the retrieved atmospheric parameters (Bowman et al., 2006; Worden et al., 2004). Connor et al. (2011) showed that the TES relative radiometric calibration was extremely stable over the time period used in their analysis: 2005 to 2009.

A new product in TES Version 6 related to radiance is the ozone band radiative flux, specifically FM ozone band flux and L1B ozone band flux. These both have units of W/m^2 and represent the TOA flux for the ozone band from 985-1080 cm^{-1}, as measured by TES (L1B) and as estimated by the radiative transfer forward model (FM) at the convergence of the L2 retrieval. The flux values were computed using the anisotropy estimate described in H. Worden et al., (2011). Both L1B and FM flux variables have reasonable values as a function of latitude, and comparing all-sky and clear-sky. Differences between L1B and FM fluxes are consistent with radiance residuals close to measurement noise. A comparison was carried out between TES ozone band fluxes and 10° latitude bins of Infrared Atmospheric Sounding Interferometer (IASI) flux values for 15 Aug 2008. IASI radiances are nominally cloud free (< 25% cloud filled pixels) and here we used scans that are closest to nadir (|sat ZA| <10°), including day/night, land/ocean. For the IASI comparison, we assumed a single value for anisotropy = 1.1 (the number in H. Worden et al., 2011 for the ozone band in cloud-free ocean scenes). For histograms of IASI ozone band flux values by latitude band, the distributions have peaks close to the TES values for clear sky at the corresponding latitude, as expected.

In April 2010, TES implemented a new strategy for observing and processing calibration measurements (see Section 4 of the Version 5 Data Validation Report, Herman et al., 2012). In order to validate TES spectra processed with the new calibration strategy, and to check comparisons of TES with Atmospheric Infrared Sounder (AIRS) over the entire TES data record from 2004 to present, we developed a more automated comparison tool based on the methods used for TES/AIRS comparisons in Shephard et al. (2008). Given the differences in ground footprints for TES and AIRS, comparisons are only meaningful for clear-sky, ocean scenes. Results for April 2009 (old calibration approach) compared to April 2010 (new calibration approach) are not significantly different, which suggests the new approach provides the same radiance accuracy as before.

- **Section 5 – Nadir Ozone:**

The TES Version 6 ozone has the following retrieval algorithm updates: (1) updated a priori ozone information into retrievals; (2) updated spectroscopic parameters and a priori information of H_2O, the primary interfering species in TES ozone measurements jointly retrieved with ozone; (3) updated a priori information of atmospheric temperature profiles. TES Version 6 nadir ozone profiles have been compared with ozonesonde measurements archived in the World Ozone and Ultraviolet Radiation Data Center (WOUDC: http://www.woudc.org). The percent differences between TES and ozonesonde were investigated in six latitude zones. The seasonal variability of ozone was investigated by using 1992 matches between coincident TES and ozonesonde observations in the 35°N to 56°N latitude zone. The criteria of ±9 h, a 300 km radius and a cloud optical depth less than 2.0 were applied to search for the TES-ozonesonde coincidence measurements. The flagged TES data were filtered out. 5149 matches were found from those TES measurements that have been processed for V006. Their latitude range is from 73.26°S to 81.82°N and time spans from 2004 to 2012.

In general, TES V006 ozone profiles are positively biased (by 0-15%) from the surface to 5 hPa relative to ozonesondes. In the altitude range from surface to 100 hPa, both V006 and V005 TES data have a mean bias of approximately +10% and rms ranging from 10 to 25%. In the altitude range from 100 to 20 hPa, V006 has a slightly larger (up to 5%) mean bias, compared to V005, with smaller (~3% better) rms of the differences. In the altitude range above 20 hPa, both the mean and rms of V006-ozonesonde showed improvements, when compared to that of V005-ozonesondes. The percent differences for all seasons for mid-to-lower tropospheric ozone also show an improvement when compared to Nassar et al. (2008) and Boxe et al. (2010).

- **Section 6 – Carbon Monoxide:**

Comparisons have been carried out between TES carbon monoxide retrievals and those from a variety of satellite and aircraft instruments. Global patterns of carbon monoxide as measured by TES are in good qualitative agreement with those seen by MOPITT (Measurement Of Pollution In The Troposphere) on the NASA Terra satellite. Comparisons of profiles of CO between TES V006 and MOPITT IR V006 show better agreement when a priori information is accounted for correctly. Their differences are within the observation errors of the two instruments and the variability of CO field in the defined pair matching region and time. TES carbon monoxide also agrees to within the estimated uncertainty of the aircraft instruments, including both errors and the variability of CO itself.

TES CO Version 6 data are very similar to Version 5 data. This is expected since neither retrieval algorithms nor operational support data related to CO retrievals are updated in Version 6. The mean difference in CO volume mixing ratio comparing two version data globally is less than 1%, with standard deviation of a few percent. This very small change is due to changes in temperature and other interfering species.

- **Section 7 – Nadir Temperature:**

TES V006 nadir temperature (TATM) retrievals have been compared with nearly coincident radiosonde (hereafter radiosonde) measurements from the National Oceanic & Atmospheric Administration (NOAA) Earth System Research Laboratory (ESRL) global radiosonde database. For TES V006 TATM minus $T_{radiosonde}$ (with averaging kernel applied), the bias is approximately +0.4 K in the lower troposphere, decreasing to negative 0.6 K in the upper troposphere. The rms

is less than 1 K in the stratosphere and upper troposphere, but increases to 1.7 K in the lower troposphere. In clear sky conditions (average cloud effective optical depth less than 0.1), the bias improves in the lower troposphere but increases to +0.6 K at 500 hPa pressure level.

To evaluate the retrieval stability the monthly mean and standard deviation of the TATM residual between TES V005 and the Global Modeling and Data Assimilation Office (GMAO) GEOS-5.2 model, which provides the first guess and a priori for the TATM retrieval, were calculated. The statistics for both Tropical Pacific and Northern Atlantic Ocean regions indicate only minor month-to-month variability and no substantial trends over the entire five-and-a-half year period. The standard deviation of the residual was generally smaller than the standard deviation of the GMAO GEOS-5.2 but larger than the TES estimated measurement error. Overall, based on this analysis it appears that the TES retrieval quality has remained stable over the years inspected, 2006 through 2011.

- **Section 8 – Sea Surface Temperature:**

TES retrievals of sea surface temperature rely on validation of previous data versions, as described in detail in the TES Validation Report V003 (Osterman et al., 2007).

- **Section 9 – Water Vapor:**

TES V006 H_2O is typically biased high relative to V005 H_2O. The changes are largely due to much higher H_2O mixing ratios in the a priori constraint, GMAO GEOS 5.9.1 (in Version 6) versus GEOS 5.2 (in Version 5). The largest effect is seen at low degrees of freedom for signal (DOFS). The user should select data using the master data quality flag ("speciesretrievalquality") and filter by DOFS. Some minor changes are due to new spectroscopic parameters in the absorption coefficient (ABSCO) tables for H_2O, a difference of at most a few percent. Comparisons have been made between TES V006 water vapor profiles and radiosonde profiles. Relative to nighttime radiosonde profiles, TES V006 water vapor is approximately 18% low at 800 hPa in the lower troposphere, 6% low at 700 to 500 hPa in the middle troposphere, and 20% low at 250 hPa in the upper troposphere. The rms increases from 30% in the lower troposphere to 50% in the upper troposphere. Results are similar for both land and water surfaces.

- **Section 10 – HDO/H_2O:**

V006 and V005 estimates of HDO/H_2O show considerable sensitivity to the isotopic composition of water vapor with typically DOFS~2 in the tropics and DOFS~1 at high latitudes. This increased sensitivity allows the TES estimates to resolve lower tropospheric and mid-tropospheric variability of the HDO/H_2O vapor ratio (see Worden et al., 2012, and Herman et al., 2014) with the expense of increased uncertainty over tropical oceans.

We find that the HDO/H_2O estimates are consistent with the previous TES release within the altitude range where the sensitivity overlaps. For validation of V005 HDO/H2O, we refer the reader to R. Herman et al. (2014). For validation of V004 HDO/H_2O, we refer the reader to J. Worden et al. (2011).

- **Section 11 – Methane:**

In order to assess the data quality of the Version 6 CH_4 product, these retrievals have been compared to in-situ aircraft profile measurements from the HIAPER Pole-to-Pole Observations (HIPPO) I and II aircraft campaigns. The latitudinal range and number of TES/HIPPO coincidences provide sufficient information to characterize the latitudinal dependence of the bias and to validate the TES error estimates. The vertical information in the TES CH_4 product is limited, with less than 2 DOFS in the troposphere. Therefore, we choose to express comparisons in terms of a "representative tropospheric volume mixing ratio" (RTVMR) approach (Payne et al., 2009) in addition to showing profiles.

Based on the prototype results for Version 6 and lower tropospheric results for Version 5, we also apply an additional global bias correction to the TES profiles equal to 0.015 times the averaging kernel to minimize the bias. The averaging kernel-based bias correction approach is based on a similar correction for HDO in Worden et al. (2012). This approximate bias correction will be further investigated in an upcoming validation paper on the Version 6 retrievals (Alvarado et al., 2014, *manuscript in preparation*). After this correction is applied, the Version 5 RTVMR is still biased high with respect to HIPPO measurements by 14.0 ppbv with an error standard deviation of 21.3 ppbv, while Version 6 only has a small negative bias of -0.3 ppbv and an error standard deviation of 19.5 ppbv after this correction. Version 6 retrievals have mean biases of approximately -10 ppbv in the upper troposphere and 5 ppbv in the lower troposphere. Overall the error bias and standard deviation are reduced in magnitude in Version 6 compared to Version 5 and this reduction occurs across latitude bands and throughout the depth of the troposphere.

- **Section 12 – Cloud Products:**

TES retrievals of cloud products rely on validation of previous data versions, as described in detail in the TES Validation Report V004 (Herman et al., 2012).

- **Section 13 – Carbon Dioxide:**

TES CO_2 is retrieved between 40S and 45N, with average cloud optical depth < 0.5, among other tests, for good quality. On average, TES CO_2 has an average of 0.65 degree of freedom for signal (DOFS) – with the most DOFS for daytime land cases (which can be on the order of 1 DOFS) and the least for nighttime or winter land cases (which can be on the order of 0.3 DOFS). Ocean targets (day or night) have intermediate DOFS with about 0.8 DOFS. The averaging kernel indicates sensitivity between the surface to above 100 mb, with the most sensitivity between about 700 and 300 mb, peaking at about 650 mb. Although a profile is retrieved and has been validated, there is very little independent information at the different profile levels and it is critical to utilize the provided averaging kernel when using TES data. The previous version, TES V005 CO_2 has been compared with aircraft vertical profiles over the Pacific from the HIAPER (High-Performance Instrumented Airborne Platform for Environmental Research) Pole-to-Pole Observation (HIPPO) program (Wofsy et al., 2011) and over land at the SGP ARM site (Riley et al., 2009). Further details of this validation can be found in Kulawik et al. (2012). The HIPPO analysis has been done with the processed PGE (Product Generation Executive) V006 data, but the SGP analysis requires a full time series of TES at the SGP site and will need to

await a more complete V006 dataset. Analysis of the PGE comparisons to HIPPO using the corrected values in the TES Lite product and a monthly regional mean, +- 5 degrees in latitude, +- 10 degrees in longitude and +- 15 days in time, show about a 1.0 ppm error and an overall 0.0 +- 0.6 ppm bias. There are some outliers in these monthly mean values. The single target error for TES CO_2 in the mid-Troposphere is on the order of 8 ppm, however averaging over 20 degrees longitude, 10 degrees latitude, and 1 month results in errors on the order of 1.0 ppm over both ocean and land targets. The Lite product has corrections applied to the observation error (increased by 1.5^2) and to the Averaging Kernel. The details of the correction to the Averaging Kernel are found in Kulawik et al. (2012), which involves a pressure-dependent scale factor. Although the TES CO_2 product is modest both in sensitivity and coverage, Nassar et al. (2011) found that TES added information to the surface flask measurements and was useful for estimating fluxes, both separately, and jointly with flask measurements.

- **Section 14 – Ammonia:**

The data quality of the TES V006 ammonia (NH_3) product has been assessed through comparisons between TES NH_3 and aircraft and surface measurements collected during two campaigns in the Central Valley in California: CalNex(Nowak et al., 2012) in the spring of 2010 and DISCOVER-AQ (Deriving Information on Surface conditions from Column and Vertically Resolved Observations Relevant to Air Quality) in January/February 2013. The Central Valley offers ideal conditions for monitoring ammonia from a satellite, since it is present in high concentrations and there is strong thermal contrast at the time of the TES overpass. During CalNex there was one aircraft track under the TES transect. The aircraft and TES measurements showed similar spatial variability. The differences are largely due to the difference in the measured parameters: while the aircraft value is a point measurement taken between 300 and 400 meters altitude, the TES measurements in this cases showed greatest sensitivity to the ammonia concentrations between 925 and 800 mbar. Additionally, total column amounts were compared between a laser spectrometer and TES. The columns show excellent agreement with differences similar to the estimated TES error.

- **Section 15 – Formic Acid (HCOOH):**

TES formic acid (HCOOH) has been validated using the prototype algorithm, which is equivalent to the algorithm implemented operationally in TES V006. To date an insufficient number of V006 observations co-located with in-situ measurements of HCOOH above the TES detection level of 0.5 ppbv have been processed operationally. However, comparisons between the prototype results and the V006 retrievals show excellent correlation and effectively no bias. The prototype algorithm was applied to TES observations taken concurrently with the Intercontinental Transport Experiment-Phase B (INTEX-B) and Megacity Initiative: Local and Global Research Observations, (MILAGRO) campaigns, during which there were numerous measurements of formic acid from the California Institute of Technology Chemical Ionization Mass Spectrometer (CIT CIMS) mounted on aircraft. Due to sampling and colocation issues it was not possible to perform meaningful comparisons of TES profiles and those obtained from the

aircraft measurements. Instead we elected to use GEOS-Chem as a transfer function, and separately compared aircraft and TES data against the model. Only aircraft data between 900-700 mbar were used, since this is the layer where TES is most sensitive to formic acid. TES observations were averaged over each GEOS-Chem grid box that contained TES data. Both TES and the in-situ measurements show that GEOS-Chem underestimates the measured HCOOH amounts, but is somewhat better correlated with measurements during MILAGRO than during INTEX-B.

- **Section 16 – Methanol (CH_3OH):**

TES methanol (CH_3OH) has been validated using the prototype algorithm, which is equivalent to the algorithm implemented operationally in TES V006. To date an insufficient number of V006 observations co-located with in-situ measurements of CH_3OH have been processed operationally. Comparisons between the prototype results and the V006 retrievals show that (1) V006 is biased low, (2) V006 is well correlated with the prototype results over regions with significant concentrations, less correlated when the methanol signal is weak, and (3) the retrieval is more sensitive to spectral noise and to the residuals remaining from previously retrieved species, namely ozone. A comparison of a few TES V006 methanol retrievals coincident with the January/February 2013 DISCOVER-AQ campaign in California suggest that V006 is biased somewhat low, but the number of data points is insufficient to generalize this statement. These data are being reprocessed with a different a priori, after which we will re-evaluate the bias.

3.1 References

3.1.1 TES References

[1] Alvarado, M. J., V. H. Payne, K. E. Cady-Pereira, J. D. Hegarty, S. S. Kulawik, K. J. Wecht, J. R. Worden, S. C. Wofsy (2014), Impacts of updated spectroscopy and a priori profiles on retrievals of CH_4 from NASA Aura Tropospheric Emission Spectrometer (TES) observations evaluated with HIPPO observations, *manuscript in preparation*.

[2] Bowman K.W., C.D. Rodgers, S.S. Kulawik, J. Worden, E. Sarkissian, G. Osterman, T. Steck, M. Lou, A. Eldering, M. Shephard, H. Worden, M. Lampel, S.A. Clough, P.D. Brown, C.P. Rinsland, M. Gunson, and R. Beer (2006), Tropospheric emission spectrometer: Retrieval method and error analysis, *IEEE Trans. Geosci. Remote Sens., 44(5)*, pp. 1297-1307, May 2006.

[3] Boxe, C.S., J.R. Worden, K.W. Bowman, S.S. Kulawik, J.L. Neu, W.C. Ford, G.B. Osterman, R.L. Herman, A. Eldering, D.W. Tarasick, A.M. Thompson, D.C. Doughty, M.R. Hoffmann, S.J. Oltmans (2010), Validation of northern latitude Tropospheric Emission Spectrometer stare ozone profiles with ARC-IONS sondes during ARCTAS: sensitivity, bias and error analysis, *Atmospheric Chemistry and Physics*, doi:10.5194/acp-10-9901-2010, October 20, 2010.

[4] Connor, T.C., M. W. Shephard, V. H. Payne, K. E. Cady-Pereira, S. S. Kulawik, M. Luo, G. Osterman, and M. Lampel (2011), Long-term stability of TES satellite radiance measurements, *Atmospheric Measurement Techniques, 4,* doi:10.5194/amt-4-1481-2011, 1481–1490, July 25, 2011.

[5] Robert Herman and Gregory Osterman (editors), Christopher Boxe, Kevin Bowman, Karen Cady-Pereira, Tony Clough, Annmarie Eldering, Brendan Fisher, Dejian Fu, Robert Herman, Daniel Jacob, Line Jourdain, Susan Kulawik, Michael Lampel, Qinbin Li, Jennifer Logan, Ming Luo, Inna Megretskaia, Ray Nassar, Gregory Osterman, Susan Paradise, Vivienne Payne, Hank Revercomb, Nigel Richards, Mark Shephard, Dave Tobin, Solene Turquety, Felicia Vilnrotter, Kevin Wecht, Helen Worden, John Worden, Lin Zhang (2012), Earth Observing System (EOS) Tropospheric Emission Spectrometer (TES) Data Validation Report (Version F06_08, F06_09 data), Version 5.0, JPL Internal Report D-33192, April 8, 2012.

[6] Robert Herman and Gregory Osterman (editors), Christopher Boxe, Kevin Bowman, Karen Cady-Pereira, Tony Clough, Annmarie Eldering, Brendan Fisher, Dejian Fu, Robert Herman, Daniel Jacob, Line Jourdain, Susan Kulawik, Michael Lampel, Qinbin Li, Jennifer Logan, Ming Luo, Inna Megretskaia, Ray Nassar, Gregory Osterman, Susan Paradise, Vivienne Payne, Hank Revercomb, Nigel Richards, Mark Shephard, Dave Tobin, Solene Turquety, Felicia Vilnrotter, Kevin Wecht, Helen Worden, John Worden, Lin Zhang (2012), Earth Observing System (EOS) Tropospheric Emission Spectrometer (TES) Data Validation Report (Version F06_08, F06_09 data), Version 5.0, JPL Internal Report D-33192, April 8, 2012.

[7] Herman, R. L., J. E. Cherry, J. Young, J. M. Welker, D. Noone, S. S. Kulawik, and J. Worden (2014), Aircraft validation of Aura Tropospheric Emission Spectrometer retrievals of HDO and H_2O, *Atmos. Meas. Tech. Discuss., 7*, 3801-3833, doi: 10.5194/amtd-7-3801-2014, 2014, April 14, 2014.

[8] Kulawik, S.S., J.R. Worden, S.C. Wofsy, S.C. Biraud, R. Nassar, D.B.A. Jones, E.T. Olsen, G.B. Osterman, (2012), Comparison of improved Aura Tropospheric Emission Spectrometer (TES) CO_2 with HIPPO and SGP aircraft profile measurements, *Atmospheric Chemistry and Physics Discussions*, *12,* 6283 – 6329, February 29, 2012.

[9] Nassar, R., J.A. Logan, H.M. Worden, I.A. Megretskaia, K.W. Bowman, G.B. Osterman, A.M. Thompson, D.W. Tarasick, S. Austin, H. Claude, M.K. Dubey, W.K. Hocking, B.J. Johnson, E. Joseph, J. Merrill, G.A. Morris, M. Newchurch, S.J. Oltmans, F. Posny, F.J. Schmidlin, H. Vömel, D.N. Whiteman, and J.C. Witte (2008), Validation of Tropospheric Emission Spectrometer (TES) Nadir Ozone Profiles Using Ozonesonde Measurements, *Journal of Geophysical Research Vol. 113*, D15S17, (doi:10.1029/2007JD008819), May 7, 2008.

[10] Nassar, R., D.B.A. Jones, S.S. Kulawik, J.R. Worden, K.W. Bowman, R.J. Andres, P. Suntharalingam, J.M. Chen, C.A.M. Brenninkmeijer, T.J. Schuck, T.J. Conway, D.E. Worthy (2011), Inverse modeling of CO_2 sources and sinks using satellite observations

of CO_2 from TES and surface flask measurements, *Atmos. Chem. Phys.,* ***11****, (12),* 6029-6047, June 24, 2011.

[11] Nowak, J. B., J.A. Neuman, R. Bahreini, R., A.M. Middlebrook, J.S. Holloway, S.A. McKeen, D.D. Parrish, T.B. Ryerson, and M. Trainer (2012), Ammonia sources in the California South Coast Air Basin and their impact on ammonium nitrate formation, *Geophysical Research Letters, Vol. 39, Issue 7,* L07804, doi: 10.1029/2012GL051197.

[12] Osterman, G., (editor), K. Bowman, K. Cady-Pereira, T. Clough, A. Eldering, B. Fisher, R. Herman, D. Jacob, L. Jourdain, S. Kulawik, M. Lampel, Q. Li, J. Logan, M. Luo, I. Megretskaia, R. Nassar, G. Osterman, S. Paradise, V. Payne, H. Revercomb., N. Richards, M. Shephard, D. Tobin, S. Turquety, F. Vilnrotter, H. Worden, J. Worden, and L. Zhang (2007), Earth Observing System (EOS) Tropospheric Emission Spectrometer (TES) Data Validation Report (Version F04_04 data), Version 3.0, JPL Internal Report D-33192, November 5, 2007.

[13] Payne, V.H., S.A. Clough, M.W. Shephard, R. Nassar and J.A. Logan (2009), Information-centered representation of retrievals with limited degrees of freedom for signal: Application to methane from the Tropospheric Emission Spectrometer, *Journal of Geophysical Research: Atmospheres, Vol. 114 Issue D10*, May 27, 2009, D10307, (doi:10:1029/2008JD010155).

[14] Shephard, M. W., H. M. Worden, K. E. Cady-Pereira, M. Lampel, M. Luo, K. W. Bowman, E. Sarkissian, R. Beer, D. M. Rider, D. C. Tobin, H. E. Revercomb, B. M. Fisher, D. Tremblay, S. A. Clough, G. B. Osterman, and M. Gunson (2008), Tropospheric Emission Spectrometer Nadir Spectral Radiance Comparisons, *Journal of Geophysical Research: Atmospheres, Vol. 113, Issue D15,* D15S05, (doi:10.1029/2007JD008856), April 22, 2008.

[15] Worden, J., S. S. Kulawik, M. W. Shephard, S. A. Clough, H. Worden, K. Bowman, and A. Goldman (2004), Predicted errors of tropospheric emission spectrometer nadir retrievals from spectral window selection, *Journal of Geophysical Research, 109*, *D09308,* May 15, 2004.

[16] Worden, J., D. Noone, J. Galewsky, A. Bailey, K. Bowman, D. Brown, J. Hurley, S. Kulawik, J. Lee, and M. Strong (2011), Estimate of bias in Aura TES HDO/H_2O profiles from comparison of TES and in situ HDO/H_2O measurements at the Mauna Loa observatory, *Atmospheric Chemistry and Physics, 11,* 4491–4503, 2011, doi:10.5194/acp-11-4491-2011, May 12, 2011.

[17] Worden, J., S. Kulawik, C. Frankenberg, V. Payne, K. Bowman, K. Cady-Peirara, K. Wecht, J.-E. Lee, D. Noone (2012), Profiles of CH_4, HDO, H_2O, and N_2O with improved lower tropospheric vertical resolution from Aura TES radiances, *Atmospheric Measurement Techniques, 5, 397–411, 2012*, doi:10.5194/amt-5-397-2012, February 20, 2012.

3.1.2 General References

[18] Riley, W.J., S.C. Biraud, M.S. Torn, M.L. Fischer,D. P. Billesbach, J.A. Berry (2009), Regional CO_2 and latent heat surface fluxes in the Southern Great Plains: Measurements, modeling, and scaling, *Journal of Geophysical Research-Biogeosciences, 114,* G04009, DOI: 10.1029/2009JG001003, 2009.

[19] Wofsy, S.C., the HIPPO Science Team and Cooperating Modellers and Satellite Teams (2011), HIAPER Pole-to-Pole Observations (HIPPO): Fine grained, global scale measurements for determining rates for transport, surface emissions, and removal of climatically important atmospheric gases and aerosols, *Phil. Trans. of the Royal Society A, vol. 369 (no. 1943),* 2073-2086, May 28, 2011.

4. TES Level 1B Radiance Data Products

Though this report is focused primarily on the TES Level 2 data products, it is important to understand that the L1B radiance products have also undergone a rigorous validation as reported in Shephard et al. (2008) and in the TES Validation Report V003 (Osterman et al., 2007). The fundamental measurement of the Tropospheric Emission Spectrometer (TES) on board the Aura spacecraft is upwelling infrared spectral radiances. Accurate radiances are critical for trace gas profile retrievals for air quality as well as sensitivity to climate processes. For example, any radiometric systematic errors (e.g. calibration) not addressed in the L1B radiances will propagate as errors into the retrieved atmospheric parameters (Bowman et al., 2006; Worden et al., 2004). Connor et al. (2011) showed that the TES relative radiometric calibration was extremely stable over the time period used in their analysis: 2005 to 2009.

A new product in TES Version 6 related to radiance is the ozone band radiative flux, specifically FM ozone band flux and L1B ozone band flux. These both have units of W/m^2 and represent the TOA flux for the ozone band from 985-1080 cm^{-1}, as measured by TES (L1B) and as estimated by the radiative transfer forward model (FM) at the convergence of the L2 retrieval. The flux values were computed using the anisotropy estimate described in H. Worden et al., (2011). Both L1B and FM flux variables have reasonable values as a function of latitude, and comparing allsky and clear-sky. Differences between L1B and FM fluxes are consistent with radiance residuals close to measurement noise. A comparison was carried out between TES ozone band fluxes and 10° latitude bins of Infrared Atmospheric Sounding Interferometer (IASI) flux values for 15 Aug 2008. IASI radiances are nominally cloud free (< 25% cloud filled pixels) and here we used scans that are closest to nadir (|sat ZA|<10°), including day/night, land/ocean. For the IASI comparison, we assumed a single value for anisotropy = 1.1 (the number in H. Worden et al., 2011 for the ozone band in cloud-free ocean scenes). For histograms of IASI ozone band flux values by latitude band, the distributions have peaks close to the TES values for clear sky at the corresponding latitude, as expected.

In April 2010, TES implemented a new strategy for observing and processing calibration measurements (see Section 4 of the Version 5 Data Validation Report, Herman and Osterman (eds.) et al., 2012). In order to validate TES spectra processed with the new calibration strategy, and to check comparisons of TES with AIRS over the entire TES data record from 2004 to present, we developed a more automated comparison tool based on the methods used for TES/AIRS comparisons in Shephard et al. (2008). Given the differences in ground footprints for TES and AIRS, comparisons are only meaningful for clear-sky, ocean scenes. Results for April 2009 (old calibration approach) compared to April 2010 (new calibration approach) are not significantly different, which suggests the new approach provides the same radiance accuracy as before.

4.1 References

4.1.1 TES L1B Radiance Validation Reference

[1] Connor, T.C., M. W. Shephard, V. H. Payne, K. E. Cady-Pereira, S. S. Kulawik, M. Luo, G. Osterman, and M. Lampel (2011), Long-term stability of TES satellite radiance measurements, *Atmospheric Measurement Techniques, 4,* doi:10.5194/amt-4-1481-2011, 1481–1490, July 25, 2011.

[2] Osterman, G., (editor), K. Bowman, K. Cady-Pereira, T. Clough, A. Eldering, B. Fisher, R. Herman, D. Jacob, L. Jourdain, S. Kulawik, M. Lampel, Q. Li, J. Logan, M. Luo, I. Megretskaia, R. Nassar, G. Osterman, S. Paradise, V. Payne, H. Revercomb., N. Richards, M. Shephard, D. Tobin, S. Turquety, F. Vilnrotter, H. Worden, J. Worden, and L. Zhang (2007), Earth Observing System (EOS) Tropospheric Emission Spectrometer (TES) Data Validation Report (Version F04_04 data), Version 3.0, JPL Internal Report D-33192, November 5, 2007.

[3] Shephard, M. W., H. M. Worden, K. E. Cady-Pereira, M. Lampel, M. Luo, K. W. Bowman, E. Sarkissian, R. Beer, D. M. Rider, D. C. Tobin, H. E. Revercomb, B. M. Fisher, D. Tremblay, S. A. Clough, G. B. Osterman, and M. Gunson (2008), Tropospheric Emission Spectrometer Nadir Spectral Radiance Comparisons, *J. Geophys. Res., 113*, D15S05, (doi:10.1029/2007JD008856), April 22, 2008.

4.1.2 TES References

[4] Bowman K. W., C. D. Rodgers, S. S. Kulawik, J. Worden, E. Sarkissian, G. Osterman, T. Steck, M. Lou, A. Eldering, M. Shephard, H. Worden, M. Lampel, S. A. Clough, P. D. Brown, C. P. Rinsland, M. Gunson, and R. Beer (2006), Tropospheric emission spectrometer: Retrieval method and error analysis, IEEE Trans. Geosci. Remote Sens., 44(5), 1297-1307, May 2006.

[5] Herman, R. and G. Osterman, (editors), C. Boxe, K. Bowman, K. Cady-Pereira, T. Clough, A. Eldering, B. Fisher, D. Fu, R. Herman, D. Jacob, L. Jourdain, S. Kulawik, M. Lampel, Q. Li, J. Logan, M. Luo, I. Megretskaia, R. Nassar, G. Osterman, S. Paradise, V. Payne, H. Revercomb, N. Richards, M. Shephard, D. Tobin, S. Turquety, F. Vilnrotter, K. Wecht, H. Worden, J. Worden, L. Zhang (2012), Earth Observing System (EOS) Tropospheric Emission Spectrometer (TES) Data Validation Report (VersionF06_08, F06_09 data), Version 5.0, JPL Internal Report D-33192, April 8, 2012.

[6] Worden, J., S. S. Kulawik, M. W. Shephard, S. A. Clough, H. Worden, K. Bowman, and A. Goldman (2004), Predicted errors of tropospheric emission spectrometer nadir retrievals from spectral window selection, *J. Geophys. Res., 109,* D09308, May 15, 2004.

5. Nadir Ozone Validation

5.1 Overview

TES V006 ozone has the following retrieval algorithm updates: (1) updated a priori ozone information into retrievals; (2) updated spectroscopic parameters and a priori information of H_2O, the primary interfering species in TES ozone measurements jointly retrieved with ozone; (3) updated a priori information of atmospheric temperature profiles. The TES V005 validation report showed data quality nearly identical to TES V004 (Herman et al., 2012). The percent and absolute biases of TES V005-ozonesonde (similarly TES V004-ozonesonde) are congruent to previous validation studies of TES V001, V002, and V003. Hence, comparisons between the percent biases and random error of TES V006-ozonesonde and that of TES V005-ozonesonde are sufficient to validate TES V006 nadir ozone profile. TES V006 nadir ozone profiles provide data that were measured in the TES global survey, step-and-stare, transect, and stare observation modes. They were compared with ozonesonde measurements archived in the World Ozone and Ultraviolet Radiation Data Center (WOUDC: http://www.woudc.org). The percent differences between TES and ozonesonde were investigated in six latitude zones. The seasonal variability of ozone was investigated by using 1992 matches between coincident TES and ozonesonde observations in the 35°N to 56°N latitude zone.

The criteria of ±9 h, a 300 km radius and a cloud optical depth less than 2.0 were applied to search for the TES-ozonesonde coincidence measurements. The flagged TES data were filtered out. 5149 matches were found from those TES measurements that have been processed for V006. Their latitude range is from 73.26°S to 81.82°N (Figure 5-1) and time spans from 2004 to 2012.

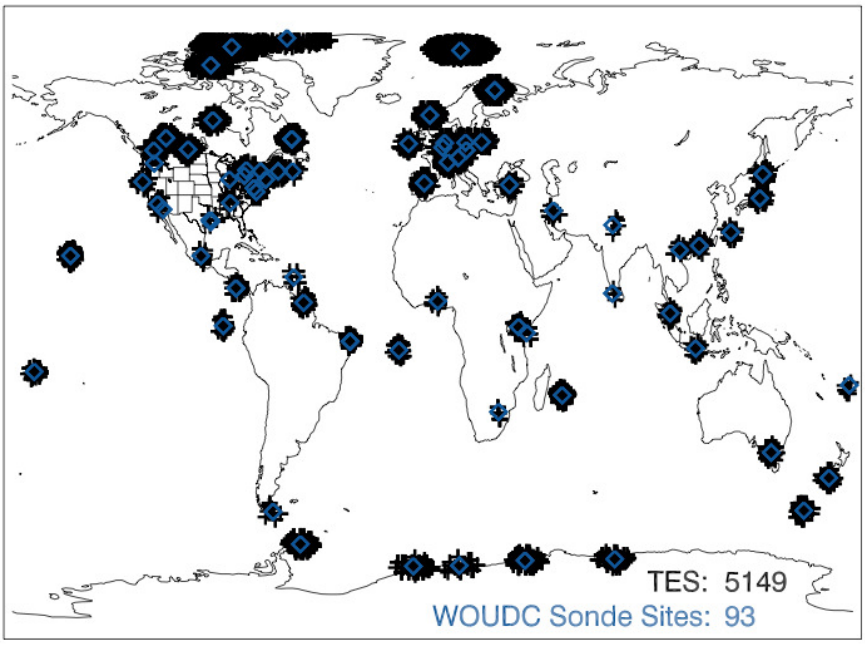

Figure 5-1 The global distribution of coincident TES (black plus) and WOUDC ozonesonde (blue diamond) measurements. Their latitude range is from 73.26°S to 81.82°N and time spans from 2004 to 2012.

The TES averaging kernel and a priori constraint were applied to the ozonesonde data in order to: (1) compare the TES ozone profiles and ozonesonde data in an unbiased quantifiable manner (i.e. not biased by the TES a priori); (2) take TES measurement sensitivity and vertical resolution into account.

In general, TES V006 ozone profiles are positively biased (by 0-15%) from the surface to 5 hPa relative to ozonesondes (Figure 5-2A). Figure 5-2B/C compares the mean and one-sigma differences between TES products (V006, V005) and ozonesonde profiles. In the altitude range from surface to 100 hPa, both V006 and V005 TES data have a mean bias of approximately +10% and rms ranging from 10 to 25%. In the altitude range from 100 to 20 hPa, V006 has a slightly larger (up to 5%) mean bias, compared to V005, with smaller (~3% better) rms of the differences. In the altitude range above 20 hPa, both the mean and rms of V006-ozonesonde differences showed improvements, when compared to that of V005-ozonesonde. The percent differences for all seasons for mid-to-lower tropospheric ozone also show an improvement when compared to Nassar et al. (2008) and Boxe et al. (2010).

5.2 TES Ozonesonde Comparisons

TES nadir ozone profiles were retrieved using the optimal estimation method (OEM). The OEM combines TES measurements and a priori into the retrieved ozone profiles. An unbiased and quantitative TES-ozonesonde comparison method, which has been applied in the validation for all versions of TES products (V001 – V006), takes the impacts of a priori into account. The method applies the TES operator (i.e., averaging kernel and a priori constraint) to ozonesonde profiles. This approach generated ozonesonde profiles for the TES-ozonesonde comparisons by smoothing the high vertical resolution ozonesonde data with the TES averaging kernels and adding a priori information into the ozonesonde data. TES-ozonesonde percent differences were calculated using TES nadir ozone profiles and the ozonesonde profiles whose vertical resolution and impacts of a priori profiles are consistent to those TES nadir ozone profiles.

The number of matches from TES V006 is nearly identical to that of TES V005 since we used the target scenes that have been processed in both TES V006 and TES V005. The differences on the data throughput of TES V006 and V005 are generally less than 1%. Ozone percent difference profiles are shown in Figure 5-2 (Figure 5-2A TES V006 minus ozonesonde; Figure 5-2B TES V005 minus ozonesonde over laid in V006-ozonesonde) for all latitude ranges. Figure 5-3 are the TES V006-ozonesonde and TES V005-ozonesonde for six latitude zones (Arctic, north midlatitudes, northern subtropics, tropics, southern low- and mid-latitudes, and Antarctic). The southern low (subtropics) and mid-latitudes were combined as a single zone to improve the number of coincident TES-ozonesonde measurements. In Figure 5-2, Figure 5-3 and Figure 5-4, all individual TES V006 – ozonesonde profiles are plotted in black; mean and standard deviation ranges are overlaid in blue solid lines and blue dash lines, respectively. *NP* is the number of TES-ozonesonde profiles plotted after removing cloudy scenes and flagged TES data.

The algorithm updates were applied for TES V006 ozone retrievals. They led to improved bias and one-sigma standard deviation of TES V006-ozonesonde differences, compared to those for TES V005. The improvements shown in right panels of Figure 5-2 - Figure 5-4 are considerable, specifically the bias of the mean and the standard deviation or root-mean-square error in the altitude range 20 to 5 hPa.

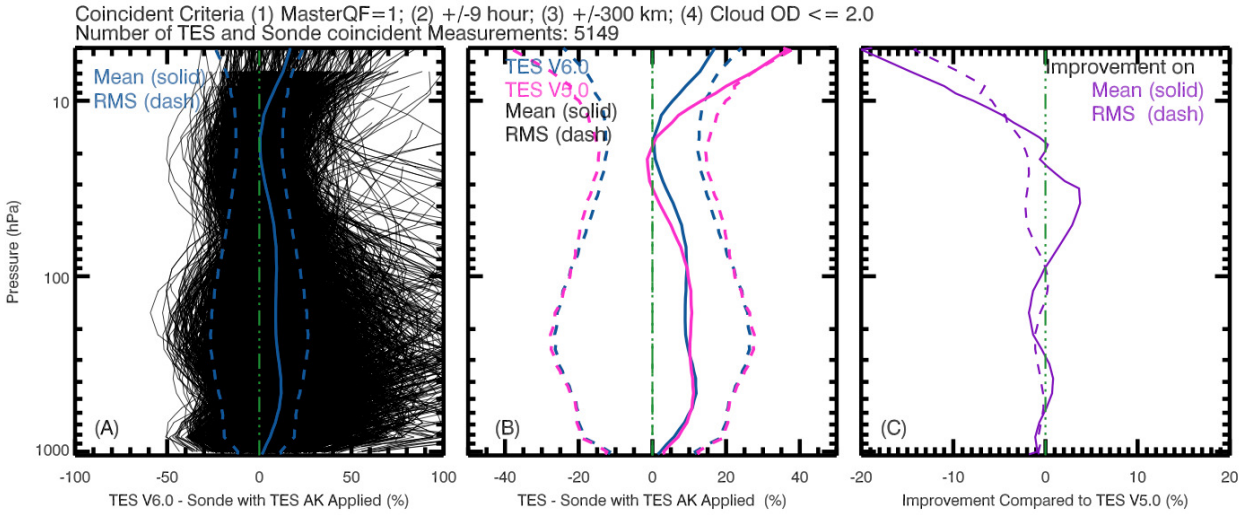

Figure 5-2 TES-ozonesonde percent differences. (Panel A) Individual profile of differences between TES V006 and ozonesonde are shown in black, mean and one standard deviation ranges are overlaid in solid blue and dash blue lines, respectively. (Panel B) The mean (solid lines) and one standard deviation (dahs lines) of differences between TES V006 and ozonesonde (blue lines) overlaid in TES V005-ozonesonde (magenta lines). (Panel C) Purples solid line is the differences between mean differences of TES V006-Sonde and that of TES V005-Sonde. Purples dash line is the differences between 1 sigma deviation of the differences of TES V006-Sonde and that of TES V005-Sonde.

An overall positive bias in the TES V006 and V005 (Figure 5-3) ozone retrievals, compared to the ozonesondes, are found in all six latitude zones. This positive bias is more apparent in the mean ozone percent difference profiles than the minor negative bias around 10 hPa. Both TES V005 and V006 mean percent bias in the troposphere is generally within 15% with an exception in the Antarctic region where both TES V005 and V006 ozone profiles showed up to 20% positive bias in the upper troposphere. Similar to comparison of TES V005 and V006 with ozonesondes, a positive bias in the TES measurements relative to the ozonesondes has been noticed in TES V002 and V004 O_3 validation report.

In Arctic and Antarctic, both TES V006-ozonesonde and TES V005-ozonesonde comparisons exhibit a positive percent bias. The exception to the general positive bias in the TES V005-ozonesonde comparisons was found over the Arctic (20 to 70 hPa) and the Antarctic (20 to 50 hPa). TES V006 displays a negative bias with a peak value about -5%, but TES V005 had a negative bias up to -10%.

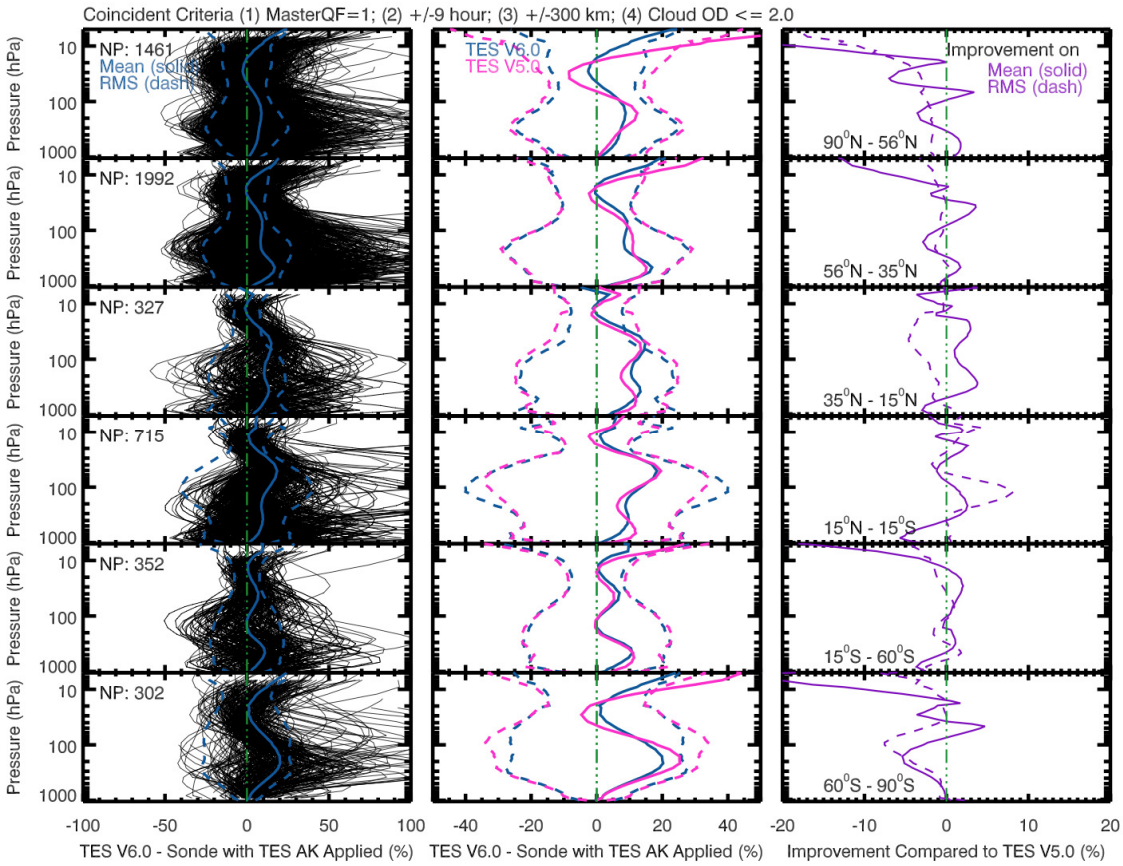

Figure 5-3 TES-ozonesonde percent differences differences in six latitude zones. 1st row (or top row): Arctic, 2nd row: Northern Midlatitudes, 3rd row: Northern Subtropics, 4th row: Tropics, 5th row: Southern low- and midlatitudes, and 6th row: Antarctic. Individual profiles are shown in black, mean and one standard deviation ranges are overlaid in blue solid lines and blue dash lines, respectively. The number of coincident comparisons is "NP." Left panels illustrate comparisons using TES V006. Middle panels showed the mean and 1 sigma deviation of differences TES V006-ozonesonde (blue lines) overlaid in TES V005-ozonesonde (magenta lines). Right panels illustrate the comparisons between TES V006-Sonde and V005-Sonde; i.e., the purple solid lines = abs(mean(TES V006-ozonesonde)) - abs(mean(TES V005-ozonesonde)) and the purple dash lines = rms(TES V006-ozonesonde) - rms(TES V005-ozonesonde).

The percent TES-ozonesonde difference of ozone profiles for winter, spring, summer, and fall in northern midlatitudes (35 to 56° N) are shown in Figure 5-4 (using 1992 coincident TES V006-ozonesonde measurements). Both TES V005 and V006 show a positive mean bias less than 15% when compared to ozonesonde measurements. It is an improvement, compared to TES V002 ozone profiles used by Nassar et al. (2008) to study the seasonal variability of ozone profiles (using 700 coincident TES-ozonesonde measurements) in northern midlatitudes. Nassar et al. (2008) illustrated that the altitude of the peak in the mean percent difference profiles was lowest in the winter and highest in the summer. It likely relates to the changing tropopause height and variability of ozone (Logan, 1999). Figure 5-4 also shows seasonal differences in the altitude of the peak ozone difference for V006. The low-altitude outliers predominantly occur in the summer and to a lesser degree in the spring and that the summer northern midlatitude bias profiles somewhat resemble the northern subtropics or the tropics in the upper troposphere. With

the exception of a small negative bias at ~ 90 to 100 hPa in the summer for V002 mean ozone percent difference, the mean O_3 percent and absolute differences generally show a positive bias for all seasons. All of these features are in agreement with Boxe et al. (2010), TES V004, V005 and V006 O_3.

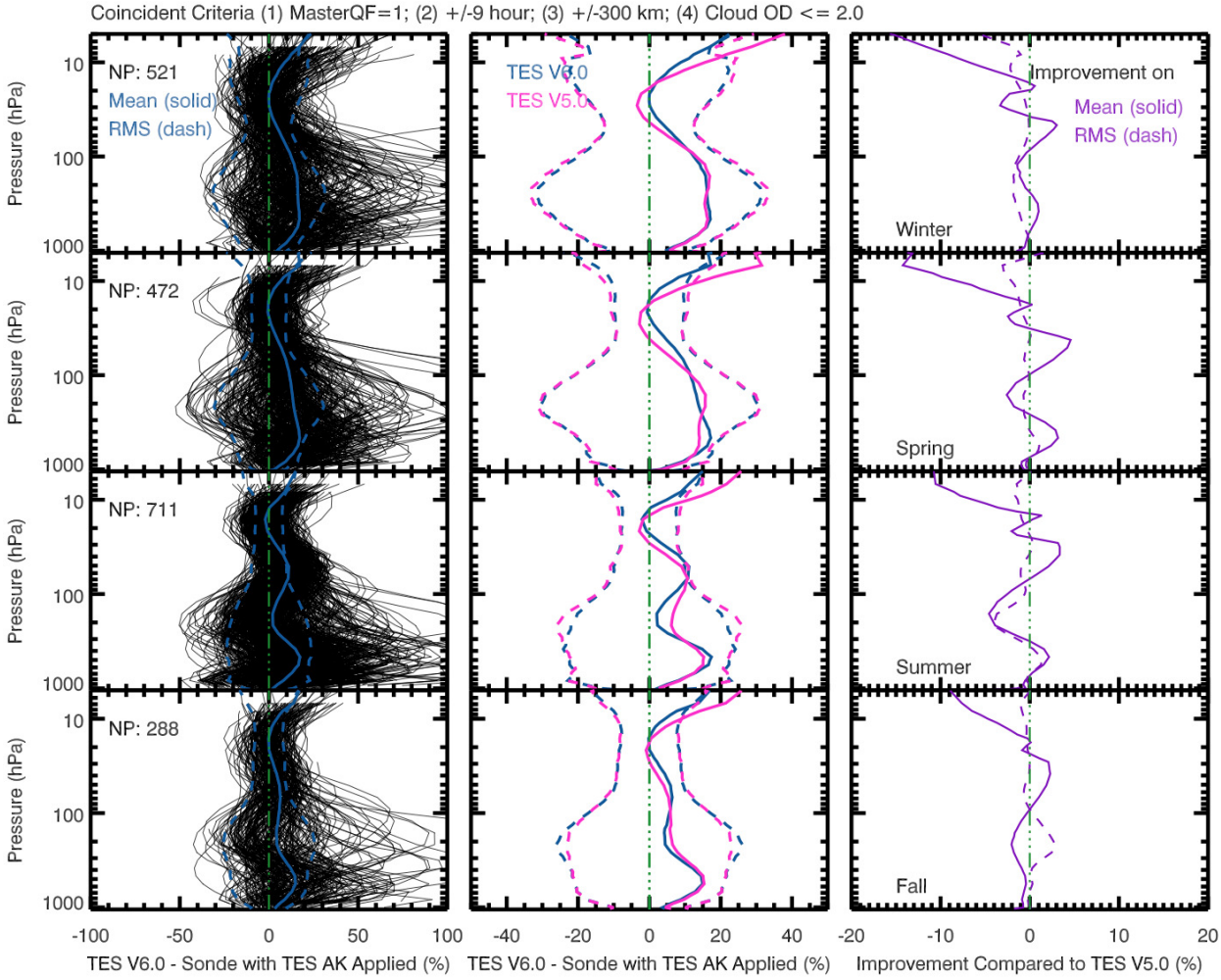

Figure 5-4 TES-ozonesonde ozone percent differences differences for the four seasons [Winter (DJF); Spring (MAM); Summer (JAJ); Fall (SON); months abbreviated in parentheses] in the northern midlatitudes (35 to 56°N). Individual profiles are shown in black, mean and one standard deviation ranges are overlaid in blue solid lines and blue dash lines, respectively. 1st row (or top row): Winter, 2nd row: Spring, 3rd row: Summer, and 4th row: Fall. The number of coincident comparisons is "NP." Left panels illustrate comparisons using TES V006. Middle panels showed the mean and 1 sigma deviation of differences TES V006-ozonesonde (blue lines) overlaid in TES V005-ozonesonde (magenta lines). Right panels illustrate the comparisons between TES V006-Sonde and V005-Sonde; i.e., the purple solid lines = abs(mean(TES V006-ozonesonde)) - abs(mean(TES V005-ozonesonde)) and the purple dash lines = rms(TES V006-ozonesonde) - rms(TES V005-ozonesonde).

5.3 References

5.3.1 Primary TES Nadir Ozone References

[1] Boxe, C.S., J.R. Worden, K.W. Bowman, S.S. Kulawik, J.L. Neu, W.C. Ford, G.B. Osterman, R.L. Herman, A. Eldering, D.W. Tarasick, A.M. Thompson, D.C. Doughty, M.R. Hoffmann, S.J. Oltmans (2010), Validation of northern latitude Tropospheric Emission Spectrometer stare ozone profiles with ARC-IONS sondes during ARCTAS: sensitivity, bias and error analysis, *Atmospheric Chemistry and Physics*, doi:10.5194/acp-10-9901-2010, October 20, 2010.

[2] Nassar, R., J.A. Logan, H.M. Worden, I.A. Megretskaia, K.W. Bowman, G.B. Osterman, A.M. Thompson, D.W. Tarasick, S. Austin, H. Claude, M.K. Dubey, W.K. Hocking, B.J. Johnson, E. Joseph, J. Merrill, G.A. Morris, M. Newchurch, S.J. Oltmans, F. Posny, F.J. Schmidlin, H. Vömel, D.N. Whiteman, J.C. Witte (2008), Validation of Tropospheric Emission Spectrometer (TES) Nadir Ozone Profiles Using Ozonesonde Measurements, *J. Geophys. Res. 113*, D15S17, (doi:10.1029/2007JD008819), May 7, 2008.

[3] Osterman, G., S. S. Kulawik, H. M. Worden, N. A. D. Richards, B. M. Fisher, A. Eldering, M. W. Shephard, L. Froidevaux, G. Labow, M. Luo, R. L. Herman, K. W. Bowman, and A. M. Thompson, Validation of Tropospheric Emission Spectrometer (TES) Measurements of the Total, Stratospheric and Tropospheric Column Abundance of Ozone, *J. Geophys. Res., 113*, D15S16, (doi:10.1029/2007JD008801) May 7, 2008.

[4] Richards, N. A. D., G. B. Osterman, E. V. Browell, J. W. Hair, M. Avery and Q. Li, Validation of Tropospheric Emission Spectrometer ozone profiles with aircraft observations during the Intercontinental Chemical Transport Experiment–B, *J. Geophys. Res., 113*, D16S29, (doi:10.1029/2007JD008815) May 23, 2008.

[5] Worden, H. M., J. Logan, J. R. Worden, R. Beer, K. Bowman, S. A. Clough, A. Eldering, B. M. Fisher, M. R. Gunson, R. L. Herman, S. S. Kulawik, M. C. Lampel, M. Luo, I. A. Megretskaia, G. B. Osterman, and M. W. Shephard (2007), Comparisons of Tropospheric Emission Spectrometer (TES) ozone profiles to ozonesondes: Methods and initial results, *J. Geophys. Res., 112*, D03309, (doi:10.1029/2006JD007258), February 15, 2007.

[6] Worden, J., X. Liu, K. Bowman, K. Chance, R. Beer, A. Eldering, M. Gunson, and H. Worden, (2007), Improved Tropospheric Ozone Profile Retrievals Using OMI and TES Radiances, *Geophys. Res. Lett., 34,* L01809, (doi:10.1029/2006GL027806) January 10, 2007.

5.3.2 TES References

[7] Beer, R., T. A. Glavich, D. M. Rider (2001), Tropospheric Emission Spectrometer for the Earth Observing System's Aura satellite, *Applied. Optics, 40 (15),* 2356-2367, May 20, 2001.

[8] Beer, R. (2006), TES on the Aura Mission: Scientific Objectives, Measurements and Analysis Overview, *IEEE Transactions on Geoscience and Remote Sensing, 44 (No.5),* 1102-1105, May 2006.

[9] Bowman K.W., C. D. Rodgers, S. S. Kulawik, J. Worden, E. Sarkissian, G. Osterman, T. Steck, M. Lou, A. Eldering, M. Shepherd, H. Worden, M. Lampel, S. Clough, P. Brown, C. Rinsland, M. Gunson, R. Beer, "Tropospheric Emission Spectrometer: Retrieval Method and Error Analysis", *IEEE Trans. Geoscience and Remote Sensing, 44, (No.5),* 1297-1307. May 2006.

[10] Eldering, A., S. S. Kulawik, J. Worden, K. Bowman, G. Osterman (2008), Implementation of cloud retrievals for TES Atmospheric retrievals: 2. Characterization of cloud top pressure and effective optical depth retrievals, *Journal of Geophysical Research, Vol. 113,* D16S37, (doi:10.1029/2007JD008858) June 10, 2008.

[11] Herman, R., and S. Kulawik, (editors), K. Bowman, K. Cady-Pereira, A. Eldering, B. Fisher, D. Fu, R. Herman, D. Jacob, L. Jourdain, S. Kulawik, M. Luo, R. Monarrez, G. Osterman, S. Paradise, V. Payne, S. Poosti, N. Richards, D. Rider, D. Shepard, M. Shephard, F. Vilnrotter, H. Worden, J. Worden, H. Yun and L. Zhang (2013), Earth Observing System (EOS) Tropospheric Emission Spectrometer (TES) Level 2 (L2) Data User's Guide (Up to & including Version 6 data), Version 6.0, JPL Internal Report D-38042, November 4, 2013.

[12] Robert Herman and Gregory Osterman (editors), Christopher Boxe, Kevin Bowman, Karen Cady-Pereira, Tony Clough, Annmarie Eldering, Brendan Fisher, Dejian Fu, Robert Herman, Daniel Jacob, Line Jourdain, Susan Kulawik, Michael Lampel, Qinbin Li, Jennifer Logan, Ming Luo, Inna Megretskaia, Ray Nassar, Gregory Osterman, Susan Paradise, Vivienne Payne, Hank Revercomb, Nigel Richards, Mark Shephard, Dave Tobin, Solene Turquety, Felicia Vilnrotter, Kevin Wecht, Helen Worden, John Worden, Lin Zhang (2012), Earth Observing System (EOS) Tropospheric Emission Spectrometer (TES) Data Validation Report (Version F06_08, F06_09 data), Version 5.0, JPL Internal Report D-33192, April 8, 2012.

[13] Jourdain, L., H. M. Worden, J. R. Worden, K. Bowman, Q. Li, A. Eldering, S. S. Kulawik, G. Osterman, K. F. Boersma, B. Fisher, C. P. Rinsland, R. Beer, M. Gunson,. (2007), Tropospheric vertical distribution of tropical Atlantic ozone observed by TES during the northern African biomass burning season, *Geophysical Research Letters, 34*, L04810, (doi:10.1029/2006GL028284) February 23, 2007.

[14] Kulawik, S. S., J. Worden, A. Eldering, K. Bowman, M. Gunson, G. B. Osterman, L. Zhang, S. Clough, M. W. Shephard, R. Beer (2006), Implementation of cloud retrievals for Tropospheric Emission Spectrometer (TES) atmospheric retrievals: part 1. Description and characterization of errors on trace gas retrievals, *J. Geophys. Res., 111*, D24204, (doi:10.1029/2005JD006733), December 22, 2006.

[15] Luo M., C. P. Rinsland, C. D. Rodgers, J. A. Logan, H. Worden, S. Kulawik, A. Eldering, A. Goldman, M. W. Shephard, M. Gunson, and M. Lampel (2007) Comparison of carbon monoxide measurements by TES and MOPITT: Influence of a priori data and instrument characteristics on nadir atmospheric species retrievals,

Journal of Geophysical Research, Vol. 112, D09303, (doi:101029/2006JD007663) May 3, 2007.

[16] Worden, J., S. S. Kulawik, M. W. Shephard, S. A. Clough, H. Worden, K. Bowman, and A. Goldman (2004), Predicted errors of tropospheric emission spectrometer nadir retrievals from spectral window selection, *J. Geophys. Res., 109*, D09308, May 15, 2004.

5.3.3 General References

[17] Bloom, S., A. da Silva, D. Dee, M. Bosilovich, J.-D. Chern, S. Pawson, S. Schubert, M. Sienkiewicz, I. Stajner, W.-W. Tan, M.-L. Wu (2005). Documentation and Validation of the Goddard Earth Observing System (GEOS) Data Assimilation System - Version 4. *Technical Report Series on Global Modeling and Data Assimilation 104606, Vol. 26,* 187 pages, April 2005. Available from (paste entire link including pdf into browser):

http://ntrs.nasa.gov/archive/nasa/casi.ntrs.nasa.gov/20050175690_2005173043.pdf

[18] Brasseur, G. P., D. A. Hauglustaine, S. Walters, R. J. Rasch, J.-F. Müller, C. Granier, and X. X. Tie (1998), MOZART, a global chemical transport model for ozone and related chemical tracers 1. Model description, *J. Geophys. Res.*, *103* (D21), 28, 265–28, 289 (1998).

[19] Draxler, R.R. and Rolph, G.D. (2003), HYSPLIT (HYbrid Single-Particle Lagrangian Integrated Trajectory) Model access via NOAA ARL READY Website (http://www.arl.noaa.gov/ready/hysplit4.html). NOAA Air Resources Laboratory, Silver Spring, MD (2003).

[20] Froidevaux, L., Y.B. Jiang, A. Lambert, N.J. Livesey, W.G. Read, J.W. Waters, E.V. Browell, J.W. Hair, M.A. Avery, T.J. McGee, L.W. Twigg, G.K. Sumnicht, K.W. Jucks, J.J. Margitan, B. Sen, R.A. Stachnik, G.C. Toon, P.F. Bernath, C.D. Boone, K.A. Walker, M.J. Filipiak, R.S. Harwood, R.A. Fuller, G.L. Manney, M.J. Schwartz, W.H. Daffer, B.J. Drouin, R.E. Cofield, D.T. Cuddy, R.F. Jarnot, B.W. Knosp, V.S. Perun, W.V. Snyder, P.C. Stek, R.P. Thurstans, P.A. Wagner (2008), Validation of Aura Microwave Limb Sounder stratospheric ozone measurements, *J. Geophys. Res., 113,* D15S20, (doi:10.1029/2007JD008771) 2008.

[21] Jiang, Y. B., L. Froidevaux, A. Lambert, N.J. Livesey, W.G. Read, J.W. Waters, B. Bojkov, T. Leblanc, I.S. McDermid, S. Godin-Beekmann, M.J. Filipiak, R.S. Harwood, R.A. Fuller, W.H. Daffer, B.J. Drouin, R.E. Cofield, D.T. Cuddy, R.F. Jarnot, B.W. Knosp, V.S. Perun, M.J. Schwartz, W.V. Snyder, P.C. Stek, R.P. Thurstans, P.A. Wagner, M. Allaart, S.B. Andersen, G. Bodeker, B. Calpini, H. Claude, G. Coetzee, J. Davies, H. De Backer, H. Dier, M. Fujiwara, B. Johnson, H. Kelder, N.P. Leme, G. Konig-Langlo, E. Kyro, G. Laneve, L.S. Fook, J. Merrill, G. Morris, M. Newchurch, S. Oltmans, M.C. Parrondos, F. Posny, F. Schmidlin, P. Skrivankova, R. Stubi, D. Tarasick, A. Thompson, V. Thouret, P. Viatte, H. Vomel, P. von der Gathen, M. Yela, G. Zablocki (2007), Validation of Aura Microwave Limb Sounder Ozone by Ozonesonde and Lidar Measurements, *Journal of Geophysical Research, 112,* D24S34, (doi:10.1029/2007JD008776) 2007.

[22] Levelt, P. F., G.H.J. van den Oord, M.R. Dobber, A. Mälkki, H. Visser, J. de Vries, P. Stammes, J. Lundell and H. Saari (2006a), The Ozone Monitoring Instrument, *IEEE Trans. Geoscience and Remote Sensing, 44, (No.5),* 1093-1101, May 2006.

[23] Levelt, P. F., E. Hilsenrath, G.W. Leppelmeier, G.H.J. van den Oord, P.K. Bhartia, J. Tamminen, J.F. de Haan en J.P. Veefkind (2006b), Science objectives of the Ozone monitoring instrument, *IEEE Trans. Geoscience and Remote Sensing, 44, (No.5),*1199-1208, May 2006.

[24] Livesey, N. J., W.G. Read, A. Lambert, R.E. Cofield, D. T. Cuddy, L. Froidevaux, R. A. Fuller, R. F. Jarnot, J. H. Jiang, Y. B. Jiang, B. W. Knosp, L. J. Kovalenko, H. M. Pickett, H. C. Pumphrey, M. L. Santee, M. J. Schwartz, P. C. Stek, P. A. Wagner, J. W. Waters, and D. L. Wu (2007), EOS MLS Version 2.2 Level 2 data quality and description document, Version 2.2x-1.0a Jet Propulsion Laboratory Internal Report D-33509, May 22, 2007.

[25] Livesey N.J., M.J. Filipiak, L. Froidevaux, W.G. Read, A. Lambert, M.L. Santee, J.H. Jiang, H.C. Pumphrey, J.W. Waters, R.E. Cofield, D.T. Cuddy, W.H. Daffer, B.J. Drouin, R.A. Fuller, R.F. Jarnot, Y.B. Jiang, B.W. Knosp, Q.B. Li, V.S. Perun, M.J. Schwartz, W.V. Snyder, P.C. Stek, R.P. Thurstans, P.A. Wagner, M. Avery, E.V. Browell, J-P. Cammas, L.E. Christensen, G.S. Diskin, R-S. Gao, H-J. Jost, M. Loewenstein, J.D. Lopez, P. Nedelec, G.B. Osterman, G.W. Sachse, and C.R. Webster (2008), Validation of Aura Microwave Limb Sounder O3 and CO observations in the upper troposphere and lower stratosphere, *J. Geophys. Res., 113*, D15S02, (doi:10.1029/2007JD008805) March 27, 2008.

[26] Logan, J.A., An analysis of ozonesonde data for the troposphere: Recommendations for testing 3-D models, and development of a gridded climatology for tropospheric ozone*, J. Geophys. Res., 104,* 16115-16149, 1999.

[27] Rodgers, C. D. (2000), *Inverse Methods for Atmospheric Sounding: Theory and Practice.* World Scientific Publishing Co. Ltd., 2000.

[28] Rodgers, C. D. and B. J. Conners (2003), Intercomparison of remote sounding instruments, *J. Geophys. Res., 108,(D3),* 4116, (doi:10.1029/2002JD002299) 2003.

[29] Schoeberl, M.R., J.R. Ziemke, B. Bojkov, N. Livesey, B. Duncan, S. Strahan, L. Froidevaux, S. Kulawik, P.K. Bhartia, S. Chandra, P.F. Levelt, J.C. Witte, A.M. Thompson, E. Cuevas, A. Redondas, D.W. Tarasick, J. Davies, G. Bodeker, G. Hansen, B.J. Johnson, S.J. Oltmans, H. Vomel, M. Allaart, H. Kelder, M. Newchurch, S. Godin-Beekmann, G. Ancellet, H. Claude, S.B. Andersen, E. Kyro, M. Parrondos, M. Yela, G. Zablocki, D. Moore, H. Dier, P. von der Gathen, P. Viatte, R. Stubi, B. Calpini, P. Skrivankova, V. Dorokhov, H. De Backer, F.J. Schmidlin, G. Coetzee, M. Fujiwara, V. Thouret, F. Posny, G. Morris, J. Merrill, C.P. Leong, G. Koenig-Langlo, and E. Joseph. (2007), A trajectory-based estimate of the tropospheric ozone column using the residual method, *J. Geophys. Res. 112*, D24S49, (doi:10.1029/2007JD008773) December 19, 2007.

[30] Waters, J.W., L. Froidevaux, R.S. Harwood, R.F. Jarnot, H.M. Pickett, W.G. Read, P.H. Siegel, R.E. Cofield, M.J. Filipiak, D.A. Flower, J.R. Holden, G.K. Lau, N.J. Livesey, G.L. Manney, H.C. Pumphrey, M.L. Santee, D.L. Wu, D.T. Cuddy, R.R. Lay,

M.S. Loo, V.S. Perun, M.J. Schwartz, P.C. Stek, R.P. Thurstans, M.A. Boyles, S. Chandra, M.C. Chavez, G-S. Chen, B.V. Chudasama, R. Dodge, R.A. Fuller, M.A. Girard, J.H. Jiang, Y. Jiang, B.W. Knosp, R.C. LaBelle, J.C. Lam, K.A. Lee, D. Miller, J.E. Oswald, N.C. Patel, D.M. Pukala, O. Quintero, D.M. Scaff, W.V. Snyder, M.C. Tope, P.A. Wagner, and M.J. Walch, (2006), The Earth Observing System Microwave Limb Sounder (EOS MLS) on the Aura satellite, *IEEE Trans. Geoscience and Remote Sensing, 44, (No.5),* 1075-1092, May 2006.

[31] Ziemke, J.R., S. Chandra, B.N. Duncan, L. Froidevaux, P.K. Bhartia, P.F. Levelt, and J.W. Waters, (2006), Tropospheric ozone determined from Aura OMI and MLS: Evaluation of measurements and comparison with the Global Modeling Initiative's Chemical Transport Model, *J. Geophys. Res., 111,* D19303 (doi:10.1029/2006JD007089) October 5, 2006.

6. Validation of TES Retrievals of Carbon Monoxide

6.1 Overview

TES CO and other species retrievals are currently being processed in version V006. All the original TES CO data validation activities, including comparisons with in-situ aircraft data, and with MOPITT data and other satellite data, have been carried out for TES V003 or V002 data. The TES CO V004 data have no systematic changes from previous versions. In TES CO V005, two major changes were made: we adopted CO a priori from MOZART (Model for OZone And Related chemical Tracers) V04 model results (eight-year monthly averages) and the new constraint matrix used in retrievals. They are the same model a priori and constraint used in MOPITT CO V4/V5 retrievals. In TES V006 CO retrievals, there are no changes made in algorithms or the a priori climatology.

We briefly describe the TES instrument performance nearly ten years on orbit, the positive effect of the optical bench warm-up conducted early Dec 2005 on filter 1A1 and the CO retrievals, and the recent (post April 2011) worsening throughputs in CO data due to instrument control system degradation. We give an overview of the characterization of TES CO retrievals, including the roles of a priori profiles and the averaging kernels. A brief overview of the global distributions of TES CO measurements is given for different seasons. For CO V006, we present comparisons of TES CO profiles with in situ measurements from several aircraft campaigns, including Intercontinental Transport Experiment-Phase B (INTEX-B), Aura Validation Experiment (AVE), and Costa Rica Aura Validation Experiment (CR-AVE). Validation of TES CO V006 data using the new MOPITT V6 data are conducted for several Global Survey runs. These comparisons not only offer good qualitative checks for TES data, e.g., the characteristics of the CO global distribution or the shapes of their vertical profiles, but also offer quantitative validations of TES CO retrievals.

6.2 Instrument performance before and after optical bench warm-up

For constant emission source, e.g., on-board black body, the signal strength in TES 1A1 filter (1900-2300 cm^{-1}) is not constant over time and the variation of the signal strength is reflected in the CO retrievals. Figure 6-1 displays the normalized integrated spectral magnitude (ISM) (top panel), beam splitter temperature (middle panel), and degree of freedom for signal (DOFS) for latitudes of 30°N-30°S as a function of time (Rinsland et al., 2006). Data after the middle of 2006 stays about the same level. The ISM is a sensitive indicator of the signal levels of the TES detectors and is calculated by integrating a spectrum over wavenumber. It is the primary quantity used to quantify and detect trends in the TES instrument alignment and performance. An overall trend of declining ISM with time and the measured beamsplitter temperature is apparent, with increases in beamsplitter temperatures when the detectors are de-iced periodically. The warming of the TES optical bench on Nov 29-Dec 2, 2005 improved the TES beamsplitter alignment, with an integrated spectral magnitude increase for the 1A1 filter by a factor of 3.4 as compared to the pre-warm up value.

The TES CO retrieval ‘sensitivity’, or the parameters describing the retrieval vertical information in the troposphere, e.g., the Degree of Freedom for signal (DOF) and the retrieval errors, are much improved after the optical bench warm up in early December 2005 as a result of the better alignment of the instrument and increased signal to noise.

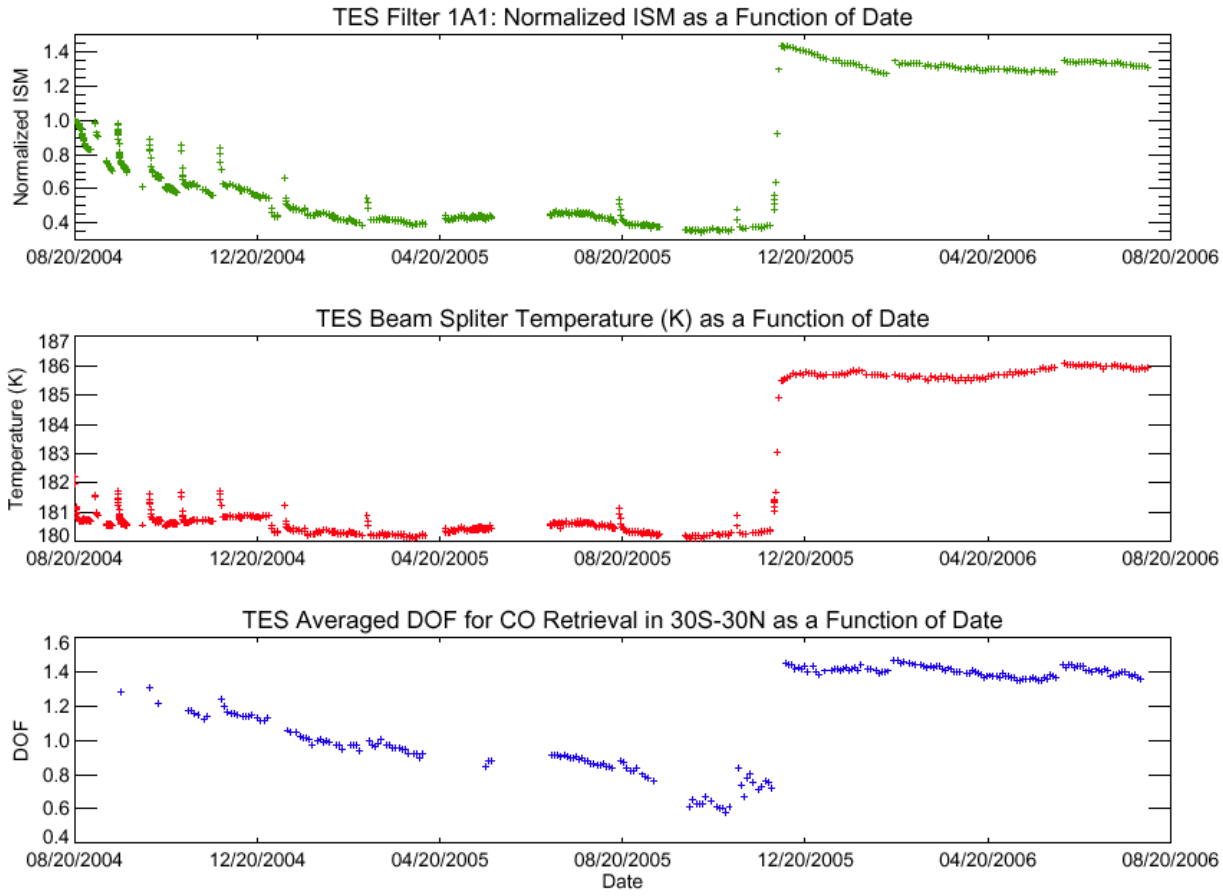

Figure 6-1 Time series of measured normalized Integrated Spectral Magnitude (ISM) (top panel), beamsplitter temperature (middle panel), and average DOFS for 30°N-30°S latitude. The ISM is normalized to 1.0 at the beginning of the time series.

6.3 Problems in filter 1A1 signal used for CO retrieval since 2011

The aging of TES mechanically moving components, e.g., Interferometer Control System (ICS) has started to affect TES measured signals since early 2011. The majority of the problematic scans show 'over/underflows' or 'spikes' in the interferogram DNs (Data Number). TES Level 1A software detects and flags these scans and removes them from the L1B and L2 processing. Compared to 2004-2010 data we therefore see drop-offs in valid number of CO retrievals in the TES product since early 2011.

To illustrate the rate of CO data drop-offs over TES lifetime, Figure 6-2 shows the percent of bad interferogram scans (Fatal Error in L1A) per science/calibration run (e.g., a Global Survey or a Transect run). This percentage number seems jump between zero (all good) and 100% (all bad) depending on a given run number. Users should definitely expect to see a lot of missing CO retrievals in data files since 2011.

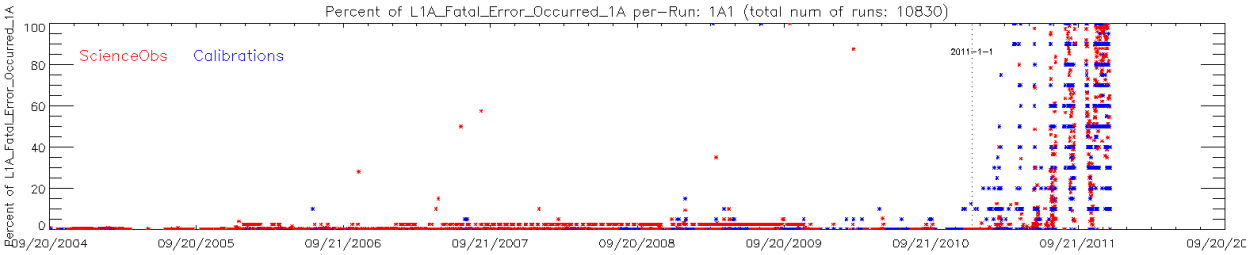

Figure 6-2 Time series of percentage of 'L1A Fatal Error in 1A1' scans per-run. The time Jan 1, 2011 is marked in dotted-line.

6.4 Major changes from V005 to V006 in CO retrieval

There are no changes made in CO step retrieval in TES V006 data processing. However, changes in other steps will slightly affect the CO retrieval results, e.g., the new temperature, water vapor and Ozone climatology. The major updates in CO retrievals were made in TES V005. The MOZART-4 model data provided to TES from the NCAR (National Center for Atmospheric Research) group are used as the CO a priori state. These model results for CO VMR were averaged monthly in 10 degree latitude by 60 degree longitude boxes as the TES CO a priori. The constraint matrix for TES CO retrievals is by adopting the same algorithm provided by the MOPITT team for deriving their V4/V5/V6 data (Deeter et al., 2010).

We examine the differences between TES V005 and V006 to see if they can be explained quantitatively by the changes made in other species retrieval steps. We also perform the comparisons of TES and MOPITT CO to evaluate their statistical differences by removing the known a priori effects as it has been done previously.

6.5 Global distributions of CO from TES measurements

Carbon monoxide is a by-product of incomplete combustion of fossil fuels and biomass, and is produced by oxidation of methane (CH_4) and other hydrocarbons. The global distributions of TES CO fields reflect this basic understanding, e.g., the enhanced CO regions and their seasonal variations are co-located with the known source regions. Figure 6-3 shows TES CO monthly mean distributions at 681.3 hPa for Jan, Apr, July, and Oct 2007. In general, the northern hemisphere (and the tropics) show much more CO than the southern hemisphere due to the known distribution of natural and industrial sources. CO values in the winter/spring are larger than summer/fall due to the longer lifetime in seasons with less photochemical activity.

In central Africa, the enhanced CO corresponding to biomass burning occurs in two time periods, in Dec/Jan/Feb for latitudes north of the equator and in Jul-Oct south of the equator, corresponding to the local dry seasons. In South America, the biomass burning induced maximum in CO concentration occurred during Aug/Sep/Oct near equator. Enhanced levels of CO over E. China can be related local pollution and can be seen throughout the year in the TES observations.

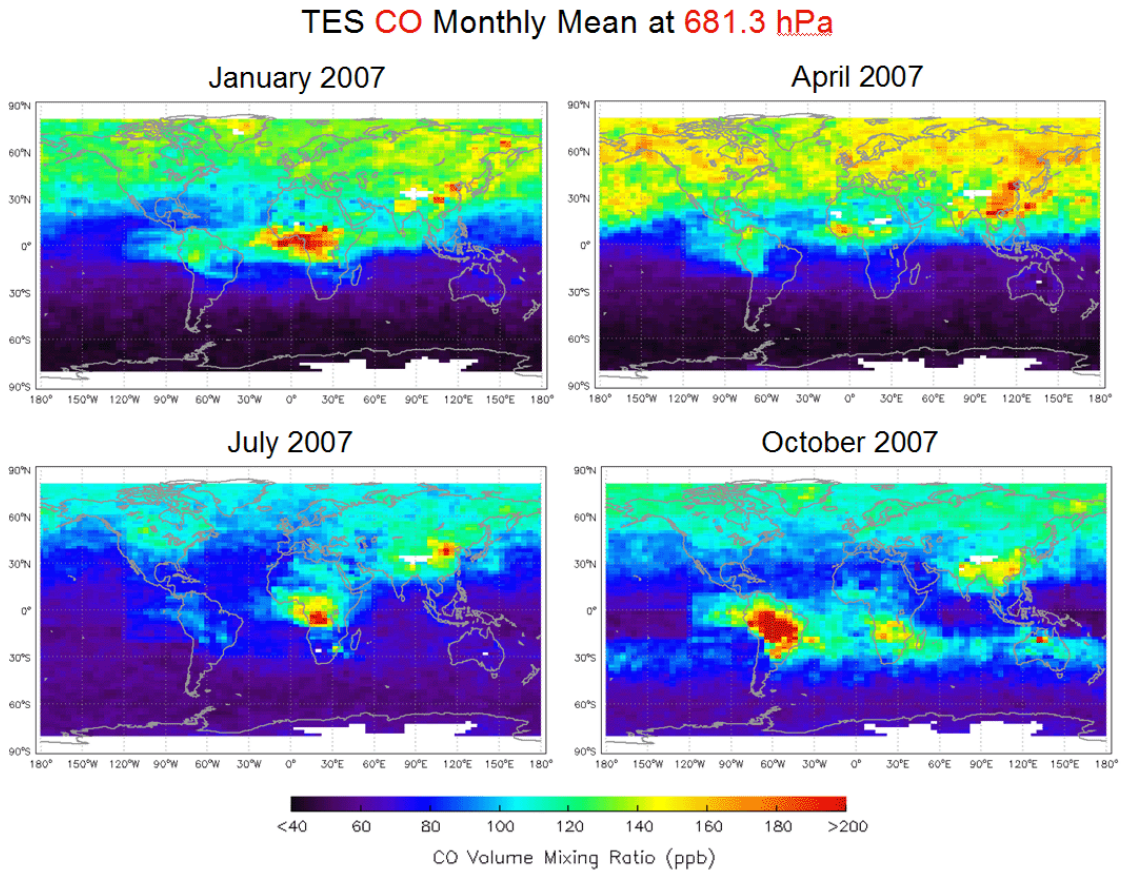

Figure 6-3 TES CO Global Distributions at 681.3 hPa for the Four Typical Months, Jan, April, July, and Oct 2007.

6.6 CO validation: Comparisons to in situ Aircraft Measurement

During the past few years, several aircraft campaigns were conducted to study tropospheric chemistry and transport, and provide data for validation of the measurements made by the instruments on the Aura satellite. The TES team participated in the Aura Validation Experiment (AVE) campaigns: Oct-Nov 2004 based near Houston, Jan-Feb 2005 based in Portsmouth, NH (PAVE), and in Jan-Feb 2006 based in Costa Rica (CR-AVE). TES also participated in INTEX-B (International Chemical Transport Experiment), which had deployments in Houston, Honolulu and Anchorage in March-May 2006. The TES CO data from the time periods of these campaigns were compared with the in situ measurements for the aircraft flights when there are the best coincidences between TES measurement location and the aircraft CO profiles. Most validation results are reported in papers by M. Luo et al., 2007b and J. Lopez et al., 2008. We plan to repeat these comparisons for TES V006 CO data since major changes in retrieval a priori and constraints are made. Here we give a brief review of the aircraft data validation for previous version TES CO data.

In all aircraft campaigns, TES made a series of step and stare nadir observations with some footprints coinciding with the aircraft tracks and the spiral profiling locations. During the AVE and CR-AVE campaigns, CO was measured by the NASA Ames Research Center Argus instrument on the WB-57 aircraft. The CO profiles were also measured by Aircraft Laser

Infrared Absorption Spectrometer (ALIAS) of JPL during CR-AVE. During the INTEX-B campaign the DACOM instrument by the NASA Langley Research Center was on board to measure CO.

For the TES and aircraft CO comparisons, all possible aircraft profiles, including profiles taken while taking-off and landing, and the vertical spirals, are extracted to match with TES profiles closest in times and locations. A few aircraft profiles and ~2-4 TES CO profiles per aircraft profile can be identified per campaign station, normally within a couple of hours and a couple to a few hundred kilometers. The next procedure is to apply TES retrieval operator to the in-situ profile, $x_{aircraft}$, to obtain the simulated aircraft profile as seen by TES, $x_{simul\text{-}aircraft}$,

$$x_{simul\text{-}aircraft} = Ax_{aircraft} + (I - A)x_a. \quad \text{(Equation 6-1)}$$

where x_a is the TES CO retrieval a priori profile from the MOZART model, and A is the averaging kernel. This profile as seen by TES is then compared to the TES retrieved CO profile.

In summary, the averaged comparisons are the best in the Houston region for the two campaigns in Oct 2004 and March 2006. The differences between Argus and TES CO profiles are within TES retrieval errors and equivalent to CO spatial/temporal variability detected in both TES and Argus measurements. The comparisons of TES and DACOM CO profiles near Hawaii and Anchorage in April-May 2006 are not as good. In these regions, the aircraft DACOM CO profiles are characterized by plumes or enhanced CO layers, consistent with known features in the tracer fields due to transpacific transport of polluted air parcels originating from East Asia. In TES V006 CO comparison, the effects of a priori should be removed and these conclusions should remain the same.

6.7 CO validation: comparisons to MOZAIC, ACE, MLS, and AIRS data sets

Some preliminary results are obtained in TES CO data validation using the CO data sets of MOZAIC (Measurements of Ozone and water vapor by In-service AIrbus aircraft, http://mozaic.aero.obs-mip.fr), ACE (Atmospheric Chemistry Experiment), MLS (Microwave Limb Sounder), and AIRS (Atmospheric Infrared Sounder). Detailed results are documented either in the previous version TES Validation Report (V003) or papers Rinsland et al., 2008, Warner et al., 2010.

6.8 CO Validation: Comparisons to MOPITT Data

Both TES and MOPITT (Measurements Of Pollution In The Troposphere) have updated CO data products to the new versions (V006 for TES and V004 for MOPITT) using updated a priori and constraints for CO retrievals from their previous version data. The a priori used by the two teams are from the same MOZART model simulation results. TES uses 10 degree latitude by 60 degree longitude monthly bins of the model data as the a priori. TES also uses the same algorithm as that of MOPITT to compute the constraint matrix used for all profile retrievals (Deeter et al., 2010), e.g., 0.3 diagonals in lnVMR (~30%) and 100 hPa vertical correlation distances. In theory, different a priori or constraints will affect final CO products and to change their global distributions from previous versions, but when proper a priori, averaging kernels, and error estimates are considered in applications, the different version data should be consistent. Here we

make comparisons between new versions of TES and MOPITT CO data using the technique that was applied in a previous study (Luo et al., 2007a). We did three TES Global Surveys, Sept 20-21, 2004, the original GS for the publication, a TES GS taken June 5-6, 2009, and a TES GS taken June 6-7, 2010 after the new instrument calibration scheme was adopted.

The retrieval results of TES 16-orbit global survey measurements in Sept 20-21, 2004 (Run ID 2147) have been examined extensively by the TES science team. In CO comparisons, MOPITT data are down-sampled to near the TES geolocations. Figure 6-4 shows TES and down-selected MOPITT CO VMR at 681 hPa and interpolated horizontally to illustrate the distribution more clearly. The two CO distribution fields are very similar partially due to the usage to the same a priori. This is an improvement from Luo et al. (2007a) using older versions of TES and MOPITT CO data.

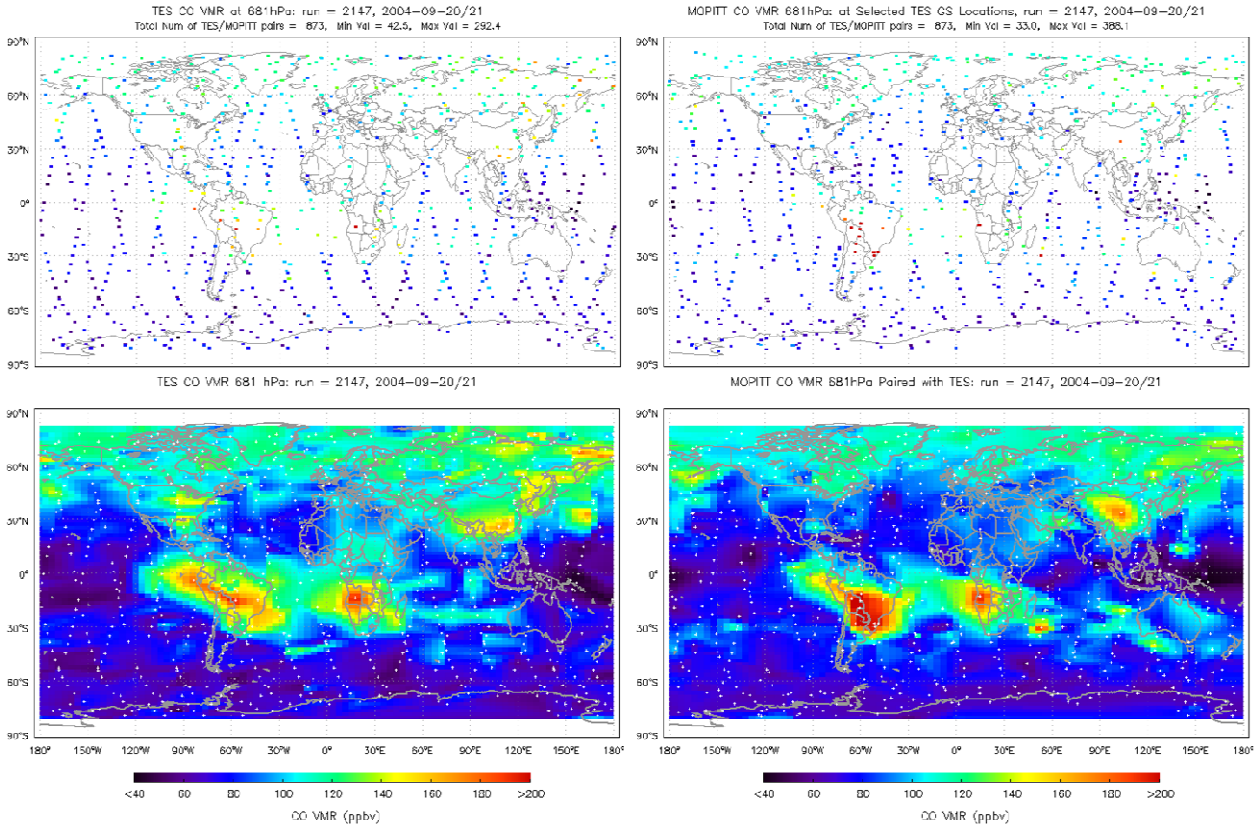

Figure 6-4 TES (left column) and down-sampled MOPITT (right column) CO VMRs at 681 hPa. The corresponding date is one TES Global Survey, Sept 20-21, 2004. Top panels are TES and MOPITT CO VMRs at or near TES geolocations. Bottom panels are horizontally interpolated CO VMR maps with footprints in white dots.

Quantitative comparisons between TES and MOPITT CO at low, mid and upper troposphere and total column for this day are carried out. Three steps are performed in the comparison, direct comparison, adjusting TES CO profiles to MOPITT a priori profile, and applying TES averaging kernels to MOPITT retrieved profiles. The final comparison is to compare TES retrieved CO profiles

adjusted to MOPITT a priori and the MOPITT retrieved CO profiles adjusted to MOPITT averaging kernel. The agreement between the two CO fields becomes better in all tropospheric levels and the total column, especially in the lower and upper troposphere where both instruments do not have much sensitivity in their measurements. Figure 6-5 shows the direct and final comparisons of the CO VMRs at 681 hPa and 215 hPa between TES and MOPITT. The final comparisons show TES CO is slightly higher than that of MOPITT by <5% in global averages.

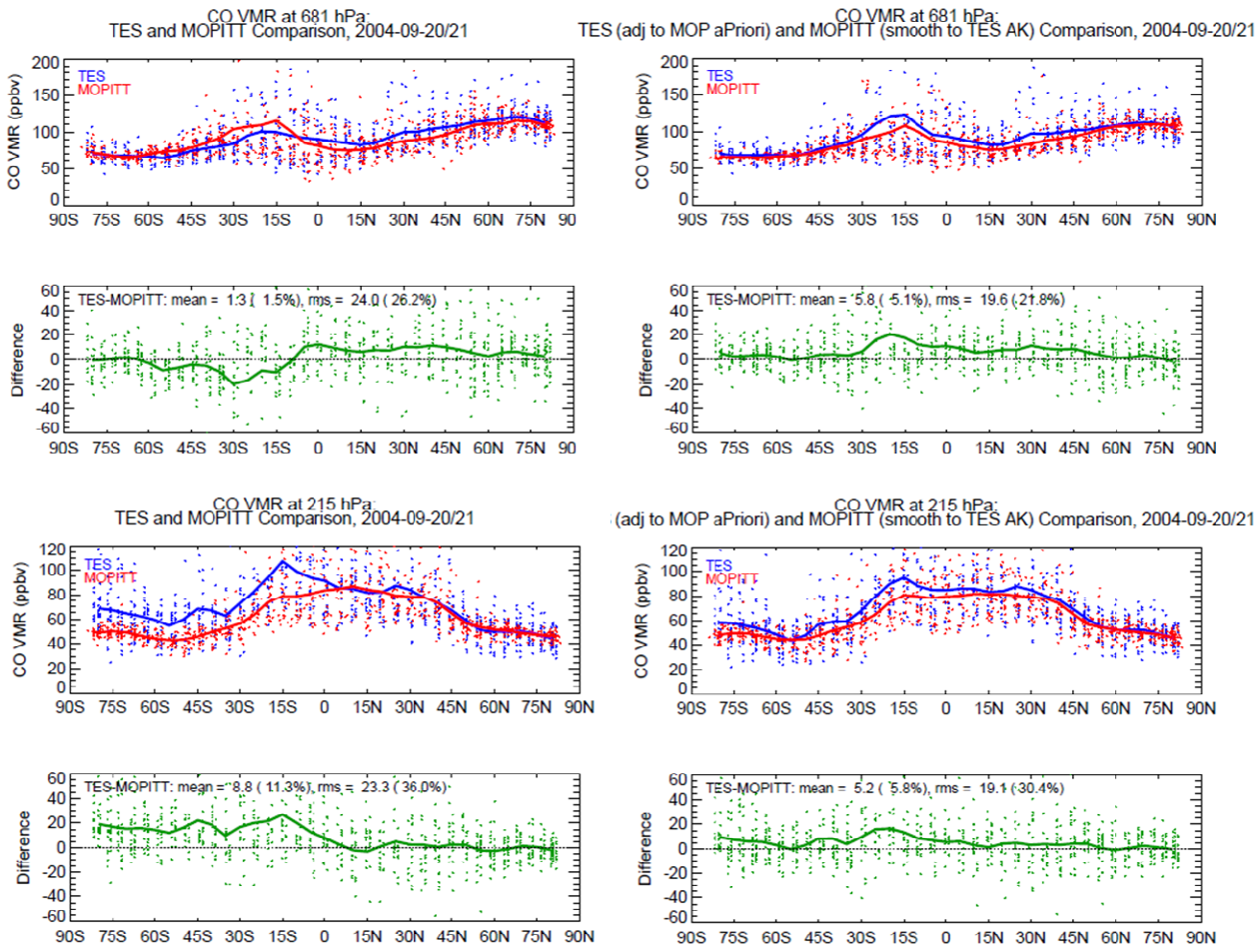

Figure 6-5 Comparisons of CO VMR reported by TES and MOPITT at 681 hPa and 215 hPa respectively. The left panels are the 'direct' comparisons. The right panels are the comparisons after the TES CO being adjusted to MOPITT a priori profile and MOPITT CO profiles being adjusted by applying TES averaging kernels (Luo et al., 2007a).

To summarize the comparison results for Sept 20-21, 2004 and other two TES GS periods, three tables are used below.

Table 6-1 TES-MOPITT CO comparisons for Sept 20-21, 2004

	681 hPa		215 hPa		Total Column	
	Mean Diff (%)	RMS of Diff (%)	Mean Diff (%)	RMS of Diff (%)	Mean Diff (%)	RMS of Diff (%)
Direct Compare	1.5%	26%	11%	36%	-1.3%	20%
TES adj to MOP aPriori vs MOP	1.4%	23%	6.2%	32%		
TES adj to MOP aPriori vs MOP adj to TES AK	5.1%	22%	5.8%	30%		
RMS of MOP in 500km/24hrs of TES location	MOP at 700hPa 5-15% (land) 5-10% (ocean)		MOP at 200hPa 2-15% (land) 3-8% (ocean)			
TES Retrieval Err	8-12%		8-20%		5-12%	
MOP Retrieval Err	25-30%		25-30%		5-12%	

Table 6-2 TES-MOPITT CO comparisons for June 5-6, 2009

	681 hPa		215 hPa		Total Column	
	Mean Diff (%)	RMS of Diff (%)	Mean Diff (%)	RMS of Diff (%)	Mean Diff (%)	RMS of Diff (%)
Direct Compare	-2.9%	22%	-0.1%	27%	-1.7%	18%
TES adj to MOP aPriori vs MOP	4.5%	21%	-1.2%	27%		
TES adj to MOP aPriori vs MOP adj to TES AK	2.6%	18%	0.8%	23%		
RMS of MOP in 500km/24hrs of TES location	5-10%		3-8%			
TES Retrieval Err	8-10%		5-15%		3-8%	
MOP Retrieval Err	25-30%		20-30%		5-10%	

Table 6-3 TES-MOPITT CO comparisons for Jun 6-7, 2010

	681 hPa		215 hPa		Total Column	
	Mean Diff (%)	RMS of Diff (%)	Mean Diff (%)	RMS of Diff (%)	Mean Diff (%)	RMS of Diff (%)
Direct Compare	7.4%	25%	-6%	28%	-0.3%	20%
TES adj to MOP aPriori vs MOP	9%	23%	-5.5%	27%		
TES adj to MOP aPriori vs MOP adj to TES AK	4%	19%	-0.9%	21%		
RMS of MOP in 500km/24hrs of TES location	5-20%		10-20%			
TES Retrieval Err	8-12%		5-15%		5-8%	
MOP Retrieval Err	25-30%		20-30%		6-10%	

In all comparisons, the RMS (root-mean-square) of the TES-MOPITT differences are seen reducing from direct comparisons to the comparisons with slight differences in a priori and averaging kernels considered as described in Luo et al. (2007a). For TES GS run2147, Sept 20-21, 2004 in Table 6-1, the comparison conclusions are similar to that of Luo et al. (2007a) made for TES and MOPITT earlier version data. Here we add the calculation of the variability (RMS) of MOPITT CO within 500km/24hrs of TES location and time. This number indicates that the comparison RMS can partially be explained by miss-matches between the two instruments in space and time. We also listed estimated retrieval errors by the two instrument teams that also contribute to the explanations of the final RMS in the differences. However, we notice a few percent of TES CO lower mean bias compared to that of MOPITT in the upper troposphere (215 hPa) in Table 6-2 and Table 6-3 (marked red) for the two GSs in 2009 and 2010.

6.9 CO validation: summary

Carbon Monoxide: Comparisons have been carried out between TES carbon monoxide retrievals and those from a variety of satellite and aircraft instruments. Global patterns of carbon monoxide as measured by TES are in good qualitative agreement with those seen by MOPITT on the NASA Terra satellite. Comparisons of profiles of CO between TES and MOPITT show better agreement when a priori information is accounted for correctly. TES carbon monoxide agrees to within the estimated uncertainty of the aircraft instruments, including both errors and the variability of CO itself. In the upper troposphere, TES CO are found to bias lower compared to that of MOPITT by a few percent.

6.10 References

6.10.1 TES Carbon Monoxide References

[1] Deeter, M.N., D.P. Edwards, J.C. Gille, L.K. Emmons, G. Francis, S.-P. Ho, D. Mao, D. Masters, H. Worden, James R. Drummond, and Paul C. Novelli (2010), The MOPITT version 4 CO product: Algorithm enhancements, validation, and long-term stability, *J. Geophys. Res.: Atmospheres, Vol. 115 Issue D7,* D07306, doi:10.1029/2009JD013005, April 15, 2010.

[2] Lopez, J.P., M. Luo, L.E. Christensen, M. Loewenstein, H. Jost, C.R. Webster, and G. Osterman (2008), TES carbon monoxide validation during two AVE campaigns using the Argus and ALIAS instruments on NASA's WB-57F, *Journal of Geophysical Research, Vol. 113, Issue D16*, (doi:10.1029/2007JD008811) D16S47, August 15, 2008.

[3] Luo, M., C.P. Rinsland, C.D. Rodgers, J.A. Logan, H. Worden, S. Kulawik, A. Eldering, A. Goldman, M.W. Shephard, M. Gunson, and M. Lampel (2007a), Comparison of carbon monoxide measurements by TES and MOPITT: the influence of a priori data and instrument characteristics on nadir atmospheric species retrievals, *J. Geophys. Res., 112*, D09303, (doi:101029/2006JD007663) May 3, 2007a.

[4] Luo, M., C. Rinsland, B. Fisher, G. Sachse, G. Diskin, J. Logan, H. Worden, S. Kulawik, G. Osterman, A. Eldering, R. Herman and M. Shephard (2007b), TES carbon monoxide validation with DACOM aircraft measurements during INTEX-B 2006, *J. Geophys. Res.*, *112,* D24S48, (doi:10.1029/2007JD008803) December 20, 2007b.

[5] Rinsland, C.P., M. Luo, J.A. Logan, R. Beer, H.M. Worden, J.R. Worden, K. Bowman, S.S. Kulawik, D. Rider, G. Osterman, M. Gunson, A. Goldman, M. Shephard, S.A. Clough, C. Rodgers, M. Lampel, and L. Chiou (2006), Nadir Measurements of carbon monoxide distributions by the Tropospheric Emission Spectrometer onboard the Aura Spacecraft: Overview of analysis approach and examples of initial results, *Geophys. Res. Lett., 33*, (L2280610.1029/2006GL027000) November 22, 2006.

[6] Rinsland, C.P., M Luo, M.W. Shephard, C. Clerbaux, C.D. Boone, P.F. Bernath, L. Chiou, and P.F. Coheur (2008), Tropospheric Emission Spectrometer (TES) and atmospheric chemistry experiment (ACE) measurements of tropospheric chemistry in tropical southeast Asia during a moderate El Niño in 2006, *Journal of Quantitative Spectroscopy and Radiative Transfer, Vol. 109, Issue 10*, pp. 1931-1942, July, 2008, http://dx.doi.org/10.1016/j.jqsrt.2007.12.020.

[7] Warner, J.X., Z. Wei, L. L. Strow, C. D. Barnet, L. C. Sparling, G. Diskin, and G. Sachse (2010), Improved agreement of AIRS tropospheric carbon monoxide products with other EOS sensors using optimal estimation retrievals, *Atmospheric Chemistry and Physics, 10(19),* pp. 9521-9533, doi:10.5194/acp-10-9521-2010, October 8, 2010.

7. Validation of TES nadir Temperature Retrievals with Radiosondes

7.1 Executive Summary

TES V006 nadir temperature (TATM) retrievals have been compared with nearly coincident radiosonde (hereafter radiosonde) measurements from the NOAA ESRL global radiosonde database. For TES V006 TATM minus $T_{radiosonde}$ (with averaging kernel applied), the bias is approximately +0.4 K in the lower troposphere, decreasing to negative 0.6 K in the upper troposphere. The rms is less than 1 K in the stratosphere and upper troposphere, but increases to 1.7 K in the lower troposphere. In clear sky conditions (average cloud effective optical depth less than 0.1), the bias improves in the lower troposphere but increases to +0.6 K at 500 hPa pressure level.

To evaluate the retrieval stability the monthly mean and standard deviation of the TATM residual between TES V005 and the Global Modeling and Data Assimilation Office (GMAO) GEOS-5.2 model, which provides the first guess and a priori for the TATM retrieval, were calculated. The statistics for both Tropical Pacific and Northern Atlantic Ocean regions indicate only minor month-to-month variability and no substantial trends over the entire five-and-a-half year period. The standard deviation of the residual was generally smaller than the standard deviation of the GMAO GEOS-5.2 but larger than the TES estimated measurement error. Overall, based on this analysis it appears that the TES retrieval quality has remained stable over the years inspected, 2006 through 2011.

7.2 Details of TES V006 TATM retrieval

For V006 TATM, there are two retrieval steps. First, for latitudes between 40° S and 40° N, there is a simultaneous retrieval of TATM, O_3, and CO_2. Second, there is a sequential retrieval of TATM using the 2B1 filter. The microwindows selected for temperature retrieval are within the CO_2 ν_2 band, spanning 671.32 to 901.48 cm^{-1} (14.896 μm to 11.093 μm wavelength). Constraints are altitude-dependent Tikhonov constraints (Kulawik et al., 2006).

The TES level 2 retrieval processes use a CO_2 climatology that incorporates improved seasonal and geographic variations in CO_2, as well as scaling to account for the annual increase in global CO_2 levels. This is highly relevant to temperature retrievals from the CO_2 ν_2 band because inaccurate assumptions about atmospheric CO_2 concentrations may lead to significant errors in atmospheric temperature retrievals, up to 0.5 K (see Figure 14 of Divakarla et al., 2006). The climatology is based on model results for the year 2004 from a chemical transport model (CTM) used in conjunction with a variety of other models to provide CO_2 surface fluxes [David Baker, pers. comm.]. The CTM used to create the time-varying three-dimensional CO_2 fields (longitude, latitude and pressure) is the Model of Atmospheric Transport and Chemistry (MATCH) (Nevison et al., 2008). Key surface CO_2 fluxes are derived from models including biospheric fluxes from the Carnegie Ames Stanford Approach (CASA) land biosphere model, oceanic fluxes from the WHOI model and a realistic, annually-varying fossil fuel source scheme (Nevison et al., 2008). The CO_2 fields generated by the model compare well to GLOBALVIEW atmospheric CO_2 data. Model results were provided to the TES team for the year 2004. Monthly mean profiles were calculated for two longitude bins and 10-degree latitude bins. This binned monthly mean climatology for 2004 was then scaled upward yearly (by 1.0055) to match the annual increase in CO_2.

7.3 A priori constraint vector

For each individual sequence and scan, the initial guess in the TES retrieval algorithm is set equal to an a priori profile (constraint vector). The TES V006 a priori constraint vectors come from NASA's Goddard Earth Observing System (GEOS) data assimilation system GEOS-5 (Rienecker et al., 2008). What is new in TES V006 is that the a priori constraint comes from the new GMAO GEOS version 5.9.1 processing stream. The TES V005 a priori constraint was based on the previous GMAO GEOS version 5.2. GEOS-5 data are produced by the Global Modeling and Assimilation Office (GMAO) at the NASA Goddard Space Flight Center (GSFC), on a 0.625° longitude by 0.5° latitude grid. GEOS-5 data are then interpolated to the locations and pressure levels of TES retrievals. The a priori covariance matrices used for retrieval regularization are described in Bowman et al. (2006). GEOS-5 assimilates a wide range of operational satellite data and in situ radiosonde measurements. Radiosonde profiles are strong constraints on the thermal structure and winds throughout the troposphere, with an emphasis on continental regions where the observing network is denser. Space-based observations include the High Resolution Infrared Sounders (HIRS) and Advanced Microwave Sounders (AMSU) instruments on NOAA's operational sounders, which directly constrain temperature and moisture. GEOS-5 includes a direct assimilation of radiances from AMSU and HIRS in a three-dimensional variational assimilation, as well as radiances from the Advanced Infrared Sounder (AIRS) and AMSU instruments on NASA's EOS Aqua platform (Zhu and Gelaro, 2008).

7.4 Current Validation Status of V006 nadir temperature

This section summarizes the latest validation comparisons for V006 TES nadir TATM retrievals. TES retrievals have been filtered by the master quality flag (see TES Data Users Guide, Herman and Kulawik (eds.) et al., 2013). The TES observation operator has been applied to the radiosonde profiles, and differences are shown as TATM minus $T_{radiosonde}$ (with averaging kernel). Levels where TES has no sensitivity to temperature (i.e., where the sum of the row of the averaging kernel equals zero) are not included in the calculation of the mean difference.

TES V006 TATM is compared with a global radiosonde database from the National Oceanic and Atmospheric Administration (NOAA) Earth System Research Laboratory (ESRL) Global Systems Division, formerly Forecast Systems Laboratory [M. Govett, pers. comm.]. The advantage of this database is that it includes the exact radiosonde release time, which improves the temporal coincidence between TES and radiosonde, and the temperature rms. The NOAA ESRL database combines the IGRA global data with North American Global Telecommunications Service (GTS) radiosonde observations. Both undergo extensive checks for errors and hydrostatic consistency.

TES global surveys from 2004-2008 are matched with radiosonde profiles from the NOAA ESRL database within 100 km and -0.5 hr to +1.5 hr. The tightly constrained time match is possible because the exact radiosonde release time is known. Times are offset so that, on average, the radiosonde has ascended to the middle troposphere by the time of the Aura overpass and TES retrieval.

Figure 7-1 shows comparisons of TES V006 TATM with NOAA ESRL radiosondes. Outliers have been removed by using an iterative 3-sigma rejection algorithm. The solid red line is the temperature bias (TES TATM minus $T_{radiosonde}$ with averaging kernel) and the dashed red line is the temperature rms. The blue line is the TES observation error (measurement error plus systematic error). For TES V006 TATM minus $T_{radiosonde}$ (with averaging kernel applied), the bias is approximately +0.4 K in the lower troposphere, decreasing to -0.6 K at 300 hPa in the upper troposphere. The rms is less than 1 K in the stratosphere and upper troposphere, but increases to 1.7 K in the lower troposphere. In clear sky conditions (average cloud effective optical depth less than 0.1), the bias improves near the surface (700 to 1000 hPa) but increases to +0.6 K at 500 hPa pressure level. There are slight day-to-night differences in the comparisons between TES V006 TATM and NOAA ESRL radiosondes (Figure 7-2). The bias in the lower troposphere (500 to 1000 hPa) is +0.5 K at daytime, but less at nighttime.

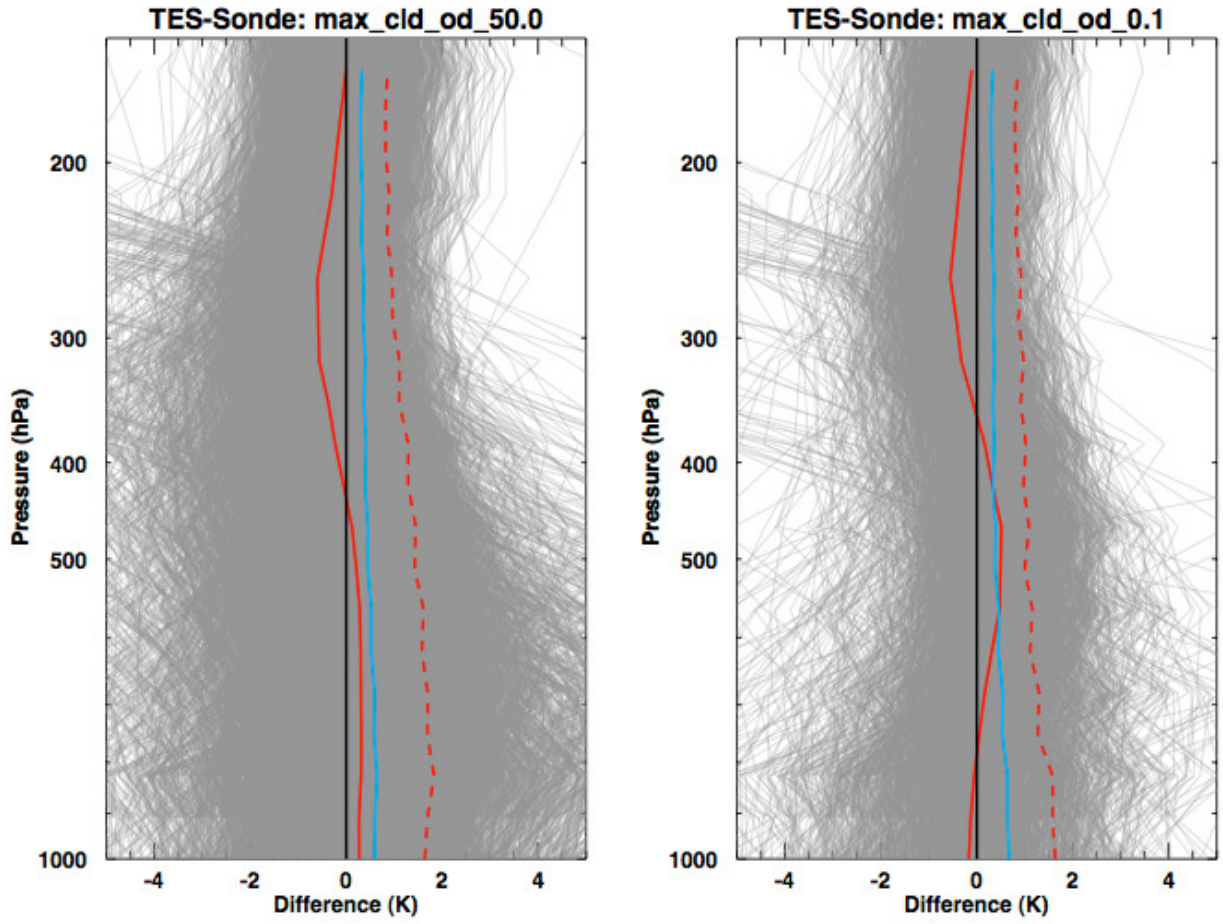

Figure 7-1 Temperature differences between TES V006 TATM and NOAA ESRL radiosondes with observation operator applied: (left) all good quality comparisons, (right) comparisons filtered by average cloud effective optical depth < 0.1. Shown are individual temperature differences (thin grey lines), bias (solid red line), rms (dashed red line), and the TES observation error (solid blue line). Figure prepared using idl code from Karen Cady-Pereira and the TES radiosonde comparison tool.

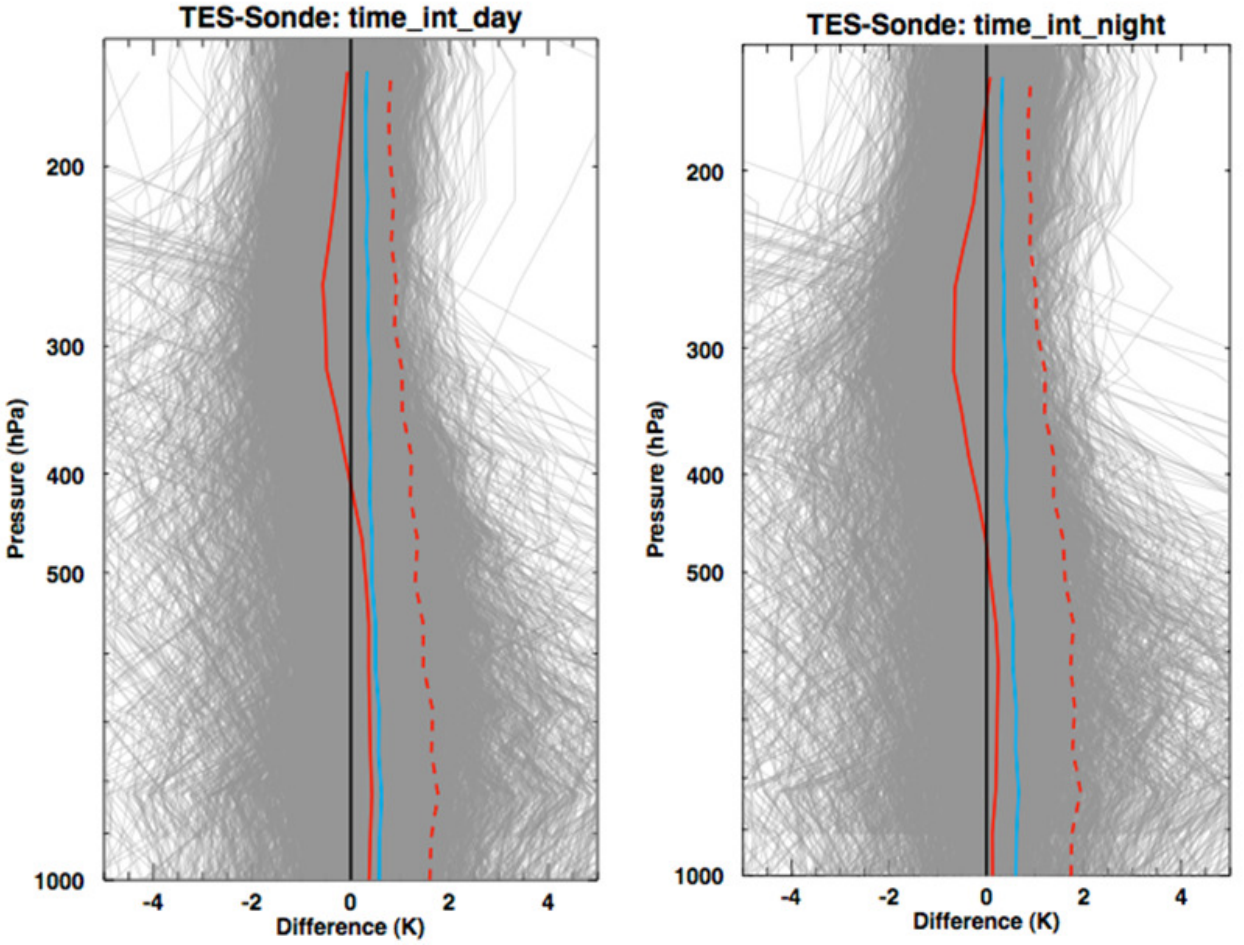

Figure 7-2 Temperature differences between TES V006 TATM and NOAA ESRL radiosondes with observation operator applied: (left) daytime comparisons, (right) nighttime comparisons. Same color lines as Figure 7-1. Figure prepared using idl code from Karen Cady-Pereira and the TES radiosonde comparison tool.

7.5 TES Temperature Retrieval Stability 2006-2011

A recent design file memorandum (DFM) by J. Hegarty et al. (2012) presented an analysis of TES TATM retrieval stability over the lifetime of the TES instrument. An excerpt of that DFM is included below (Hegarty et al., 2012).

7.5.1 Background on retrieval stability

The TES retrievals have been validated with radiosondes, ozonsondes, aircraft measurements, and other satellite measurements (e.g. Osterman et al., 2007, 2008; Nasser et al., 2008; Richards et al., 2008; see http://tes.jpl.nasa.gov/documents/publications/ for a comprehensive list of studies). In addition, the radiance measurements within 30° of the equator were shown to be stable over a four year period from 2005 - 2009 (Connor et al., 2011). However, the TES instrument exceeded its five-year expected lifetime in 2009 and has since experienced several

age-related mechanical problems that have required some mitigating changes to its operations. The question arises as to whether these changes and any other age-related degradation of the instrument may have altered the retrieval quality or its characteristics in any meaningful way. We present here a long-term evaluation of TES retrieval stability using TATM retrievals from January 2006 – July 2011. TATM was chosen for the evaluation because it is the first parameter retrieved and its quality impacts the subsequent retrieval of all the other parameters.

7.5.2 Analysis and Results

The TES V005 TATM retrieval stability evaluation used global survey (GS) data in two geographical boxes referred to as the Tropical Pacific Box (10° S – 10° N, 160° W – 120° W) and the North Atlantic Box (30° N – 60° N, 60° W – 20° W). Though both boxes were centered over oceans, the North Atlantic Box intersected the North American and European land masses and both contained some island points. To avoid the complicating factor introduced by highly variable land surface emissivity all the land points within the boxes were screened from the evaluation data set using the TES surface type flag. Additionally points were screened for quality using the TES retrieval quality flag and for optically thick clouds using an average cloud effective optical depth threshold of 0.5.

To evaluate the retrieval stability the monthly mean and standard deviation of the TATM residual between TES and the Global Modeling and Data Assimilation Office (GMAO) GEOS-5 model (Rienecker et al., 2008), which provides the first guess and a priori for the TATM retrieval, were calculated. These statistics were produced for the surface and at four standard TES pressure levels; 825 hPa, 464 hPa, 261 hPa, and 100 hPa. The statistics for both geographical boxes, shown in Figure 7-3, indicate only minor month-to-month variability and no substantial trends over the entire five-and-a-half year period. The TES TATM retrieval in the Tropical Pacific Box had an average bias of -0.8 K at the surface and -1.0 K near the tropopause (100 hPa). In the North Atlantic Box the TES surface and tropopause (261 hPa) TATM were also biased by -0.6 K and -0.8 K, respectively. There were no substantial biases at other levels.

The standard deviation of the residual was generally smaller than the standard deviation of the GMAO GEOS-5 but larger than the TES estimated measurement error (Figure 7-3). The exception was for the surface temperature (TSUR) in the Tropical Pacific Box which had a slight increase in standard deviation early in 2011 to a maximum value of 2.13 K in April. The TSUR bias also decreased to its lowest value of -1.4 K during February of 2011 and was -1.25 during April 2011. However, both statistics relaxed back to values more in line with those of the entire period during the months of May - July of 2011.

Overall, based on this analysis it appears that the TES retrieval quality has remained stable from 2006 - 2011.

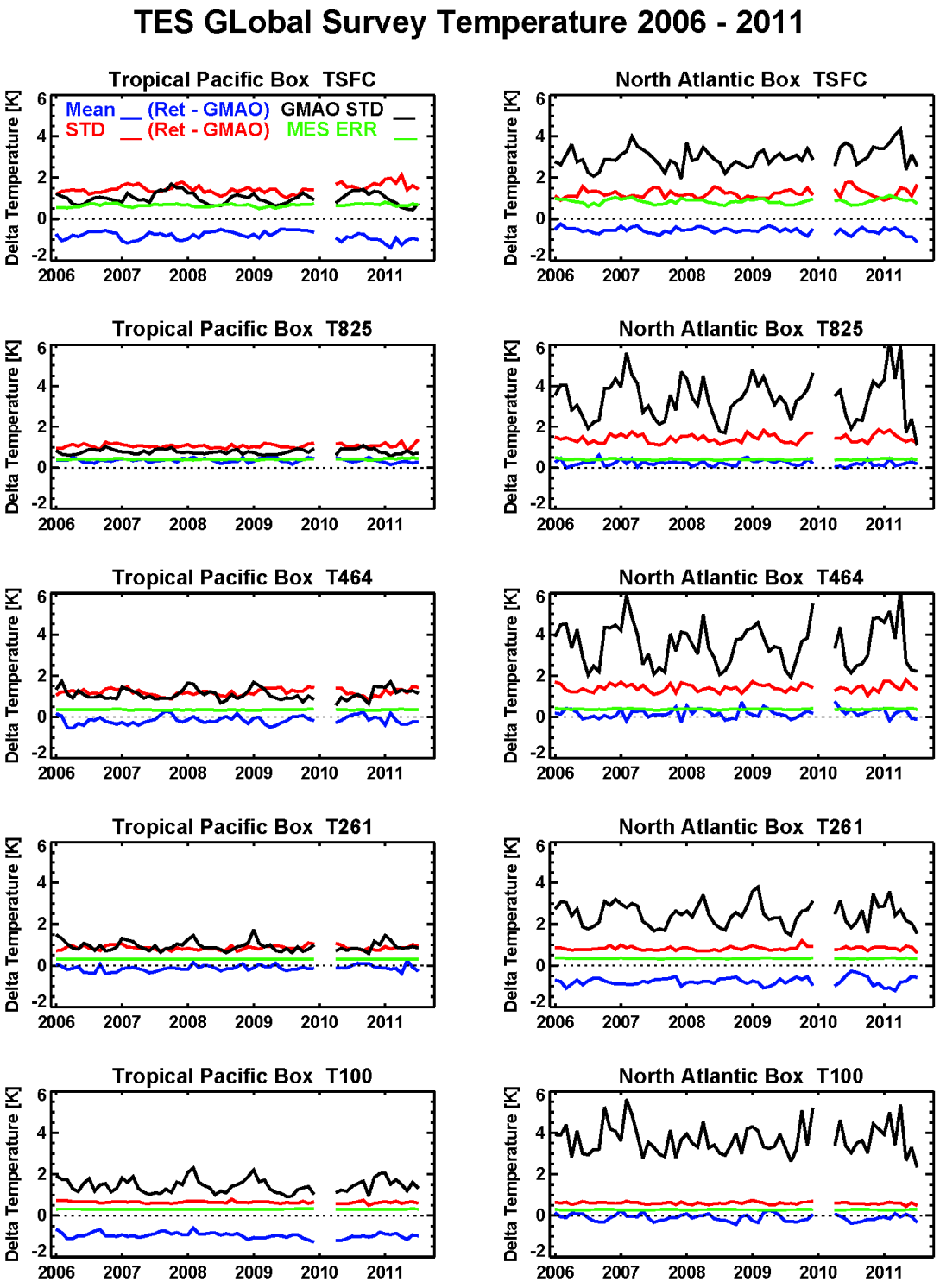

Figure 7-3 Mean (blue) and standard deviation (red) of TES TATM minus GMAO GEOS-5 temperature residuals with GMAO standard deviation (GMAO STD, black) and TES measurement error estimate (TES ERR, green) for the surface (TSUR), 825, 464, 261, and 100 hPa pressure levels. Figure courtesy of J. Hegarty, AER (Hegarty et al., 2012).

7.6 References

7.6.1 TES Temperature References

[1] Hegarty, J., S.S. Kulawik, V.H. Payne, K.E. Cady-Pereira, TES Temperature Retrieval Stability 2006-2011, TES Internal DFM, 2012.

7.6.2 TES References

[2] Bowman, K. W., J. Worden, T. Steck, H. M. Worden, S. Clough, and C. Rodgers (2002), Capturing time and vertical variability of tropospheric ozone: A study using TES nadir retrievals, *J. Geophys. Res., 107, No. D23*, 4723, (doi:10.1029/2002JD002150) December 14, 2002.

[3] Bowman, K. W., C. D. Rodgers, S. S. Kulawik, J. Worden, E. Sarkissian, G. Osterman, T. Steck, M. Luo, A. Eldering, M. W. Shephard, H. Worden, M. Lampel, S. A. Clough, P. Brown, C. Rinsland, M. Gunson, R. Beer (2006), Tropospheric emission spectrometer: Retrieval method and error analysis, *IEEE Trans. Geosci. Remote Sens., 44(5)*, 1297-1307, May 2006.

[4] Connor, T.C., M.W. Shephard, V.H. Payne, K.E. Cady-Pereira, S.S. Kulawik, M. Luo, G. Osterman, M. Lampel (2011), Long-term stability of TES satellite radiance measurements, *Atmospheric Measurement Techniques, 4,* doi:10.5194/amt-4-1481-2011, 1481–1490, July 25, 2011.

[5] Robert Herman and Susan Kulawik (editors), Kevin Bowman, Karen Cady-Pereira, Annmarie Eldering, Brendan Fisher, Dejian Fu, Robert Herman, Daniel Jacob, Line Jourdain, Susan Kulawik, Ming Luo, Ruth Monarrez, Gregory Osterman, Susan Paradise, Vivienne Payne, Sassaneh Poosti, Nigel Richards, David Rider, Douglas Shepard, Mark Shephard, Felicia Vilnrotter, Helen Worden, John Worden, Hyejung Yun, Lin Zhang (2013), Earth Observing System (EOS) Tropospheric Emission Spectrometer (TES) Level 2 (L2) Data User's Guide (Up to & including Version 6 data), Version 6.0, JPL Internal Report D-38042, November 5, 2013.

[6] Robert Herman and Gregory Osterman (editors), Christopher Boxe, Kevin Bowman, Karen Cady-Pereira, Tony Clough, Annmarie Eldering, Brendan Fisher, Dejian Fu, Robert Herman, Daniel Jacob, Line Jourdain, Susan Kulawik, Michael Lampel, Qinbin Li, Jennifer Logan, Ming Luo, Inna Megretskaia, Ray Nassar, Gregory Osterman, Susan Paradise, Vivienne Payne, Hank Revercomb, Nigel Richards, Mark Shephard, Dave Tobin, Solene Turquety, Felicia Vilnrotter, Kevin Wecht, Helen Worden, John Worden, Lin Zhang (2012), Earth Observing System (EOS) Tropospheric Emission Spectrometer (TES) Data Validation Report (Version F06_08, F06_09 data), Version 5.0, JPL Internal Report D-33192, April 8, 2012.

[7] Kulawik, S. S., G. B. Osterman, D. B. A. Jones, and K. W. Bowman (2006), Calculation of Altitude-Dependent Tikhonov Constraints for TES Nadir Retrievals, *IEEE Transactions on Geoscience and Remote Sensing, 44 (No.5),* Special Issue on Aura, 1334-1342, May 2006.

[8] Nassar, R., J.A. Logan, H.M. Worden, I.A. Megretskaia, K.W. Bowman, G.B. Osterman, A.M. Thompson, D.W. Tarasick, S. Austin, H. Claude, M.K. Dubey, W.K.

Hocking, B.J. Johnson, E. Joseph, J. Merrill, G.A. Morris, M. Newchurch, S.J. Oltmans, F. Posny, F.J. Schmidlin, H. Vömel, D.N. Whiteman, J.C. Witte (2008), Validation of Tropospheric Emission Spectrometer (TES) Nadir Ozone Profiles Using Ozonesonde Measurements, *J. Geophys. Res. 113*, D15S17, (doi:10.1029/2007JD008819), May 7, 2008.

[9] Osterman, G., S.S. Kulawik, H.M. Worden, N.A.D. Richards, B.M. Fisher, A. Eldering, M.W. Shephard, L. Froidevaux, G. Labow, M. Luo, R.L. Herman, K.W. Bowman, A.M. Thompson (2008), Validation of Tropospheric Emission Spectrometer (TES) Measurements of the Total, Stratospheric and Tropospheric Column Abundance of Ozone, *J. Geophys. Res., 113*, D15S16, (doi:10.1029/2007JD008801) May 7, 2008.

[10] Osterman, G. B. (editor), K. Bowman, K. Cady-Pereira, T. Clough, A. Eldering, B. Fisher, R. Herman, D. Jacob, L. Jourdain, S. Kulawik, M. Lampel, Q. Li, J. Logan, M. Luo, I. Megretskaia, R. Nassar, G. Osterman, S. Paradise, V. Payne, H. Revercomb., N. Richards, M. Shephard, D. Tobin, S. Turquety, F. Vilnrotter, H. Worden, J. Worden, and L. Zhang (2007), Earth Observing System (EOS) Tropospheric Emission Spectrometer (TES) Data Validation Report (Version F04_04 data), Version 3.0, JPL Internal Report D-33192, November 5, 2007, available at: https://eosweb.larc.nasa.gov/project/tes/validation

[11] Richards, N.A.D., G.B. Osterman, E.V. Browell, J.W. Hair, M. Avery and Q.Li, Validation of Tropospheric Emission Spectrometer ozone profiles with aircraft observations during the Intercontinental Chemical Transport Experiment–B, *J. Geophys. Res., 113*, D16S29, (doi:10.1029/2007JD008815) May 23, 2008.

[12] Worden, J., S. S. Kulawik, M. W. Shephard, S. A. Clough, H. Worden, K. Bowman, and A. Goldman (2004), Predicted errors of tropospheric emission spectrometer nadir retrievals from spectral window selection, *J. Geophys. Res., 109*, D09308, May 15, 2004.

7.6.3 General References

[13] Bloom, S., A. da Silva, D. Dee, M. Bosilovich, J.-D. Chern, S. Pawson, S. Schubert, M. Sienkiewicz, I. Stajner, W.-W. Tan, M.-L. Wu (2005). Documentation and Validation of the Goddard Earth Observing System (GEOS) Data Assimilation System - Version 4. *Technical Report Series on Global Modeling and Data Assimilation 104606, Vol. 26,* 187 pages, April 2005. Available from (paste entire link including pdf into browser):

http://ntrs.nasa.gov/archive/nasa/casi.ntrs.nasa.gov/20050175690_2005173043.pdf.

[14] Divakarla, M. G., C. D. Barnet, M. D. Goldberg, L. M. McMillin, E. Maddy, W. Wolf, L. Zhou, and X. Liu (2006), Validation of Atmospheric Infrared Sounder temperature and water vapor retrievals with matched radiosonde measurements and forecasts, *J. Geophys. Res., 111,* D09S15, (doi: 10.1029/2005JD006116) April 6, 2006.

[15] Nevison, C. D., N. M. Mahowald, S. C. Doney, I. D. Lima, G. R. van der Werf, J. T. Randerson, D. F. Baker, P. Kasibhatla, and G. A. McKinley (2008), Contribution of ocean, fossil fuel, land biosphere and biomass burning carbon fluxes to seasonal and interannual variability in atmospheric CO_2, *J. Geophys. Res., 113,* G01010, (doi:10.1029/2007JG000408) February 12, 2008.

[16] Rienecker, M. M., M. J. Suarez (editor), R. Todling, J. Bacmeister, L. Takacs, H.-C. Liu, W. Gu, M. Sienkiewicz, R. D. Koster, R. Gelaro, I. Stajner and J.E. Nielson (2008), The GEOS-5 Data Assimilation System- Documentation of Versions 5.0.1, 5.1.0, and 5.2.0 *NASA Technical Report Series on Global Modeling and Data Assimilation 104606, Vol.27.*, December 2008.

[17] Tobin, D. C., H. E. Revercomb, R. O. Knuteson, B. M. Lesht, L. L. Strow, S. E. Hannon, W. F. Felt, L. A. Moy, E. J. Fetzer, and T. S. Cress (2006), Atmospheric Radiation Measurement site atmospheric state best estimates for Atmospheric Infrared Sounder temperature and water vapor retrieval validation, *J. Geophys. Res., 111,* doi: 10.1029/2005JD006103.

[18] Zhu, Y., and R. Gelaro (2008), Observation Sensitivity Calculations Using the Adjoint of the Gridpoint Statistical Interpolation (GSI) Analysis System, *Monthly Weather Review, Volume 136, Issue 1*, pp. 335-351, (DOI:10.1175/MWR3525.1) January 2008 - available from http://gmao.gsfc.nasa.gov/pubs/ref/archive/ref_2008.php.

8. Sea Surface Temperature

TES retrievals of sea surface temperature rely on validation of previous data versions, as described in detail in the TES Validation Report V003 (Osterman et al., 2007). V003 sea surface temperature (SST) was compared with Reynolds Optimally Interpolated (ROI) weekly SST for the time period Jan 2005 through July 2008. In clear sky conditions, TES SST versus ROI has a bias of -0.04 K (daytime) and -0.20 K (nighttime). The day/night difference is within the uncertainty of the predicted value based on ocean skin versus ocean bulk SST [D. Kerola, pers. comm.].

8.1 References

8.1.1 TES References

[1] Osterman, G., (editor), K. Bowman, K. Cady-Pereira, T. Clough, A. Eldering, B. Fisher, R. Herman, D. Jacob, L. Jourdain, S. Kulawik, M. Lampel, Q. Li, J. Logan, M. Luo, I. Megretskaia, R. Nassar, G. Osterman, S. Paradise, V. Payne, H. Revercomb., N. Richards, M. Shephard, D. Tobin, S. Turquety, F. Vilnrotter, H. Worden, J. Worden, and L. Zhang (2007), Earth Observing System (EOS) Tropospheric Emission Spectrometer (TES) Data Validation Report (Version F04_04 data), Version 3.0, JPL Internal Report D-33192, November 5, 2007

9. Water Vapor

The main objectives for obtaining retrieved water vapor from TES are to measure the isotopic ratio of HDO/H_2O and to obtain the most likely state of the atmosphere within the field-of-view. This applies whether water vapor is a tracer of air mass, of chemical interest, or whether it is an interferent. A number of comparisons have been made between TES V006 water vapor and other data sources, including radiosondes and aircraft. More than most species retrieved by TES, tropospheric water vapor is highly variable over short distances. Therefore, the key to water validation is to perform statistics on large datasets to determine possible biases. The most mature of all these analyses is the comparison to radiosondes and that work is presented in this document.

9.1 Executive Summary

TES V006 H_2O is typically biased high relative to V005 H_2O. The changes are largely due to much higher H_2O mixing ratios in the a priori constraint, GMAO GEOS 5.9.1 (in Version 6) versus GEOS 5.2 (in Version 5). The largest effect is seen at low degrees of freedom for signal (DOFS). The user should select data using the master data quality flag ("speciesretrievalquality") and filter by DOFS. Some minor changes are due to new spectroscopic parameters in the ABSCO tables for H_2O, a difference of at most a few percent. Comparisons have been made between TES V006 water vapor profiles and radiosonde profiles. Relative to nighttime radiosonde profiles, TES V006 water vapor is approximately 18% low at 800 hPa in the lower troposphere, 6% low at 700 to 500 hPa in the middle troposphere, and 20% low at 250 hPa in the upper troposphere. The rms increases from 30% in the lower troposphere to 50% in the upper troposphere. Results are similar for both land and water surfaces.

9.2 Background

TES uses an optimal estimation non-linear least squares retrieval (Bowman et al., 2006). TES versions V005 and V006 use a wide band retrieval (1100 to 1330 cm^{-1}) to jointly estimate the mixing ratios of four species: HDO, H_2O, CH_4, and N_2O (Worden et al., 2012). This retrieval dramatically improves the vertical resolution in the lower troposphere for water vapor, compared to V004.

9.3 A priori constraint vector

For each individual sequence and scan, the initial guess in the TES retrieval algorithm is set equal to an a priori profile (constraint vector). The TES V006 a priori constraint vectors come from NASA's Goddard Earth Observing System (GEOS) data assimilation system GEOS-5 (Rienecker et al., 2008). What is new in TES V006 is that the a priori constraint comes from the new GMAO GEOS version 5.9.1 processing stream. The TES V005 a priori constraint was based on the previous GMAO GEOS version 5.2. GEOS-5 data are produced by the Global Modeling and Assimilation Office (GMAO) at the NASA Goddard Space Flight Center (GSFC), on a 0.625° longitude by 0.5° latitude grid. GEOS-5 data are then interpolated to the locations and pressure levels of TES retrievals. The a priori covariance matrices used for retrieval regularization are described in Bowman et al. (2006). GEOS-5 assimilates a wide range of operational satellite data and in situ radiosonde measurements. Radiosonde profiles are strong

constraints on the thermal structure and winds throughout the troposphere, with an emphasis on continental regions where the observing network is denser. Space-based observations include the High Resolution Infrared Sounders (HIRS) and Advanced Microwave Sounders (AMSU) instruments on NOAA's operational sounders, which directly constrain temperature and moisture. GEOS-5 includes a direct assimilation of radiances from AMSU and HIRS in a three-dimensional variational assimilation, as well as radiances from the Advanced Infrared Sounder (AIRS) and AMSU instruments on NASA's EOS Aqua platform (Zhu and Gelaro, 2008).

9.4 Comparison of TES Water Vapor with Radiosondes

Radiosonde data come from a global database from the National Oceanic and Atmospheric Administration (NOAA) Earth System Research Laboratory (ESRL) Global Systems Division [M. Govett, pers. comm.]. The NOAA ESRL database combines the IGRA global data with North American Global Telecommunications Service (GTS) radiosonde observations. This database features the exact radiosonde launch time, which improves the temporal coincidence between TES and radiosonde significantly. The disadvantage of radiosondes is the spatial mismatch between the satellite retrieval footprint (8 km by 5 km for TES) and the radiosonde data (a vertical profile of in-situ measurement with no horizontal information). Coincidence constraints are TES-radiosonde matches within 100 km and -0.5 hours to +1.5 hours. The tightly constrained time match is possible because the exact launch time of the radiosonde is known. Times are offset so that, on average, the radiosonde has ascended to the middle troposphere by the time of the Aura overpass and TES retrieval. The TES observation operator (averaging kernel) has been applied to the radiosonde profiles, and standard water data quality flags applied to the TES retrieval (Herman and Kulawik (eds.), et al., TES Data User's Guide D-38042, 2013). Outliers have been removed by using an iterative three-sigma rejection algorithm. Figure 9-1 below shows the comparison between TES V006 water vapor and radiosondes for the cases of all cloud optical depths from 0 to 50 (left panel) and "clear sky" average cloud effective optical depth less than 0.1 (right panel). Not much difference is seen in the bias, but the rms is improved slightly in the clear sky case. The bias ranges from +10% to -10% in the lower troposphere, with a positive bias up to +10% in the middle troposphere at 400 hPa.

One complication with this comparison is that radiosondes have a daytime bias. For the standard radiosondes, Vaisala model RS-92, the accuracy of reported water vapor is degraded during daytime due to solar heating of the Relative Humidity sensor and consequent solar radiation error (Milosevich et al., 2006; Voemel et al., 2007). The radiosondes in the NOAA ESRL database have not been corrected for solar heating, as shown in Figure 9-2 below. Daytime radiosonde bias increases with height, up to 50% in the upper troposphere. In contrast, the nighttime radiosonde profiles have insignificant bias from the surface up to 300 hPa, relative to GMAO GEOS 5.9.1.

As a result, we use nighttime comparisons between TES and radiosondes for a statistical estimate of the TES water vapor bias and rms. In Figure 9-3, nighttime TES minus radiosonde comparisons are shown for land surface (left panel) and ocean surface (right panel). It is seen that TES has a dry bias relative to the radiosondes: TES V006 water vapor is approximately 18% low at 800 hPa in the lower troposphere, 6% low at 700 to 500 hPa in the middle troposphere, gradually changing to 20% low at 250 hPa in the upper troposphere. The rms increases from 30% in the lower troposphere to 50% in the upper troposphere. Results are similar for both land and water surfaces.

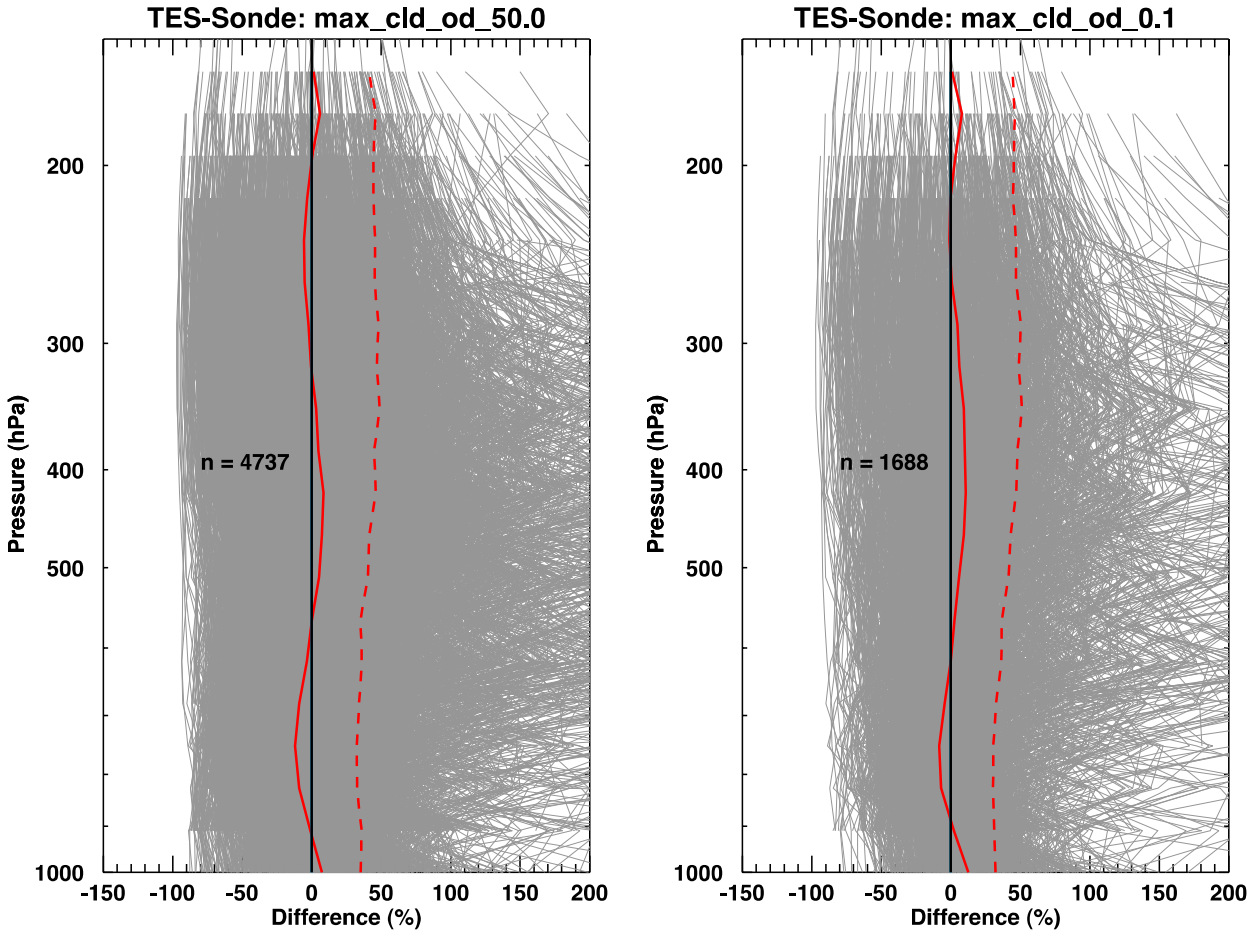

Figure 9-1 Water vapor percent differences between TES V006 retrievals and radiosondes (with averaging kernel applied) from the NOAA ESRL database. Matches are selected for TES geolocation coincidence within 100 km distance and -0.5 to +1.5 hours of radiosonde launch time. In each panel, n individual matches are shown (thin grey lines) with rms (dashed red lines) and bias (solid red lines). Percent differences are calculated as 100(TES-radiosonde)/TES. Figure prepared using idl code from K. Cady-Pereira and the TES sonde comparison tool.

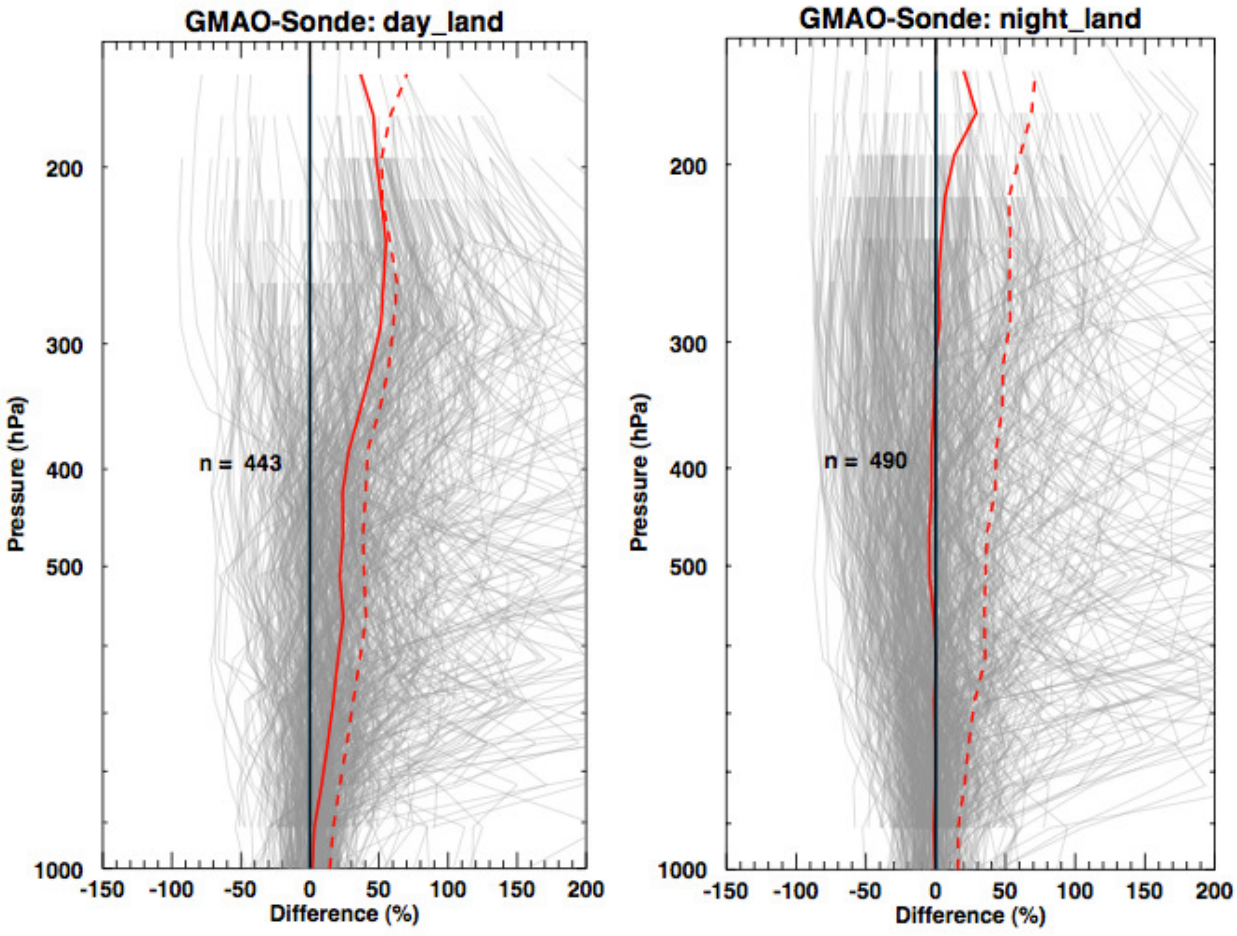

Figure 9-2 Water vapor percent differences between GMAO GEOS 5.9.1 and radiosondes from the NOAA ESRL database. This figure shows n individual matches (thin grey lines) with rms (dashed red lines) and bias (solid red lines). The radiosondes have a significant bias during daytime, but not at night.

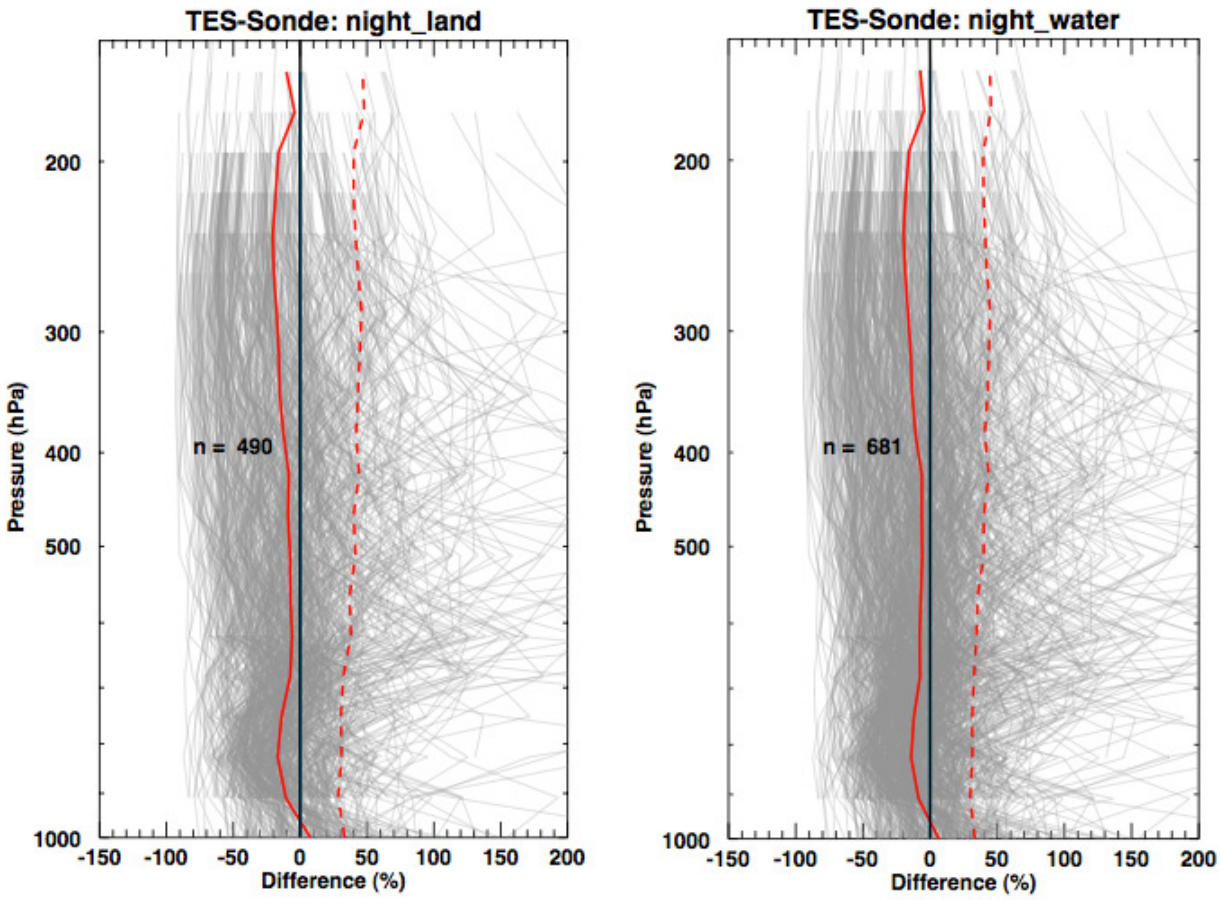

Figure 9-3 Water vapor percent differences between TES V006 retrievals and radiosondes (with averaging kernel applied) from the NOAA ESRL database (similar to Figure 9-1). Figure prepared using idl code from K. Cady-Pereira and the TES sonde comparison tool.

9.5 References

9.5.1 TES H_2O References

[1] Worden, J., S. Kulawik, C. Frankenberg, V. Payne, K. Bowman, K. Cady-Peirara, K. Wecht, J.-E. Lee, D. Noone (2012), Profiles of CH_4, HDO, H_2O, and N_2O with improved lower tropospheric vertical resolution from Aura TES radiances, *Atmospheric Measurement Techniques, 5, 397–411, 2012*, doi:10.5194/amt-5-397-2012, February 20, 2012.

9.5.2 TES References

[2] Bowman K. W., C. D. Rodgers, S. S. Kulawik, J. Worden, E. Sarkissian, G. Osterman, T. Steck, M. Lou, A. Eldering, M. Shephard, H. Worden, M. Lampel, S. A. Clough, P. D. Brown, C. P. Rinsland, M. Gunson, and R. Beer (2006), Tropospheric emission

spectrometer: Retrieval method and error analysis, *IEEE Transactions on Geoscience and Remote Sensing, 44(5)*, 1297-1307, May 2006.

[3] Robert Herman and Susan Kulawik (editors), Kevin Bowman, Karen Cady-Pereira, Annmarie Eldering, Brendan Fisher, Dejian Fu, Robert Herman, Daniel Jacob, Line Jourdain, Susan Kulawik, Ming Luo, Ruth Monarrez, Gregory Osterman, Susan Paradise, Vivienne Payne, Sassaneh Poosti, Nigel Richards, David Rider, Douglas Shepard, Mark Shephard, Felicia Vilnrotter, Helen Worden, John Worden, Hyejung Yun, Lin Zhang (2013), Earth Observing System (EOS) Tropospheric Emission Spectrometer (TES) Level 2 (L2) Data User's Guide (Up to & including Version 6 data), Version 6.0, JPL Internal Report D-38042, November 5, 2013.

[4] Shephard, M. W., R.L. Herman, B.M. Fisher, K.E. Cady-Pereira, S. A. Clough, V. H. Payne, D.N. Whiteman, J. P. Comer, H. Vömel, L.M. Miloshevich, Ricardo Forno, M. Adam, G. B. Osterman, A. Eldering, J. R. Worden, L. R. Brown, H. M. Worden, S. S. Kulawik, D. M. Rider, A. Goldman, R. Beer, K. W. Bowman, C. D. Rodgers, M. Luo, C. P. Rinsland, M. Lampel, M. R. Gunson (2008), Comparison of Tropospheric Emission Spectrometer nadir water vapor retrievals with in situ measurements, *J. Geophys. Res., 113*, D15S24, (doi:10.1029/2007JD008822) May 16, 2008.

9.5.3 General References

[5] Bloom, S., A. da Silva, D. Dee, M. Bosilovich, J.-D. Chern, S. Pawson, S. Schubert, M. Sienkiewicz, I. Stajner, W.-W. Tan, M.-L. Wu (2005). Documentation and Validation of the Goddard Earth Observing System (GEOS) Data Assimilation System - Version 4. *Technical Report Series on Global Modeling and Data Assimilation 104606, Vol. 26,* 187 pages, April 2005. Available from (paste entire link including pdf into browser):

http://ntrs.nasa.gov/archive/nasa/casi.ntrs.nasa.gov/20050175690_2005173043.pdf

[6] Rienecker, M. M., M. J. Suarez (editor), R. Todling, J. Bacmeister, L. Takacs, H.-C. Liu, W. Gu, M. Sienkiewicz, R. D. Koster, R. Gelaro, I. Stajner and J.E. Nielson (2008), The GEOS-5 Data Assimilation System- Documentation of Versions 5.0.1, 5.1.0, and 5.2.0 *NASA Technical Report Series on Global Modeling and Data Assimilation 104606, Vol.27.*, December 2008.

[7] Miloshevich, L.M., H. Voemel, D.N. Whiteman, B.M. Lesht, F.J. Schmidlin, and F. Russo (2006), Absolute accuracy of water vapor measurements from six operational radiosonde types launched during AWEX-G, and implications for AIRS validation. *J. Geophys. Res., 111,* D09S10, doi:10.1029/2005JD006083, 2006.

[8] Voemel, H., H. Selkirk, L. Miloshevich, J. Valverde-Canossa, J. Valdes, E. Kyro, R. Kivi, W. Stolz, G. Peng, and J.A. Diaz (2007), Radiation Dry Bias of the Vaisala RS92 Humidity Sensor, *J. Atmos. Ocean. Tech., 24,* pp. 953-963, doi: 10.1175/JTECH2019.1, 2007.

[9] Zhu, Y., and R. Gelaro (2008), Observation Sensitivity Calculations Using the Adjoint of the Gridpoint Statistical Interpolation (GSI) Analysis System, *Monthly Weather Review, Volume 136, Issue 1*, pp. 335-351, (DOI:10.1175/MWR3525.1) January 2008 - available from http://gmao.gsfc.nasa.gov/pubs/ref/archive/ref_2008.php.

10. HDO/H_2O

10.1 Comparison of V006 to V005 HDO/H_2O

TES V006 estimates of HDO/H_2O have been compared to V005, as shown in Figure 10-1 below. Differences are mostly uniform across all latitudes. In the free troposphere, V006 is biased slightly lower than V005 by -1.1 per mil. In the boundary layer, however, V006 is biased *higher* than V005 by approximately +6 per mil.

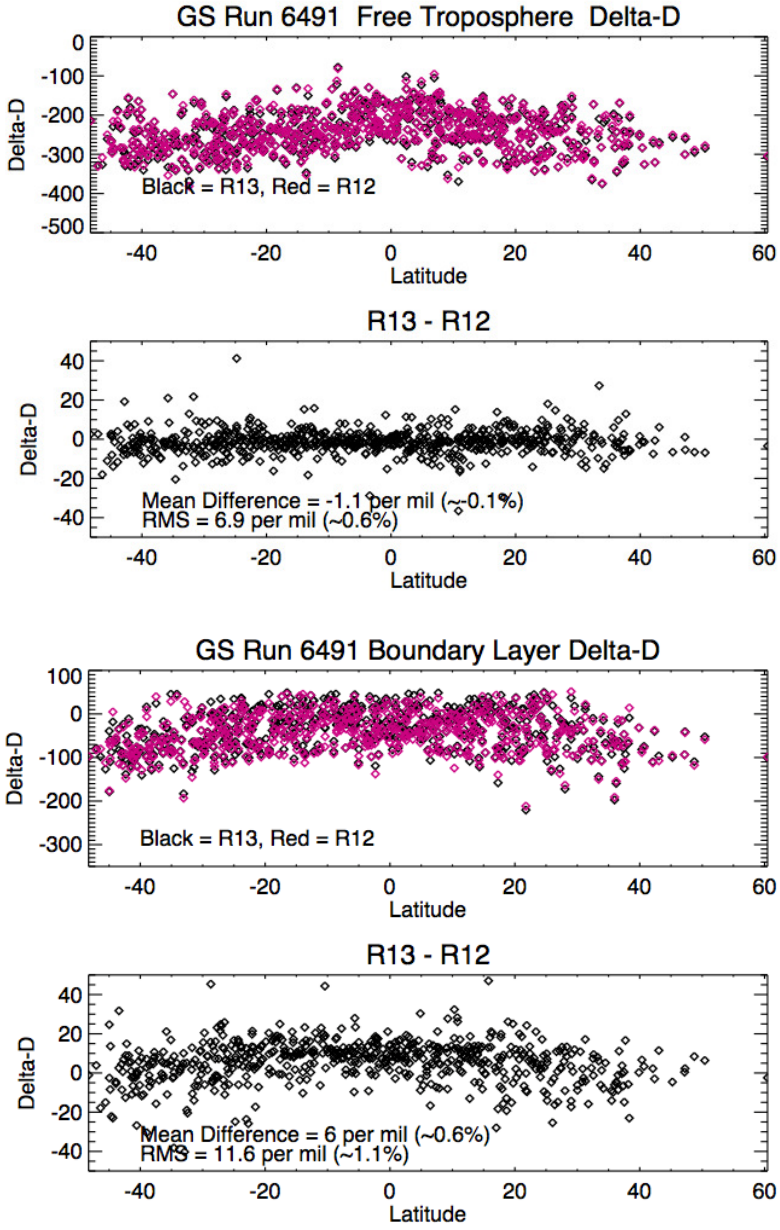

Figure 10-1 Comparisons of TES V006 ("R13") and V005 ("R12") delta-D isotopic signature of HDO/H_2O from Global Survey runid 6491. (botton panel) Difference between V006 and

V005 HDO/H_2O estimates for the overlapping data shown in the top panel. Delta-D δ-D is defined as 1000(HDO/H_2O/3.11x10^{-4} - 1.).

V006 and V005 estimates of HDO/H2O show considerable sensitivity to the isotopic composition of water vapor with typically DOFS~2 in the tropics and DOFS~1 at high latitudes. This increased sensitivity allows the TES estimates to resolve lower tropospheric and mid-tropospheric variability of the HDO/H2O vapor ratio (see Worden et al., 2012, and Herman et al., 2014) with the expense of increased uncertainty over tropical oceans.

We find that the HDO/H2O estimates are consistent with the previous TES release within the altitude range where the sensitivity overlaps. For validation of V005 HDO/H2O, we refer the reader to R. Herman et al. (2014). For validation of V004 HDO/H2O, we refer the reader to J. Worden et al. (2011).

10.2 References

10.2.1 TES HDO/H_2O References

[1] Herman, R. L., J. E. Cherry, J. Young, J. M. Welker, D. Noone, S. S. Kulawik, and J. Worden (2014), Aircraft validation of Aura Tropospheric Emission Spectrometer retrievals of HDO and H_2O. *Atmos. Meas. Tech. Discuss., 7*, pp. 3801-3833, doi: 10.5194/amtd-7-3801-2014, 2014, April 14, 2014.

[2] Worden, J., D. Noone, J. Galewsky, A. Bailey, K. Bowman, D. Brown, J. Hurley, S. Kulawik, J. Lee, M. Strong (2011), Estimate of bias in Aura TES HDO/H_2O profiles from comparison of TES and in situ HDO/H_2O measurements at the Mauna Loa observatory, *Atmospheric Chemistry and Physics, 11,* pp. 4491–4503, doi:10.5194/acp-11-4491-2011, May 12, 2011.

10.2.2 TES References

[3] Worden, J., S. Kulawik, C. Frankenberg, V. Payne, K. Bowman, K. Cady-Peirara, K. Wecht, J.-E. Lee, D. Noone (2012), Profiles of CH_4, HDO, H_2O, and N_2O with improved lower tropospheric vertical resolution from Aura TES radiances, *Atmospheric Measurement Techniques, 5,* pp. 397–411, 2012, doi:10.5194/amt-5-397-2012, February 20, 2012.

11. Nadir Methane

In order to assess the data quality of the Version 6 CH_4 product we compared Version 6 retrievals to in-situ aircraft profile measurements from the HIPPO I and II aircraft campaigns. The latitudinal range and number of TES/HIPPO coincidences provide sufficient information to characterize the latitudinal dependence of the bias and to validate the TES error estimates. The vertical information in the TES CH_4 product is limited, with less than 2 DOFS in the troposphere. Therefore, we choose to express comparisons in terms of a "representative tropospheric volume mixing ratio" (RTVMR) approach (Payne et al., 2009) in addition to showing profiles. All comparisons shown here include the application of the "N_2O correction" described in Worden et al. (2012). The TES Lite files include CH_4 profiles with the N_2O correction already applied, but the Level 2 HDF files only include the uncorrected CH_4 profiles.

Previously Version 5 CH_4 retrievals had been compared to the same in-situ aircraft data and had been found to generally capture the latitudinal gradient in CH_4 as observed by the HIPPO measurements (Wecht et al., 2012). In the Wecht et al. work, profiles were categorized according to the DOFS. For TES profiles with DOFS < 1.6, a single RTVMR value was calculated. For TES profiles with DOFS > 1.6, both lower and upper tropospheric representative mixing ratios (Y_U and Y_L respectively) were calculated. For the current assessment we repeat the validation of Version 5 and perform a new validation of Version 6 CH_4 using a single RTVMR value for all profiles regardless of DOFs.

Changes between Version 6 and Version 5 that could affect the CH_4 result include updates to spectroscopy and updates to various datasets used as initial guess and a priori information. Version 6 includes spectroscopy updates for CO_2, H_2O and CH_4. Of these, the CH_4 spectroscopy update is the only one expected to have an appreciable effect on the CH_4 retrievals. Version 6 also includes updated GMAO v5.9.1 fields (TES CH_4 retrievals are somewhat sensitive to changes in temperature and H_2O), as well as updates to the CH_4 and N_2O climatologies used as initial guess and a priori information.

The TES retrievals were matched with the HIPPO profiles using a coincidence window of 750 km and +/- 24 hours following the procedure described in Wecht et al. (2012). After the matches were completed a final screening was applied to the pairs to remove those for which the stratosphere exerted too strong an influence on the tropospheric CH_4 retrieval. The screening removed all pairs for which the ratio of the sum of the 560 hPa CH_4 averaging kernel (AK) above the tropopause to the sum of the 560 hPa CH_4 AK for the entire vertical column was greater than or equal to 0.2. Based on the prototype results for Version 6 and lower tropospheric results for Version 5, we also apply an additional global bias correction to the TES profiles equal to 0.015 times the averaging kernel to minimize the bias. The averaging kernel-based bias correction approach is based on a similar correction for HDO in Worden et al. (2012). This approximate bias correction will be further investigated in an upcoming validation paper on the Version 6 retrievals (Alvarado et al., 2014, *manuscript in preparation*). After this correction is applied, the Version 5 RTVMR is still biased high with respect to HIPPO measurements by 14.0 ppbv with an error standard deviation of 21.3 ppbv (Table 11-1), while Version 6 only has a small negative bias of -0.3 ppbv and an error standard deviation of 19.5 ppbv after this

correction. Note that a similar correction to Version 5 could have resulted in a similar low bias, but this post hoc correction would have to have been much stronger for Version 5 than it is in Version 6.

Table 11-1 TES Version 5 and Version 6 TES - HIPPO RTVMR validation statistics.

	Mean Bias (ppbv)	Standard Deviation (ppbv)	Number of TES Retrievals	Number of HIPPO Profiles
Version 5	14.0	21.3	329	168
Version 6	-0.3	19.5	302	149

The TES-HIPPO RTVMR differences do not show any apparent variation with latitude south of 40 °N for either Version 5 or Version 6 (Figure 11-1). However, between 40° N and 60° N the bias shifts downward by about 15 ppbv and the standard deviation increases by about 10 ppbv for both versions. The difference between Version 5 and Version 6 is more apparent in the plots of vertical error profiles (Figure 11-2). Version 5 retrievals have mean biases of approximately 30 ppbv in the upper troposphere and -15 ppbv in the lower troposphere. In contrast Version 6 retrievals have mean biases of approximately -10 ppbv in the upper troposphere and 5 ppbv in the lower troposphere. Overall the error bias and standard deviation are reduced in magnitude in Version 6 compared to Version 5 and this reduction occurs across latitude bands and throughout the depth of the troposphere.

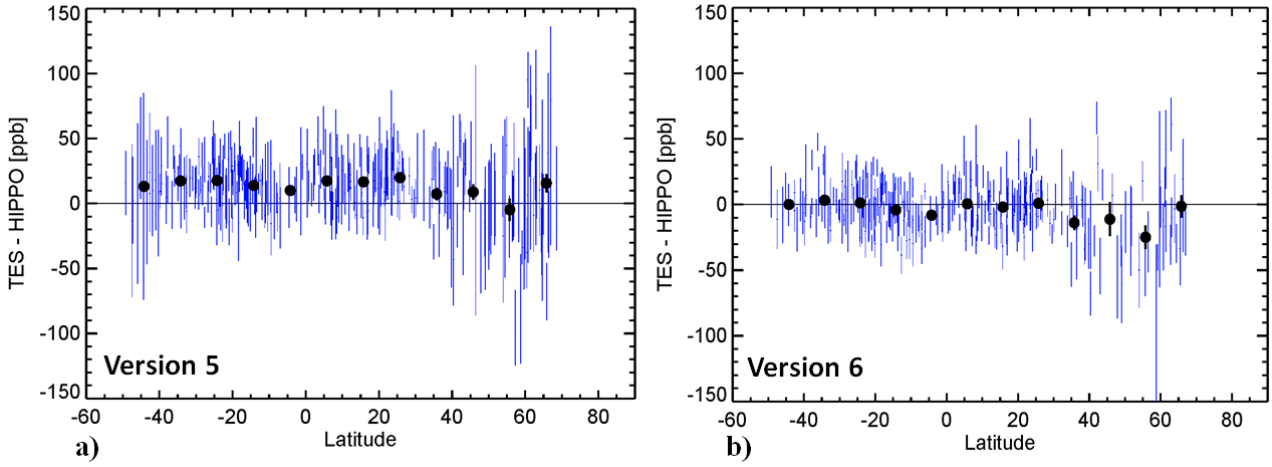

Figure 11-1 Latitudinal profile of TES- HIPPO CH4 RTVMR difference (ppbv) for a) Version 5 and b) Version 6 during HIPPO I and II. Black circles and vertical bars are the means and errors in the means (i.e., standard deviation divided by the square root of the number of points) of the TES-HIPPO RTVMR binned by 10° latitude. Blue vertical bars are the theoretical standard deviations reported in the TES retrievals.

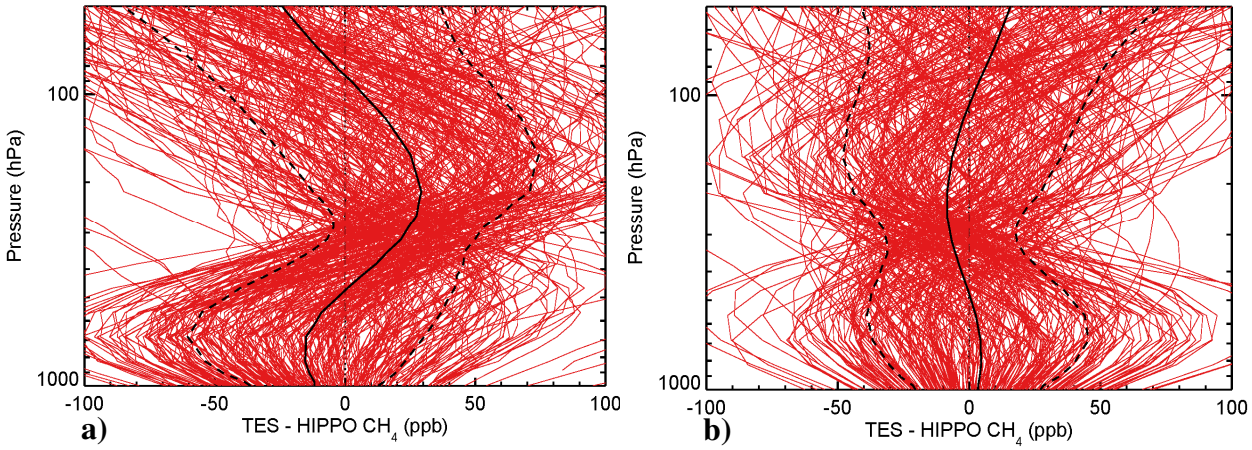

Figure 11-2 TES - HIPPO CH_4 vertical error profiles (ppbv) for HIPPO I and II for a) Version 5 and b) Version 6. The means and standard deviations are shown as black solid and dashed lines respectively.

11.1 References

11.1.1 TES CH_4 References

[1] Alvarado, M. J., V. H. Payne, K. E. Cady-Pereira, J. D. Hegarty, S. S. Kulawik, K. J. Wecht, J. R. Worden, S. C. Wofsy (2014), Impacts of updated spectroscopy and a priori profiles on retrievals of CH_4 from NASA Aura Tropospheric Emission Spectrometer (TES) observations evaluated with HIPPO observations, *manuscript in preparation*.

[2] Payne, V.H., S.A. Clough, M.W. Shephard, R. Nassar and J.A. Logan (2009), Information-centered representation of retrievals with limited degrees of freedom for signal: Application to methane from the Tropospheric Emission Spectrometer, *Journal of Geophysical Research: Atmospheres, Vol. 114 Issue D10*, May 27, 2009, D10307, (doi:10:1029/2008JD010155).

[3] Wecht, K.J., D.J. Jacob, S.C. Wofsy, E.A. Kort, J.R. Worden, S.S. Kulawik, D.K. Henze, M. Kopacz, and V. H. Payne (2012), Validation of TES methane with HIPPO aircraft observations: implications for inverse modeling of methane sources, *Atmos. Chem. Phys., 12,* pp. 1823–1832, doi:10.5194/acp-12-1823-2012, February 17, 2012.

[4] Worden, J., S. Kulawik, C. Frankenberg, V. Payne, K. Bowman, K. Cady-Pereira, K. Wecht, J.-E. Lee, and D. Noone (2012), Profiles of CH_4, HDO, H_2O, and N_2O with improved lower tropospheric vertical resolution from Aura TES radiances, *Atmospheric Measurement Techniques, 5,* pp. 397–411, doi:10.5194/amt-5-397-2012, February 20, 2012.

12. Cloud Products

TES retrievals of cloud products rely on validation of previous data versions, as described in detail in the TES Validation Report V005 (Herman and Osterman (eds.) et al., 2012).

12.1 References

12.1.1 TES References

[1] Robert Herman and Gregory Osterman (editors), Christopher Boxe, Kevin Bowman, Karen Cady-Pereira, Tony Clough, Annmarie Eldering, Brendan Fisher, Dejian Fu, Robert Herman, Daniel Jacob, Line Jourdain, Susan Kulawik, Michael Lampel, Qinbin Li, Jennifer Logan, Ming Luo, Inna Megretskaia, Ray Nassar, Gregory Osterman, Susan Paradise, Vivienne Payne, Hank Revercomb, Nigel Richards, Mark Shephard, Dave Tobin, Solene Turquety, Felicia Vilnrotter, Kevin Wecht, Helen Worden, John Worden, Lin Zhang (2012), Earth Observing System (EOS) Tropospheric Emission Spectrometer (TES) Data Validation Report (Version F06_08, F06_09 data), Version 5.0, JPL Internal Report D-33192, April 8, 2012.

13. Carbon Dioxide Validation

13.1 Overview of current validation status of TES V006 CO_2

TES CO_2 is retrieved between 40S and 45N, with average cloud optical depth < 0.5, among other tests, for good quality. On average, TES CO_2 has an average of 0.65 degree of freedom for signal (DOFS) – with the most DOFS for daytime land cases (which can be on the order of 1 DOFS) and the least for nighttime or winter land cases (which can be on the order of 0.3 DOFS). Ocean targets (day or night) have intermediate DOFS with about 0.8 DOFS. The averaging kernel indicates sensitivity between the surface to above 100 mb, with the most sensitivity between about 700 and 300 mb, peaking at about 650 mb. Although a profile is retrieved and has been validated, there is very little independent information at the different profile levels and it is critical to utilize the provided averaging kernel when using TES data. The previous version, TES V005 CO_2 has been compared with aircraft vertical profiles over the Pacific from the HIAPER (High-Performance Instrumented Airborne Platform for Environmental Research) Pole-to-Pole Observation (HIPPO) program (Wofsy et al., 2011) and over land at the SGP Arm site (Riley et al., 2009). Further details of this validation can be found in Kulawik et al. (2012). The HIPPO analysis has been done with the processed PGE (Product Generation Executive) V006 data, but the SGP analysis requires a full time series of TES at the SGP site and will need to await a more complete V006 dataset. Analysis of the PGE comparisons to HIPPO using the corrected values in the TES Lite product and a monthly regional mean, +- 5 degrees in latitude, +- 10 degrees in longitude and +- 15 days in time, show about a 1.0 ppm error and an overall 0.0 +- 0.6 ppm bias. There are some outliers in these monthly mean values. The single target error for TES CO_2 in the mid-Troposphere is on the order of 8 ppm, however averaging over 20 degrees longitude, 10 degrees latitude, and 1 month results in errors on the order of 1.0 ppm over both ocean and land targets. The Lite product has corrections applied to the observation error (increased by 1.5^2) and to the Averaging Kernel. The details of the correction to the Averaging Kernel are found in Kulawik et al. (2012) which involves a pressure-dependent scale factor. Although the TES CO_2 product is modest both in sensitivity and coverage, Nassar et al. (2011) found that TES added information to the surface flask measurements and is useful for estimating fluxes, both separately, and jointly with flask measurements.

13.2 Differences between the V006 and V005 retrievals

V006 has spectroscopy updates from Lamouroux et al. (2010). Testing indicated a neutral impact on the CO_2 results. Given that the spectroscopic community regards Lamouroux et al. (2010) an improvement over our previous spectroscopy (Niro et al., 2005) we updated to Lamouroux et al. (2010). Note that inconsistency between the v2 and laser band spectroscopy was seen with both sets of spectroscopic parameters. Comparison of v005 and v006 results shows v006 is higher than v005 by ~1 ppm. After 2010, the bias is ~0.5 ppm.

13.3 Differences between the V005 and V004 retrievals

This is the first version of this product, although TES prototype CO_2 has been shown and published in, e.g. Nassar et al. (2011) and Kulawik et al. (2010). The improvement over the

previous prototype results is most seen over land, with improved correlations and reduced errors so that the predicted and actual errors are now reasonably consistent over land as well as ocean. Both land and ocean results are usable for V005.

13.4 Comparisons to HIPPO-1, HIPPO-2 and HIPPO-3

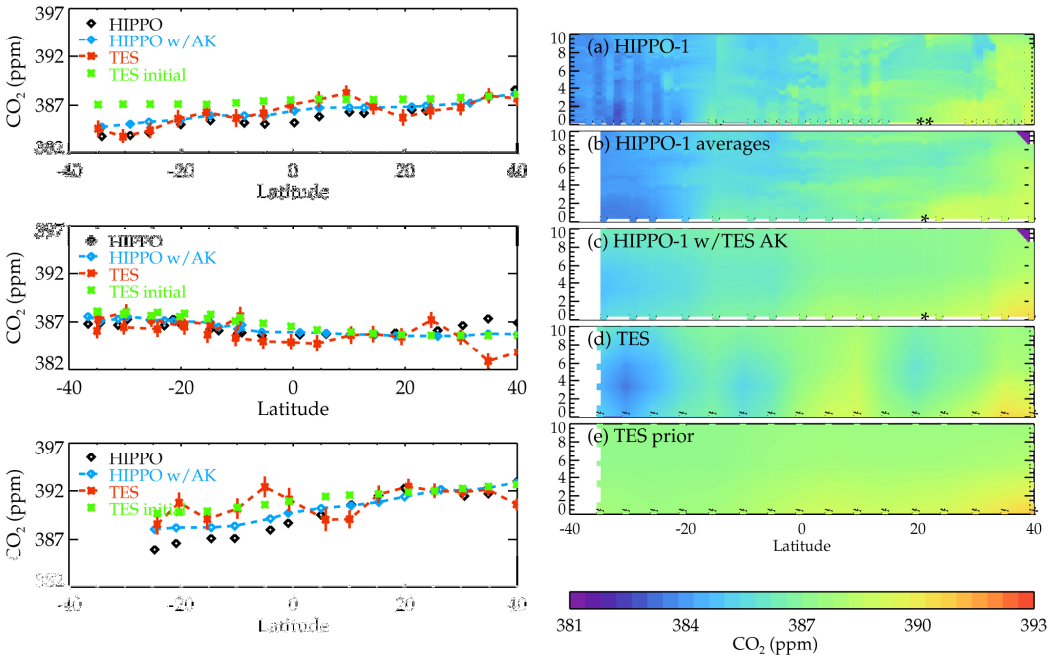

Figure 13-1 Comparison of monthly averaged TES V005 observations at 511 hPa to HIPPO-identified profiles of CO2_X, which is CO_2 from two (harmonized) sensors averaged to 10s. Left shows TES (red) compared to HIPPO at the altitude of maximum TES sensitivity with and without the averaging kernel applied (blue dashed line and black dots, respectively). The green dotted line shows the TES prior. Right shows a curtain plot of the HIPPO-1 measurements (a) HIPPO profile measurements (b) averaged over same latitude bins as TES (c) applying the TES averaging kernel to account for TES vertical sensitivity (d) TES measurements, averaged over +-10 degrees longitude, +- 5 degrees latitude, and +- 15 days, and (e) the TES prior.

As discussed in Kulawik et al. (2012), the HIPPO datasets are unique for validation in that they provide CO_2 profiles between the surface up through 9 - 13 km, far higher than most regular aircraft measurements which go up to 5 km. Other validation datasets, while still extremely valuable, are less suitable for validation, e.g. CONTRAIL, while very useful in that it crosses over a wide range of latitudes is less useful in that most measurements are between 9-11 km.

TES, while capturing most latitudinal patterns, has issues in HIPPO-2 at +-15 degrees, and HIPPO-1 north of 30N. These seem to be regions where the systematic errors are not random and so do not average out.

13.5 References

13.5.1 TES CO_2 References

[1] Kulawik, S.S., D.B.A. Jones, R. Nassar, F.W. Irion, J.R. Worden, K.W. Bowman, T. Machida, H. Matsueda, Y. Sawa, S.C. Biraud, M.L. Fischer, A.R. Jacobson (2010), Characterization of Tropospheric Emission Spectrometer (TES) CO_2 for carbon cycle science, *Atmos. Chem. Phys., 10, (12),* 5601-5623, 2010.

[2] Kulawik, S.S., J.R. Worden, S.C. Wofsy, S.C. Biraud, R. Nassar, D.B.A. Jones, E.T. Olsen, G.B. Osterman, (2012), Comparison of improved Aura Tropospheric Emission Spectrometer (TES) CO_2 with HIPPO and SGP aircraft profile measurements, *Atmospheric Chemistry and Physics Discussions, 12,* 6283 – 6329, February 29, 2012.

[3] Lamouroux, J., Tran, H, Laraia, A. L., Gamache, R. R., Rothman, L. S., Gordon, I. E., Hartmann, J.-M.: Updated database plus software for line-mixing in CO_2 infrared spectra and their test using laboratory spectra in the 1.5-2.3 μm region, J. Quant. Spectrosc. Radiat. Transfer, 111, 2321, DOI: 10.1016/j.jqsrt.2010.03.006, 2010.

[4] Nassar, R., D.B.A. Jones, S.S. Kulawik, J.R. Worden, K.W. Bowman, R.J. Andres, P. Suntharalingam, J.M. Chen, C.A.M. Brenninkmeijer, T.J. Schuck, T.J. Conway, D.E. Worthy (2011), Inverse modeling of CO_2 sources and sinks using satellite observations of CO_2 from TES and surface flask measurements, *Atmos. Chem. Phys., **11**, (12),* 6029-6047, June 24, 2011.

13.5.2 General References

[5] Niro, F., K. Jucks, and J.-M. Hartmann (2005), Spectra calculations in central and wing regions of CO_2 IR bands. IV: Software and database for the computation of atmospheric spectra, *J Quant Spectrosc Radiat Transfer, Vol. 95,* pp. 469-481.

[6] Riley, W.J., S.C. Biraud, M.S. Torn, M.L. Fischer,D. P. Billesbach, J.A. Berry (2009), Regional CO_2 and latent heat surface fluxes in the Southern Great Plains: Measurements, modeling, and scaling, *Journal of Geophysical Research-Biogeosciences, 114,* G04009, DOI: 10.1029/2009JG001003, 2009.

[7] Wofsy, S.C., the HIPPO Science Team and Cooperating Modellers and Satellite Teams (2011), HIAPER Pole-to-Pole Observations (HIPPO): Fine grained, global scale measurements for determining rates for transport, surface emissions, and removal of climatically important atmospheric gases and aerosols, *Phil. Trans. of the Royal Society A, vol. 369 (no. 1943),* 2073-2086, May 28, 2011.

14. Ammonia

The TES ammonia algorithm is described in Shepard et al. (2011), which also presented global retrievals using a prototype algorithm equivalent to TES V005. TES V005 ammonia was validated against in situ measurements in North Carolina over seven months in 2009 (Pinder et al., 2011). This analysis showed that ammonia from TES transects, averaged by month or by density of livestock facilities captured the same spatial and temporal variability as the two week means of in situ surface measurements. Due to sampling issues, this analysis was restricted to daytime only observations, with DOFS greater than 0.1. Only the TES transects from August 2009 have been reprocessed with V006. The daytime values of the V006 retrievals with DOFS greater than 0.1 are within 1 ppbv of the V005 results and the two datasets are 92% correlated. This provides some confidence that a repeat of the analysis over North Carolina with the full seven months of V006 data would return the same results, and that therefore TES V006 ammonia, when averaged over sufficient number of observations, will provide reliable information on temporal and spatial variability.

TES V005 data over North America were assimilated by Zhu et al. (2013) in an inverse modeling effort with the GEOS-Chem adjoint to constrain NH_3 emissions. The optimized model showed better agreement with surface measurements from National Atmospheric Deposition Program (NADP) AmmoniaMonitoring Network (AMoN).

The data quality of the TES V006 ammonia product was assessed through comparisons between TES ammonia and aircraft and surface measurements collected during two campaigns in the Central Valley in California: CalNex (Nowak et al., 2012) in the spring of 2010 and DISCOVER-AQ in January/February 2013. The Central Valley offers ideal conditions for monitoring ammonia from a satellite, since it is present in high concentrations and there is strong thermal contrast at the time of the TES overpass.

During CalNex there was one aircraft track under the TES transect on May 12. Ammonia measurements were taken with the CIMS instrument on the NOAA WP-3D aircraft and compared with the TES retrieved ammonia value at the pressure level of the peak of the averaging kernel (Figure 14-1). The aircraft and TES measurements present similar spatial variability, showing a small peak around 35.1N and a sharp increase in NH_3 around 36N. The difference in magnitude is due to the difference in the measured parameters: while the aircraft value is a point measurement taken between 300 and 400 m altitude, the TES measurements in this cases showed greatest sensitivity to the ammonia concentrations between 925 and 800 mbar.

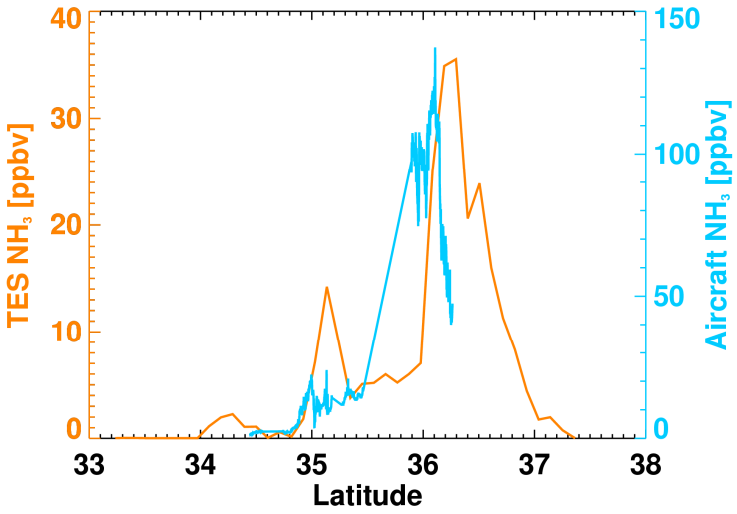

Figure 14-1 NH3 measurements from the CIMS instrument (blue) and TES (gold) on May 12, 2010 in the California Central Valley.

During DISCOVER-AQ in January 2013, there were three TES transects coincident with either aircraft or surface measurements. On January 21 and January 30 both the Proton-Transfer-Reaction (PTR) and Picarro instruments flying aboard the NASA P3-B aircraft collected ammonia data under the TES track. These data were averaged over the TES footprint and compared with the TES NH_3 value at the averaging kernel peak, as was done for the CalNex comparison (Figure 14-2). Once again TES captures the spatial gradients measured by the in situ instruments. The large change in NH_3 measured by the aircraft between January 21 and January 30 and difference in the ratio between TES and the aircraft instruments (~10 on January 21 and ~4 on January 30) are likely due to the difference in the boundary layer (BL) height between these two days. On January 21 the BL height ranged between 300 and 400 m, while on January 30 it varied from 600 to 1000m. A shallow BL leads to greater NH_3 concentrations at lower levels, where TES is less sensitive.

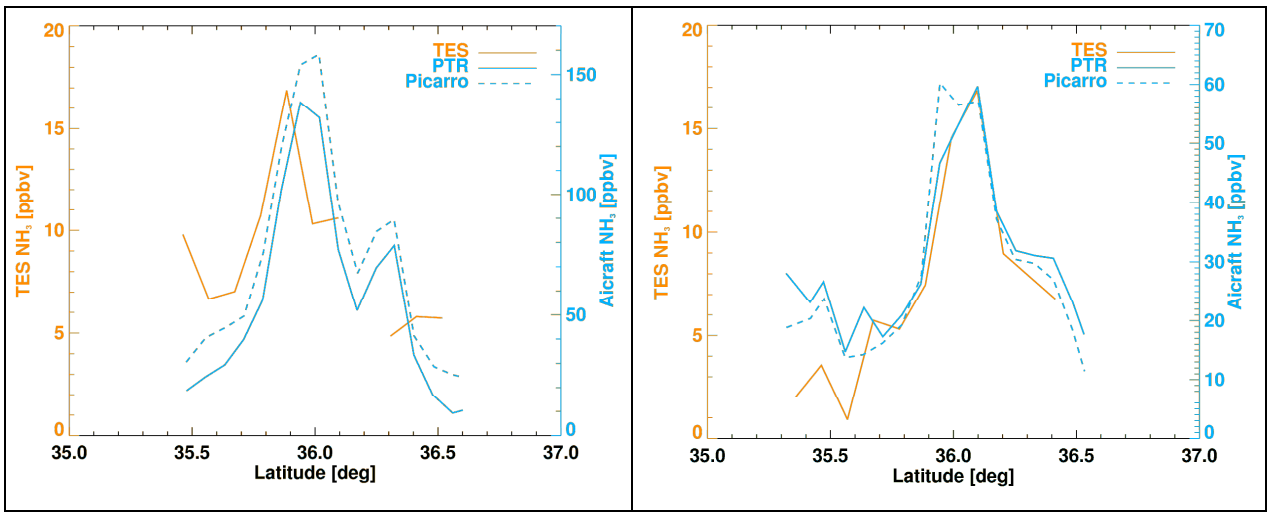

Figure 14-2 2013 NH3 measurements in the California Central Valley from the PTR and Picarro instruments (blue) and TES (gold) on January 21 (left) and January 30 (right).

On January 28 there were no aircraft measurements, but an Open Quantum Cascade Laser (QCL) was mounted on an automobile and driven along a path directly under the TES track (Miller et al., 2014). The NH_3 from the averaged QCL at the surface and from TES at the peak of the averaging kernel are very well correlated (Figure 14-3), though again the magnitudes are very different.

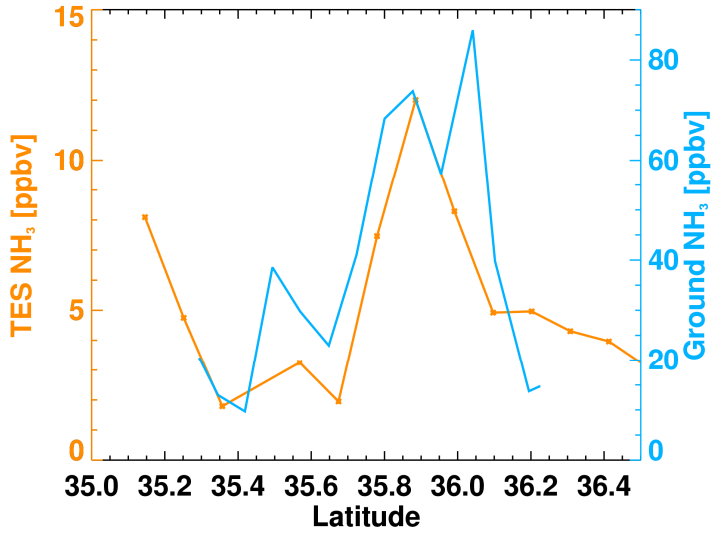

Figure 14-3 2013 NH3 measurements in the California Central Valley from the QCL instrument (blue) and TES (gold) on January 28.

A different perspective on the relative magnitudes of the measurements from these two instruments was obtained by comparing the total column amounts, as shown below in Figure 14-4 [Mark Zondlo and Kang Sun, pers. comm.]. The column amounts were estimated from the aircraft measurements by assuming that NH_3 in the BL was well mixed, and that it was negligible above the BL top. These assumptions are justified based on the analysis of the few NH_3 profiles collected during the campaign at other locations in the valley. The column show excellent agreement and the aircraft values are within or close to the estimated TES error.

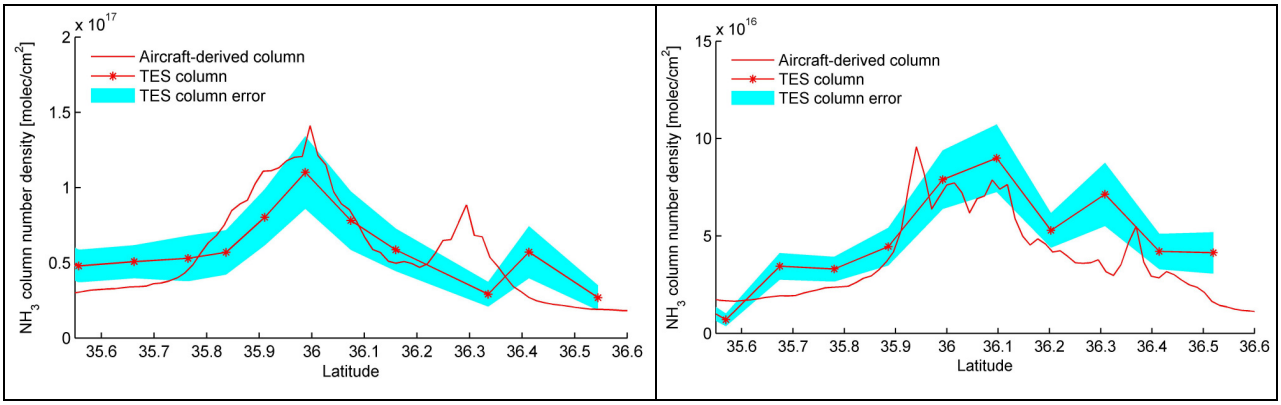

Figure 14-4 NH3 column amounts during DISCOVER-AQ from TES and the Picarro instrument on January 21 (left) and January 30 (right).

14.1 References

14.1.1 TES NH_3 references

[1] Pinder, R.W., J.T. Walker, J.O. Bash, K.E. Cady-Pereira, D.K. Henze, M. Luo, G.B. Osterman, and M.W. Shephard (2011), Quantifying spatial and seasonal variability in atmospheric ammonia with in situ and space-based observations (2011), *Geophysical Research Letters Vol. 38, Issue 4,* L04802, doi: 10.1029/2010GL046146, February 18, 2011.

[2] Shephard, M.W., K.E. Cady-Pereira, M. Luo, D.K. Henze, R.W. Pinder, J.T Walker, C.P. Rinsland, J.O. Bash, L. Zhu, V.H. Payne, and L. Clarisse (2011), TES ammonia retrieval strategy and global observations of the spatial and seasonal variability of ammonia, *Atmos. Chem. Phys., 11,* pp. 10743–10763, doi:10.5194/acp-11-10743-2011, October 31, 2011.

[3] Zhu, L., D. K. Henze, K. E. Cady-Pereira, M. W. Shephard, M. Luo, R. W. Pinder, J. O. Bash, and G.-R. Jeong (2013), Constraining U.S. ammonia emissions using TES remote sensing observations and the GEOS-Chem adjoint model. *J. Geophys. Res.*, *Vol. 118,* pp. 1-14, January 3, 2013, doi:10.1002/jgrd.50166, 2013.

14.1.2 General References

[4] Miller, D. J., K. Sun, L. Tao, M.A. Khan, and M. A. Zondlo (2014), Open-path, quantum cascade-laser-based sensor for high-resolution atmospheric ammonia measurements, *Atmos. Meas. Tech., 7,* pp. 81-93, doi:10.5194/amt-7-81-2014, 2014.

[5] Nowak, J. B., J.A. Neuman, R. Bahreini, R., A.M. Middlebrook, J.S. Holloway, S.A. McKeen, D.D. Parrish, T.B. Ryerson, and M. Trainer (2012), Ammonia sources in the California South Coast Air Basin and their impact on ammonium nitrate formation, *Geophysical Research Letters, Vol. 39, Issue 7,* L07804, doi: 10.1029/2012GL051197.

15. Formic Acid

The TES formic acid (HCOOH) algorithm is described in Cady-Pereira et al. (2014), which also presents seasonal global retrievals using a prototype algorithm equivalent to TES V006, and compares these results against GEOS-Chem output (Figure 15-1). TES and GEOS-Chem show some similarities in the broad spatial distribution of HCOOH: both model and TES see elevated HCOOH concentrations in the tropics and in the Northern Hemisphere during summer. However, the model Representative Volume Mixing Ratios (RVMRs) are persistently low compared to TES, typically by a factor of two or more. The TES data thus corroborate other recent studies based on aircraft, surface FTS, and satellite measurements that have pointed to large scale missing sources of atmospheric HCOOH (Stavrakou et al., 2012; Paulot et al., 2011).

The prototype algorithm was also applied to TES observations taken concurrently with the Intercontinental Transport Experiment-Phase B (INTEX-B) and Megacity Initiative: Local and Global Research Observations (MILAGRO) campaigns, during which there were numerous measurements of formic acid from the Caltech Chemical Ionization Mass Spectrometer (CIT CIMS) mounted on aircraft. Due to sampling and colocation issues it was not possible to perform meaningful comparisons of TES profiles and those obtained from the aircraft measurements. Instead we elected to use GEOS-Chem as a transfer function, and separately compared aircraft and TES data against the model. Only aircraft data between 900-700 mbar were used, since this is the layer to which TES is most sensitive to formic acid. TES observations were averaged over each GEOS-Chem grid box that contained TES data. There is good qualitative agreement (Figure 15-2) between TES and the in situ measurements: both show that GEOS-Chem correlates better with the MILAGRO measurements, and severely underestimates the INTEX-B measurements (Sreelekha et al., *manuscript in preparation*).

Only a limited number of the TES runs coincident with MILAGRO have been processed operationally with the V006 algorithm (Table 15-1). There were 742 observations processed but only 147 passed quality checks and had DOFS greater than 0.1. Since the detectability level for TES HCOOH is approximately 0.5 ppbv, and this level is above the expected background concentration, the small number of retrievals with information is not unexpected. Only 48 of these retrievals had been processed successfully with the prototype code and 12 of these were rejected due to large fractional error (>100%). The remaining 36 retrievals have a mean value of 1.6 ppbv, with a mean estimated error of 24.6%. The V006 results are well correlated with the prototype results (correlation coefficient is 0.9) and are biased slightly high (0.25 ppbv). This bias is due to adopting slightly different thresholds for selecting clean or enhanced profiles as a priori.

Table 15-1 MILAGRO V006 results compared against prototype code

	MILAGRO
Quality runs	147
Quality runs with error <100%	36
Mean HCOOH (ppbv)	1.6
Mean error	24.6%
Bias (V006-prototype) (ppbv)	0.26
Correlation (V006, prototype)	0.9

A preliminary direct assessment of the data quality of the TES V006 formic acid product was carried out through comparisons between the TES V006 formic acid and measurements from the Proton-Transfer-Reaction Mass Spectrometry (PTR-MS) instrument mounted on the NASA P3-B aircraft during DISCOVER-AQ in the California Central Valley January/February 2013. The Central Valley offers ideal conditions for satellite monitoring of species that tend to have higher concentrations in the boundary layer, as there is strong thermal contrast at the time of the TES overpass. During DISCOVER-AQ, there were three TES transects coincident with the aircraft flights: on January 21 and 30, and on February 6. A total of 60 transects were taken, but this set yielded only 29 TES retrievals with good quality flags and DOFS greater than 1, and only 13 of these were over the range covered by the aircraft measurements. The in situ measurements show HCOOH at approximately 0.5 ppbv, close to the expected TES detectability level. Examination of the TES spectra showed very weak HCOOH signals, with amplitude near the noise level at 1105 cm^{-1} (0.2K).

The TES RVMRs were compared against the closest aircraft measurements, which were taken between 400 and 900 m altitude (Figure 15-3). There is decent correlation between the two datasets, but while the estimated error ranges between 22% and 33%, TES is obviously overestimating HCOOH by a greater amount: the PTR measurements are taken at a lower altitude level than that of the maximum TES sensitivity, and thus are expected to be higher rather than lower. We expect these high values are caused by the selection of an enhanced a priori, when in fact a more moderate profile would be a better choice for these cases with weak signals. Currently the algorithm has only two a priori profiles, clean and enhanced. This analysis suggests that a third intermediate profile should also be included as a possible choice. This would also require slightly modifying the a priori selection algorithm.

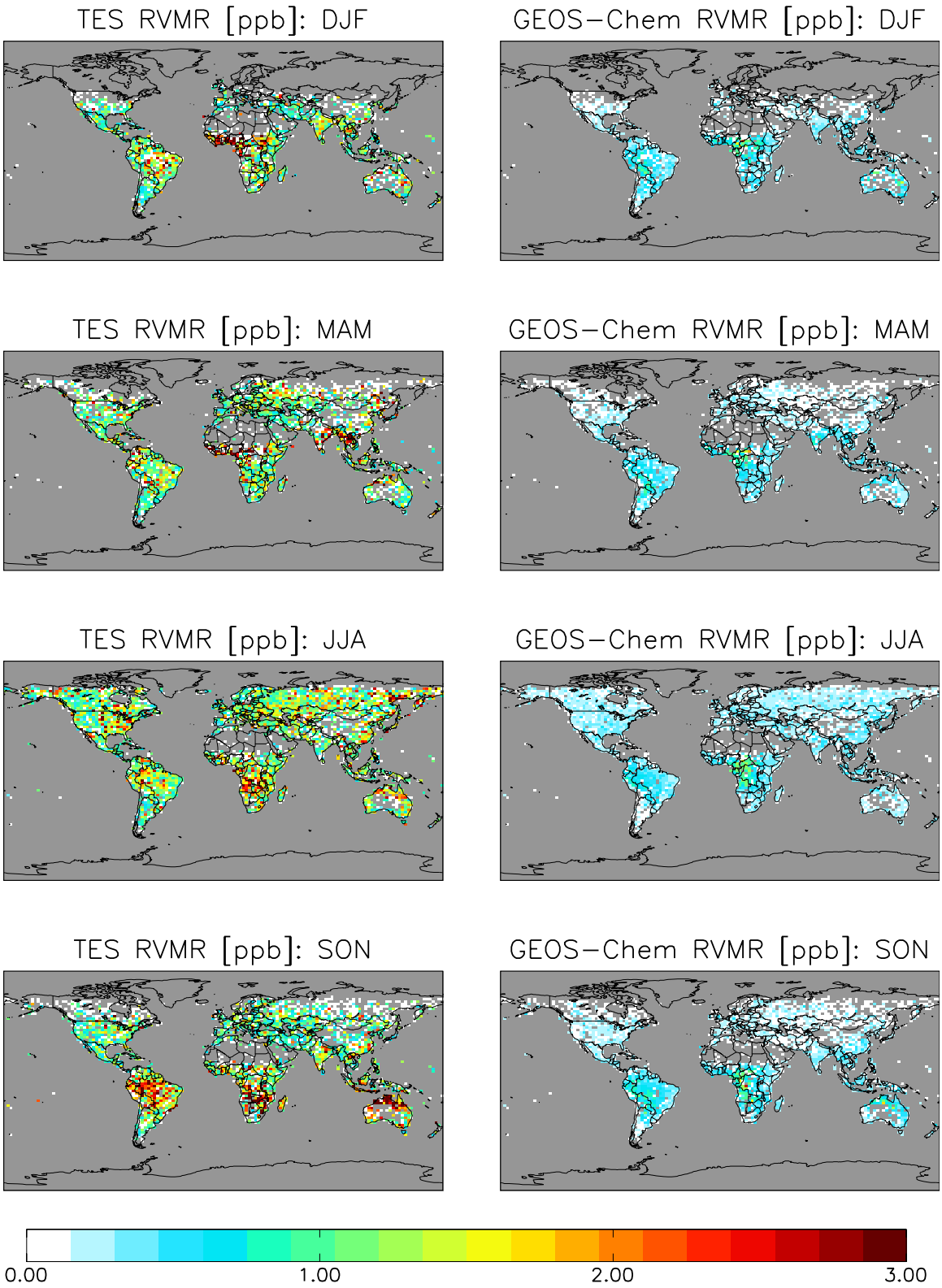

Figure 15-1 HCOOH from TES (left column) and GEOS-Chem with TES operator applied (right column). DJF: December, January, February; MAM: March, April, May; JJA: June, July, August; SON: September, October, November.

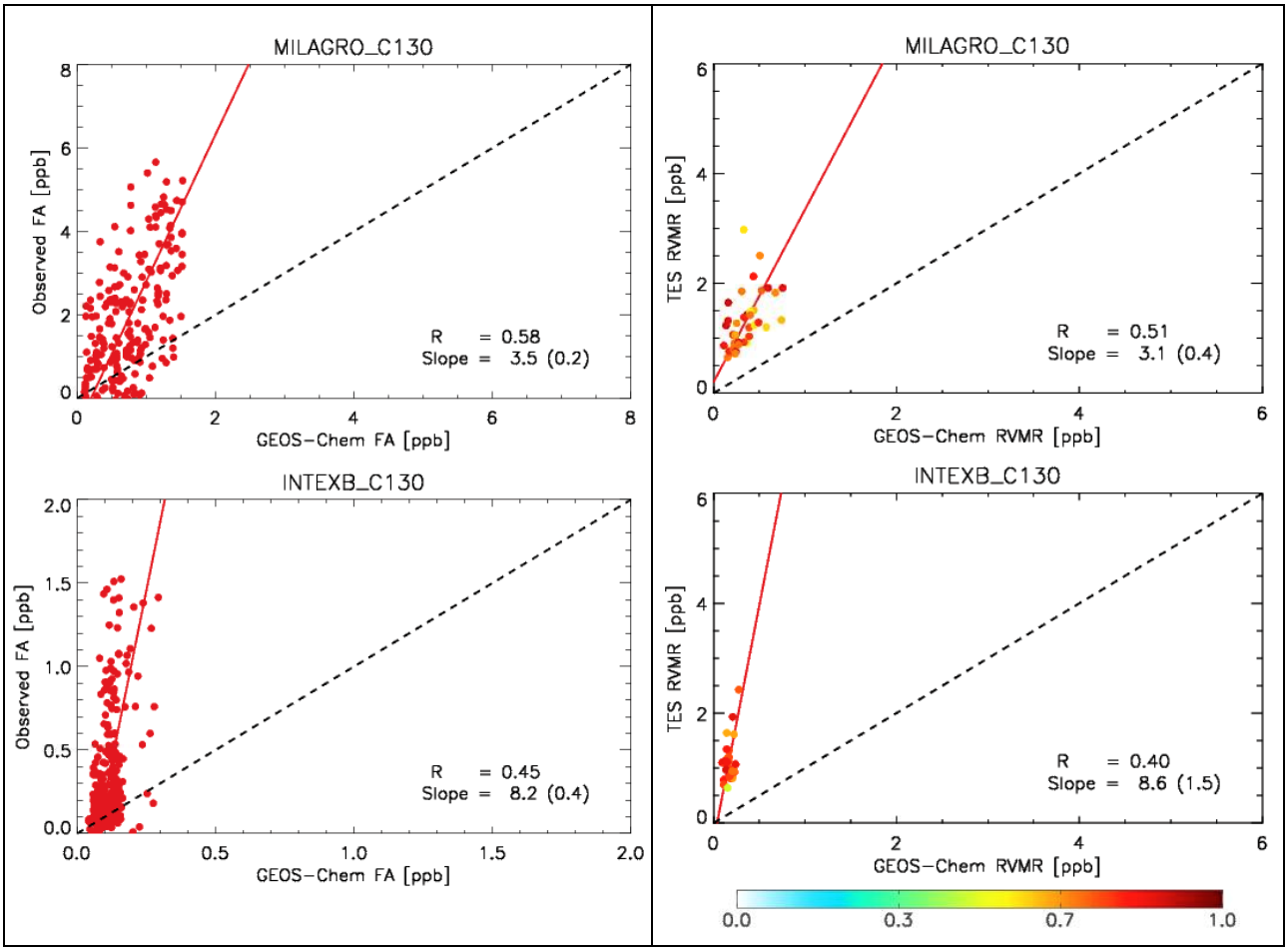

Figure 15-2 Formic acid measurements compared against GEO-Chem output from aircraft (left) and TES (right). Top panels show MILAGRO data, bottom panel INTEX-B. Colors of TES retrieval indicate DOFS.

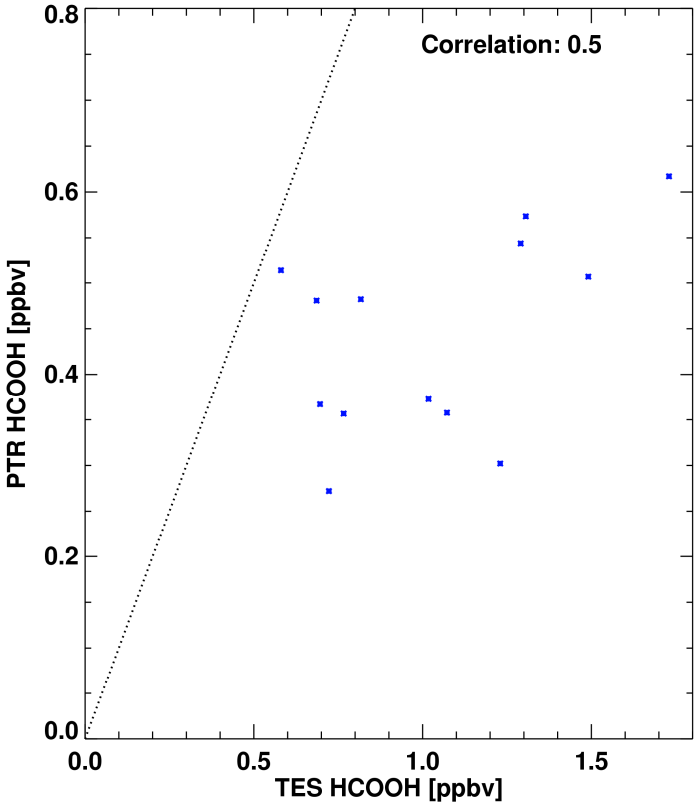

Figure 15-3 PTR HCOOH vs TES HCOOH during the DISCOVER-AQ campaign in the Central Valley in California in January/February 2013.

15.1 References

15.1.1 TES HCOOH references

[1] Cady-Pereira, K. E., S. Chaliyakunnel, M.W. Shephard, D. B Millet, M. Luo, and K. C. Wells (2014), HCOOH measurements from space: TES retrieval algorithm and observed global distribution, *Atmos. Meas. Tech. Discuss., 7,* pp. 1975-2015, doi:10.5194/amtd-7-1975-2014, 2014.

[2] Chaliyakunnel, S., D.B. Millet, K.C. Wells, K.E. Cady-Pereira, M.W. Shephard, M. Luo and F. Paulot, Global tropospheric formic acid measurements from the TES satellite sensor: retrieval evaluation and the importance of pyrogenic sources *(in preparation).*

15.1.2 General References

[3] Paulot, F., D. Wunch, J.D. Crounse, G.C. Toon, D.B. Millet, P.F. DeCarlo, C. Vigouroux, N.M. Deutscher, G. González Abad, J. Notholt, T. Warneke, J.W. Hannigan, C. Warneke, J.A. de Gouw, E.J. Dunlea, M. De Mazière, D. W. T. Griffith, P. Bernath, J.L. Jimenez, and P.O. Wennberg (2011), Importance of secondary sources in the atmospheric budgets of formic and acetic acids, *Atmos. Chem. Phys., 11,* pp. 1989-2013, 2011, doi:10.5194/acp-11-1989-2011.

[4] Stavrakou, T., J-F. Müller, J. Peeters, A. Razavi, L. Clarisse, C. Clerbaux, P-F. Coheur, D. Hurtmans, M. De Mazière, C. Vigouroux, N.M. Deutscher, D.W.T. Griffith, N. Jones, C. Paton-Walsh (2012), Satellite evidence for a large source of formic acid from boreal and tropical forests, *Nature Geoscience, Vol. 5, Issue 1,* pp. 26–30, (2012) doi:10.1038/ngeo1354, 2012.

16. Methanol

The TES methanol (CH_3OH) algorithm is described in Cady-Pereira et al. (2012), which also presents seasonal global retrievals using a prototype algorithm equivalent to TES V006, and compares these results against GEOS-Chem output (Figure 16-1). TES and GEOS-Chem exhibit similar large-scale patterns: substantially higher methanol abundance during summer, when the biosphere is active, and low values during the boreal winter. However the regional details can be quite different. For example, the observed seasonal variation in methanol over South America, with higher TES values during the dry season and lower TES values in other months, is substantially stronger than in the model; it may be that the model is underestimating the seasonal importance of biomass burning methanol emissions in these tropical regions. It is also possible that biogenic methanol emissions from tropical forests undergo stronger seasonal swings than presently thought (Myneni et al., 2007).

Wells et al. (2012) compared aircraft measurements and TES retrievals obtained with the prototype algorithm against GEOS-Chem output, as shown below in Figure 16-2. Data were available from the following campaigns: MILAGRO (Singh et al., 2009; Kleb et al., 2011) over Mexico, the Gulf of Mexico, and southern Texas (March 2006); INTEX-B (Singh et al., 2009; Kleb et al., 2011) over the Pacific Ocean and western US (April/May 2006); Aerosol, Radiation, and Cloud Processes affecting Arctic Climate(ARCPAC) (Brock et al., 2011) over the US (transit flight to Alaska, April 2008); Arctic Research of the Composition of the Troposphere from Aircraft and Satellites (ARCTAS) (Jacob et al., 2010) over Canada and the western US (June/July 2008, which comprised the latter phase of the study); and Second Texas Air Quality Study (TexAQS-II) (Parrish et al., 2009) over the Houston area (September/October 2006). Due to sampling and colocation issues it was not possible to perform meaningful comparisons of TES profiles and those obtained from the aircraft measurements. Instead we elected to use GEOS-Chem as a transfer function, and separately compared aircraft and TES data against the model. TES observations were averaged over each GEOS-Chem grid box that contained TES data.

For the INTEX-B comparisons, the TES retrievals are consistent with both the C-130 and DC-8 airborne measurements. In both cases, the TES:model slope is statistically indistinguishable from the corresponding aircraft:model slope, and the correlation coefficients are also very similar. In the case of MILAGRO, the C-130 data contain a pronounced urban influence as sampling was focused over Mexico City; TES exhibits lower concentrations (and a higher correlation with the model) because its orbit did not track directly over Mexico City. For the DC-8 flight tracks during MILAGRO, the TES data did not correlate with the model. This campaign focused on sampling Mexico City outflow during transport over the Gulf of Mexico; it may be that the satellite measurements include some plumes that are not captured at the $2° \times 2.5°$ resolution of GEOS-Chem.

The ARCPAC data exhibit the only instance with an aircraft:model slope near 1, although a 1-2 ppb offset exists between the observations and the model. As this was a transit flight for the campaign with little vertical profiling, the influence of near-field emissions is lower than in the other campaigns. For ARCPAC, most of the TES RVMR values fall in the same range as the aircraft observations, but a few high retrieved concentrations lead to an overall low correlation with the model. Two of these high TES values occurred over the Colorado Front Range near Colorado Springs and Pueblo, and may include urban boundary-layer pollution that was not sampled by the aircraft. The other two occurred over central/eastern Oklahoma and may be influenced by large wildfires that were burning in central Oklahoma during the campaign. For the ARCTAS campaign, the TES:model slope is very similar to the aircraft:model slope, and with a similar degree of correlation. The TES data are low compared to the aircraft data during TexAQS-II, probably because there were few TES observations directly over the urban core during this campaign. In summary, when TES and the aircraft are sampling the same airmass, their data present similar correlation and bias with respect to the model. In these cases both aircraft and TES show that the model is usually underestimating the atmospheric levels of methanol in these areas of North America. Wells et al. (2012) used IASI data to adjust methanol emissions over North America, and evaluated the effect of these new emissions with TES data, obtaining better model/measurement agreement.

Only a limited number of the TES runs coincident with MILAGRO and ARCTAS have been processed operationally with the V006 algorithm (Table 16-1), and only a fraction of these passed quality checks and had any information (10% for MILAGRO and 39% for ARCTAS). Furthermore, not all these runs generated successful retrievals in the prototype algorithm, which used V005 data. Based on the limited set of coincident runs we can state that in when methanol levels are high (i.e., during the ARCTAS campaign) V006 is well correlated with the prototype results, but is biased low. When methanol is low, the retrieval is more sensitive to changes in the species retrieved prior to methanol, and the results from the two algorithms are less correlated. The prototype algorithm results during ARCTAS agreed qualitatively with the aircraft measurements, but that analysis cannot determine the true bias of the TES methanol product.

Table 16-1 MILAGRO V006 results compared against prototype code

	MILAGRO	ARCTAS
Quality runs (total)	87 (742)	498 (1273)
Quality runs with coincidence	25	88
Mean CH_3OH (ppbv)	1.1	4.2
Mean error	45%	47%
Bias (V006-prototype) (ppbv)	-3.5	-3.0
Correlation (V006, prototype)	0.52	0.91

Thus there is a pressing need for a direct assessment of the data quality of the TES V006; however, the sparse coverage provided by TES leads to few close coincidences between in situ and TES observations. The DISCOVER-AQ in the California Central Valley during January/February 2013 provided one such opportunity. We compared the TES V006 methanol and measurements from the Proton-Transfer-Reaction Mass Spectrometry (PTR-MS) instrument mounted on the NASA P3-B aircraft. The Central Valley offers ideal conditions for satellite monitoring of species that tend to have higher concentrations in the boundary layer, as there is strong thermal contrast at the time of the TES overpass. During DISCOVER-AQ, there were three TES transects coincident with the aircraft flights: on January 21 and 30, and on February 6. A total of 60 transects were taken, but this set yielded only 11 TES retrievals with good quality flags and DOFS greater than 1. The PTR measurements, taken between 400 and 900 m altitude, show methanol ranging between 1.3 and 6.0 ppbv, with a mean of 3.1 ppbv, while the mean of the maximum of the TES values was 1.3 ppbv. All TES retrievals during these transects selected a clean a priori. It is likely that by changing the selection to an enhanced a priori, the TES retrievals would agree more closely with the PTR measurements.

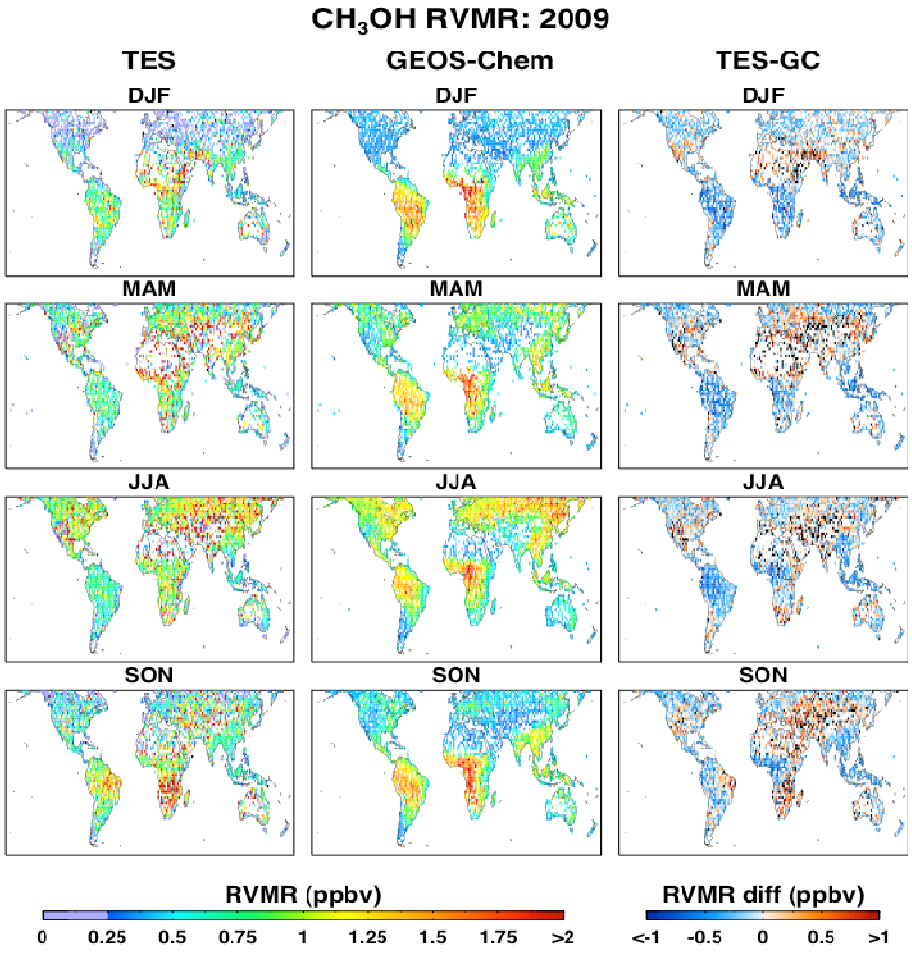

Figure 16-1 CH_3OH RVMR from TES (left column) and GEOS-Chem with TES operator applied (right column).

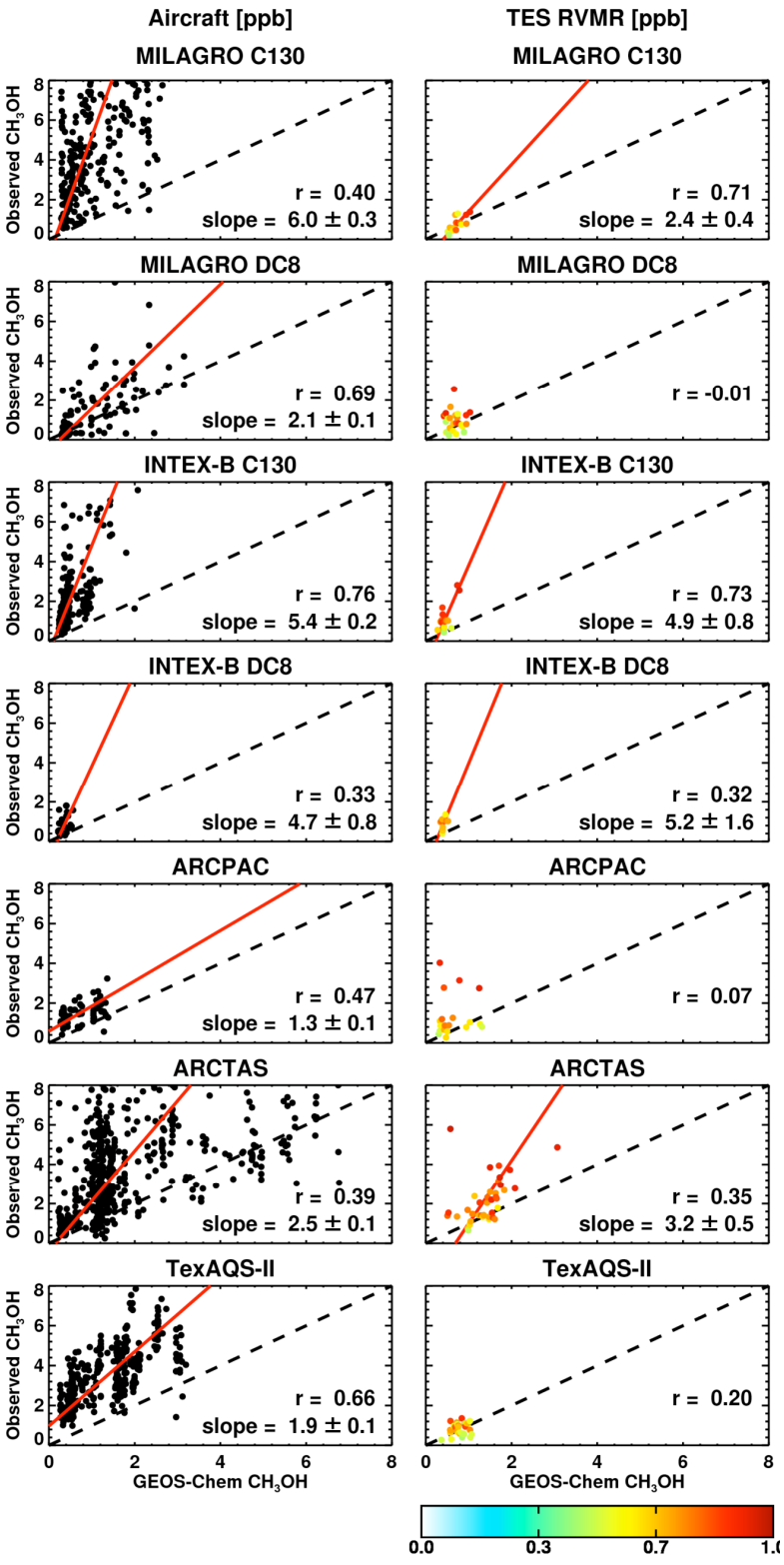

Figure 16-2 CH3OH measurements compared against GEOS-Chem output from aircraft (left) and TES (right). Colors of TES retrieval indicate DOFS.

16.1 References

16.1.1 TES references

[1] Brock, C.A., J. Cozic, R. Bahreini, K.D. Froyd, A.M. Middlebrook, A. McComiskey, J. Brioude, O.R. Cooper, A. Stohl, K.C. Aiken, J.A. de Gouw, D.W. Fahey, R.A. Farrare, R.-S. Gao, W. Gore, J.S. Holloway, G. Hubler, A. Jefferson, D.A. Lack, S. Lance, R.H. Moore, D.M. Murphy, A. Nenes, P.C. Novelli, J.B. Nowak, J.A. Ogren, J. Peischl, R.B. Pierce, P. Pilweskie, PK. Quinn, T.B. Ryerson, K.S. Schmidt, J.P. Schwarz, H. Sodemann, J.R. Spackman, H. Stark, D.S.Thomson, T. Thornberry, P. Veres, L.A. Watts, C. Warneke, and A.G. Wollney (2011), Characteristics, sources, and transport of aerosols measured in spring 2008 during the aerosol, radiation, and cloud processes affecting Arctic Climate (ARCPAC) Project, *Atmos. Chem. Phys., 11,* pp. 2423-2453, doi:10.5194/acp-11-2423-2011, 2011.

[2] Cady-Pereira, K. E., M.W. Shephard, D.B. Millet, M. Luo, K.C. Wells, Y. Xiao, V.H. Payne, and J. Worden (2012), Methanol from TES global observations: retrieval algorithm and seasonal and spatial variability, *Atmos. Chem. Phys., 12,* pp. 8189-8203, doi:10.5194/acp-12-8189-2012, 2012.

[3] Jacob, D.J., J.H. Crawford, H. Maring, A.D. Clarke, J.E.Dibb, L.K. Emmons, R.A. Ferrare, C.A. Hostetler, P.B. Russell, H.B. Singh, A.M. Thompson, G.E. Shaw, E. McCauley, J.R. Pederson, and J.A. Fisher (2010), The Arctic Research of the Composition of the Troposphere from Aircraft and Satellites (ARCTAS) mission: design, execution, and first results, *Atmos. Chem. Phys., 10,* pp. 5191-5212, doi:10.5194/acp-10-5191-2010, 2010.

[4] Kleb, M.M., G. Chen, J.H. Crawford, F.M. Flocke, and C.C. Brown (2011), An overview of measurement comparisons from the INTEX-B/MILAGRO airborne field campaign, *Atmos. Meas. Tech., 4,* pp. 9-27, doi:10.5194/amt-4-9-2011, 2011.

[5] Myneni, R. B., W. Yang, R.R. Nemani, A.R. Huete, R.E. Dickinson, Y. Knyazikhin, K. Didan, R. Fu, R.I. Negrón Juárez, S.S. Saatchi, H. Hashimoto, K. Ichii, N.V. Shabanov, B. Tan, P. Ratana, J.L. Privette, J.T. Morisette, E.F. Vermote, D.P. Roy, R.E. Wolfe, M.A. Friedl, S.W. Running, P. Votava, Nazmi El-Saleous, Sadashiva Devadiga, Y. Su, and V.V. Salomonson (2007), Large seasonal swings in leaf area of Amazon rainforests. *Proceedings of the National Academy of Sciences, vol. 104 no.12,* doi:10.1073/pnas.0611338104 pp. 4820-4823, March 20, 2007.

[6] Parrish, D.D., D.T. Allen, T.S. Bates, M. Estes, F.C. Fehsenfeld, G. Feingold, R. Ferrare, R.M. Hardesty, J.F. Meagher, J.W. Nielsen-Gammon, R.B. Pierce, T.B.

Ryerson, J.H. Seinfeld, and E.J. Williams (2009), Overview of the Second Texas Air Quality Study (TexAQS II) and the Gulf of Mexico Atmospheric Composition and Climate Study (GoMACCS), *Journal of Geophysical Research, Vol. 114 Issue D7,* D00F13, doi:10.1029/2009JD011842, 2009.

[7] Singh, H.B., W.H. Brune, J.H. Crawford, F. Flocke, and D.J. Jacob (2009), Chemistry and transport of pollution over the Gulf of Mexico and the Pacific: spring 2006 INTEX-B campaign overview and first results, *Atmos. Chem. Phys., 9,* 2301-2318, doi:10.5194/acp-9-2301-2009, 2009.

[8] Wells, K. C., D.B. Millet, L. Hu, K.E. Cady-Pereira, Y. Xiao, M.W. Shephard, C.L. Clerbaux, L. Clarisse, P.-F. Coheur, E.C. Apel, J. de Gouw, C. Warneke, H.B. Singh, A.H. Goldstein, and B.C. Sive (2012), Tropospheric methanol observations from space: retrieval evaluation and constraints on the seasonality of biogenic emissions, *Atmos. Chem. Phys., 12,* pp. 5897-5912, doi:10.5194/acp-12-5897-2012, 2012.

[9] Wells, K.C., D.B. Millet, K.E. Cady-Pereira, M.W. Shephard, D.K. Henze, N. Bousserez, E.C. Apel, J. de Gouw, C. Warneke, and H.B. Singh (2013), Quantifying global terrestrial methanol emissions using observations from the TES satellite sensor, *Atmos. Chem. Phys. Discuss., 13,* pp. 21883-21926, doi:10.5194/acpd-13-21883-2013, 2013.

Appendices

A. Acronyms

ABSCO	Absorption Coefficient
ACE	Atmospheric Chemistry Experiment
AER	Atmospheric and Environmental Research
AIRS	Atmospheric Infrared Sounder
AK	Averaging Kernel
AKVMR	Averaging Kernel weighted Volume Mixing Ratio
ALIAS	Aircraft Laser Infrared Absorption Spectrometer
AMoN	AmmoniaMonitoring Network
AMSU	Advanced Microwave Sounding Unit
ASDC	Atmospheric Science Data Center
ARCIONS	Arctic Intensive Ozonesonde Network Study
ARCPAC	Aerosol, Radiation, and Cloud Processes affecting Arctic Climate
ARCTAS	Arctic Research on the Composition of the Troposphere from Aircraft and Satellites
ARM	Atmospheric Radiation Measurement
ARM-SGP	Atmospheric Radiation Measurement – Southern Great Plains
ASHOE	Airborne Southern Hemisphere Ozone Experiment
AVE	Aura Validation Experiment
BL	Boundary Layer
CalNex	California Nexus
CAMNET	Coordinated Air Monitoring NETwork
CASA	Carnegie Ames Stanford Approach
CFH	Cryogenic Frostpoint Hygrometer
CH_3OH	Methanol
CH_4	Methane, Natural Gas
CIMS	Chemical Ionization Mass Spectrometer
CIT	California Institute of Technology
CMAQ	Community Multi-scale Air Quality
CO	Carbon Monoxide

CO_2	Carbon Dioxide
CONTRAIL	CONdensation TRAIL
CR-AVE	Costa Rica Aura Validation Experiment
CTM	Chemical Transport Model
DACOM	Differential-Absorption Carbon Monoxide Monitor
DFM	Design File Memorandum
DISCOVER-AQ	Deriving Information on Surface conditions from Column and Vertically Resolved Observations Relevant to Air Quality
DN	Data Number
DOE	Department of Energy
DOF	Degrees of Freedom
DOFS	Degrees of Freedom for Signal
DPS	Data Products Specification
EOS	Earth Observing System
EPA	Environmental Protection Agency
ESDT	Earth Science Data Type
ESRL	Earth System Research Laboratory
FM	Forward Model
FPH	Frost-Point Hygrometer
FTIR	Fourier Transform Infrared Spectrometer
FTP	File Transfer Protocol
FTS	Fourier Transform Spectrometer
GMD-ESRL	Global Monitoring Division of the Earth System Research Laboratory
GEOS	Global Earth Observing System
GEOS	Goddard Earth Observing System
GoMACCS	Gulf of Mexico Atmospheric Composition and Climate Study
GMAO	Global Modeling Assimilation Office
GSFC	Goddard Space Flight Center
GSI	Gridpoint Statistical Interpolation
GTS	Global Telecommunications Service
H_2O	Dihydrogen Monoxide (Water)
HCOOH	Formic Acid
HDF	Hierarchical Data Format

HDO	Hydrogen Deuterium Monoxide (“Heavy Water”)
HIAPER	High-Performance Instrumented Airborne Platform for Environmental Research
HIPPO	HIAPER Pole-to-Pole Observations
HIRDLS	High Resolution Dynamics Limb Sounder
HIRS	High Resolution Infrared Sounders
HIS	High-Resolution Interferometer Sounder
HITRAN	HIgh-resolution TRANsmission molecular absorption database
hPa	Hectopascal, a unit used for air pressure
HYSPLIT	Hybrid Single-Particle Lagrangian Integrated Trajectory
IASI	Infrared Atmospheric Sounding Interferometer
ICS	Interferometer Control System
IDL	Interactive Data Language
IEEE	Institute of Electrical and Electronics Engineers
IGRA	Integrated Global Radiosonde Archive
INTEX	International Chemical Transport Experiment
INTEX-B	Intercontinental Transport Experiment-Phase B
IONS	INTEX Ozonesonde Network Study
ISM	Integrated Spectral Magnitude
JPL	Jet Propulsion Laboratory
K	Kelvin
L1B	Level 1B
L2	Level 2
LBLRTM	Line-by-Line Radiative Transfer Model
LT	Lower Troposphere
MACPEX	Mid-Latitude Airborne Cirrus Properties EXperiment
MATCH	Model of Atmospheric Transport and Chemistry
MILAGRO	Megacity Initiative: Local and Global Research Observations
MISR	Multi-angle Imaging SpectroRadiometer
MLS	Microwave Limb Sounder
MODIS	Moderate Resolution Imaging Spectroradiometer
MOHAVE	Measurements of Humidity in the Atmosphere Validation Experiments
MOPITT	Measurement Of Pollution In The Troposphere

MOZAIC	Measurement of OZONE on Airbus In-service Aircraft
MOZART	Model for OZone And Related chemical Tracers
N_2O	Nitrous Oxide
NADP	National Atmospheric Deposition Program
NASA	National Aeronautics and Space Administration
NCAR	National Center for Atmospheric Research
NCEP	National Centers for Environmental Prediction
NDACC	Network for the Detection of Atmospheric Composition Change
NESR	Noise Equivalent Spectra Radiance
NH	New Hampshire
NH_3	Ammonia
NOAA	National Oceanic & Atmospheric Administration
O_3	Ozone
OD	Optical Depth
OEM	Optimal Estimation Method
OMI	Ozone Monitoring Instrument
PAVE	Polar Aura Validation Experiment
PBL	Planetary Boundary Layer
PCS	Pointing Control System
PGE	Product Generation Executive
PI	Principal Investigator
PM	Particulate Matter
POLARIS	Photochemistry of Ozone Loss in the Arctic Region in Summer
PTR	Proton-Transfer-Reaction
PTR-MS	Proton-Transfer-Reaction Mass Spectrometry
QCL	Quantum Cascade Laser
RMS, rms	Root-Mean-Square
ROI	Reynolds Optimally Interpolated
RTVMR	Representative Tropospheric Volume Mixing Ratio
RVMR	Representative Volume Mixing Ratio
Run ID	TES run identification number
SCIAMACHY	Scanning Imaging Absorption Spectrometer for Atmospheric Cartography

SGP	Southern Great Plains
SHADOZ	Southern Hemisphere Additional Ozonesondes
SO	Special Observation
SRF	Spectral Response Function
SST	Sea Surface Temperature
STRAT	Stratospheric Tracers of Atmospheric Transport
TATM	Temperature
TES	Tropospheric Emission Spectrometer
TexAQS-II	Second Texas Air Quality Study
TOA	Top Of Atmosphere
TOPP	Tropospheric Ozone Pollution Project
TSUR	Surface Temperature
UT	Upper Troposphere
UTC	Universal Time Coordinated
VMR	Volume Mixing Ratio
WACCM	Whole Atmosphere Community Climate Model
WAVES	Water Vapor Validation Experiments
WOUDC	World Ozone and Ultraviolet Radiation Data Centre
WP-3D	Lockheed Research Aircraft used by NOAA